

**High-resolution, multi-proxy climate reconstructions of the late Holocene
derived from the varved sediments of two lakes in the Swiss Alps**

Inauguraldissertation
der Philosophisch-naturwissenschaftlichen Fakultät
der Universität Bern

Vorgelegt von

Monique M. Stewart

von Lexington, Massachusetts, U.S.A.

Leiter der Arbeit:
Prof. Dr. M. Grosjean
Universität Bern

**High-resolution, multi-proxy climate reconstructions of the late Holocene
derived from the varved sediments of two lakes in the Swiss Alps**

Inauguraldissertation
der Philosophisch-naturwissenschaftlichen Fakultät
der Universität Bern

Vorgelegt von

Monique M. Stewart

von Lexington, Massachusetts, U.S.A.

Leiter der Arbeit:

Prof. Dr. M. Grosjean

Universität Bern

Von der Philosophisch-naturwissenschaftlichen Fakultät angenommen.

Bern, 14 April 2011

Der Dekan:
Herr Prof. Dr. Silvio Decurtins

Virescit Vulnere Virtus

Table of Contents

Table of Contents.....	1
Figures.....	3
Tables.....	7
Abstract.....	9
1. Introduction	
a. Problem Framing.....	11
b. Research Questions.....	14
c. Outline.....	15
2. Study sites	
a. Lake Silvaplana, Upper Engadine, Switzerland.....	21
b. Lake Seeberg, Bernese Oberland, Switzerland.....	24
3. Methods	
a. Data.....	29
b. Field Methods.....	29
c. Laboratory Methods.....	32
d. Statistical Methods.....	42
4. Quantitative inter-annual and decadal summer temperature variability ca. 570 BC - AD 120 (Iron Age - Roman Period) reconstructed from the varved sediments of Lake Silvaplana, Switzerland [Journal of Quaternary Sciences, accepted]	
a. Abstract.....	51
b. Introduction.....	52
c. Study site.....	53
d. Methods.....	55
e. Results.....	59
f. Discussion.....	70
g. Summary and Conclusions.....	73
5. Reconstructions of Late Holocene palaeofloods and glacier activity in the Upper Engadine, Switzerland (ca. 1450 BC - AD 420) [Palaeogeography, Palaeoclimatology, Palaeoecology, submitted]	
a. Abstract.....	79
b. Introduction.....	80
c. Study site.....	83
d. Methods.....	84
e. Results and Discussion.....	86
f. Conclusion.....	96
6. The potential of sediments from Lake Seeberg, Switzerland, as an archive of past climate [Journal of Paleolimnology, in preparation]	
a. Abstract.....	103
b. Introduction.....	104
c. Study site.....	105
d. Methods.....	109
e. Results.....	115

f. Discussion.....	124
g. Summary and Conclusions.....	126
7. Conclusions and Outlook	
a. Conclusions.....	133
b. Outlook.....	136
Acknowledgements.....	141
Appendix A.....	143
Appendix B.....	161
Appendix C.....	165
Appendix D.....	167
Eklärung.....	169
Curriculum Vitae.....	171

Figures

Figure 1.1 <i>An increase in the mean and variability of temperatures.....</i>	11
Figure 1.2 <i>Typical palaeoclimate archives and their maximum temporal resolutions and ranges.....</i>	12
Figure 1.3 <i>The spatial correlation of June-July-August temperatures from meteorostation Sils Maria to European meteorostations with Pearson's r values indicated in color.....</i>	13
Figure 2.1 <i>Characteristics of the Lake Silvaplana catchment, the location of Lake Silvaplana in Switzerland, and Sils Maria monthly temperature and precipitation means from AD 1961 to AD 1990.....</i>	21
Figure 2.2 <i>Characteristics of the Lake Seeberg catchment, the position of Lake Seeberg in Switzerland, and Château-d'Oex monthly temperature and precipitation means from AD 1961 to AD 1990.....</i>	24
Figure 3.1 <i>The mooring arrangement in Lake Seeberg.....</i>	30
Figure 3.2 <i>Reflectance spectra of sediments from several years between (a.) ca. 1450 BC and AD 420 and (b.) AD 1177 and AD 1950.....</i>	36
Figure 3.3 <i>Calculation of the Trough₅₉₀₋₆₄₀.....</i>	37
Figure 4.1 <i>Site characteristics of Lake Silvaplana and the contributing watershed and the location of Lake Silvaplana in Switzerland.....</i>	54
Figure 4.2 <i>Core photo showing the lithology of Lake Silvaplana sediments.....</i>	60
Figure 4.3 <i>Age-depth model with the three series of varve counts.....</i>	60
Figure 4.4 <i>Results of (a.) chironomid assemblages, (b.) inferred mean July air temperatures (MJAT) and (c.) % organic matter (OM).....</i>	62
Figure 4.5 <i>Results of (a.) mass accumulation rates (MAR), (b.) biogenic silica (bSi) concentrations, (c.) bSi fluxes, (d.) bSi June-July-August (JJA) temperature reconstruction, (e.) chironomid JJA temperature reconstruction (f.) combined bSi&chironomid JJA temperature reconstruction with the 95% confidence interval in grey.....</i>	63
Figure 4.6 <i>(a.) the biogenic silica (bSi) & chironomid June-July-August (JJA) temperature reconstruction from AD 1177 - AD 1950 with the 95% confidence interval in grey, (b.) the bSi&chironomid JJA temperature reconstruction from ca.</i>	

570 BC - AD 120 with the 95% confidence interval in grey, (c.) the 30 year moving averages for the bSi&chironomid JJA temperature reconstruction from AD 1177 - AD 1950, (d.) the 30 year moving averages for the bSi&chironomid JJA temperature reconstruction from ca. 570 BC - AD 120, (e.) the 30 year moving detrended standard deviations for the bSi&chironomid JJA temperature reconstruction from AD 1177 - AD 1950, (f.) the 30 year moving detrended standard deviations for the bSi&chironomid JJA temperature reconstruction from ca. 570 BC - AD 120, (g.) the decadal, 30 year and centennial trends for the bSi&chironomid JJA temperature reconstruction from AD 1177 - AD 1950, (h.) the decadal, 30 year and centennial trends for the bSi&chironomid JJA temperature reconstruction from ca. 570 BC - AD 120, (i.) the decadal and 30 year trends in the 1st and 99th percentile for the bSi&chironomid JJA temperature reconstruction from AD 1177 - AD 1950, (j.) the decadal and 30 year trends in the 1st and 99th percentile for the bSi&chironomid JJA temperature reconstruction from ca. 570 BC - AD 120, (k.) the changepoints for the bSi&chironomid JJA temperature reconstruction from AD 1177 - AD 1950, (l.) the changepoints for the bSi&chironomid JJA temperature reconstruction from ca. 570 BC - AD 120, (m.) subsets D, E, and F for the bSi&chironomid JJA temperature reconstruction from AD 1177 - AD 1950, (n.) subsets C, B and A for the bSi&chironomid JJA temperature reconstruction from ca. 570 BC - AD 120..... 65

Figure 4.7 Morlet wavelets for (a.) the biogenic silica (bSi) & chironomid June-July-August (JJA) temperature reconstruction from ca. 570 BC - AD 120 and (b.) the bSi&chironomid JJA temperature reconstruction from AD 1177 - AD 1950..... 67

Figure 4.8 Mean-Variability Change (MVC) plot for the entire June-July-August (JJA) temperature reconstruction (ca. 570 BC - AD 120), for the entire combined reconstructed and instrumental temperature record (AD 1177 - AD 1950) and for subsets with a significant ($p < 0.05$) MVC relationship..... 68

Figure 5.1 The Lake Silvaplana catchment including major fluvial systems, glacier cover and mean temperature and precipitation (Sils Maria; AD 1961 - AD 1990)..... 83

Figure 5.2 A high-resolution scan of a polished sediment block (approx. 5.77 m sediment depth) with a turbidite across the center..... 87

Figure 5.3 The age-depth model including the three series of varve counts and the four elected calibrated AMS radiocarbon dates with error bars denoting two standard deviations..... 88

Figure 5.4 (a.) mass accumulation rates (MAR) overlain by $MAR_{LP}^{1/2}$, (b.) turbidite thicknesses and the centennial turbidite frequency, (c.) reconstructed June-July-August temperatures from biogenic silica (bSi) flux and chironomids (ca. 570 BC - AD 120) in the sediments of Lake Silvaplana, (d.) the Lake Le Bourget magnetic susceptibility record, (e.) the Grosser Aletschgletscher extension curve, (f.) lake level fluctuations in Central Europe. Cultures on the Alps and associated Epochs are presented alongside the aforementioned figures... 91

Figure 5.5 (a.) centennial anomalies in the square-root of low-frequency mass accumulation rates ($MAR_{LP}^{1/2}$) and centennial turbidite frequency, ranked according to $MAR_{LP}^{1/2}$ and 100 year smoothed (ca. 1450 BC - AD 420), (b.) centennial anomalies in $MAR_{LP}^{1/2}$ and centennial turbidite thickness, ranked according to $MAR_{LP}^{1/2}$ and 100 year smoothed (ca. 1450 BC - AD 420), (c.) centennial linear trends in $MAR_{LP}^{1/2}$ and centennial turbidite frequency, ranked according to $MAR_{LP}^{1/2}$ and 100 year smoothed (ca. 1450 BC - AD 420), (d.) centennial linear trends in $MAR_{LP}^{1/2}$ and centennial turbidite thickness, ranked according to $MAR_{LP}^{1/2}$ and 100 year smoothed (ca. 1450 BC - AD 420), (e.) centennial June-July-August (JJA) temperatures and centennial turbidite frequency, ranked according to JJA temperatures and 100 year smoothed (ca. 570 BC - AD 120), (f.) centennial JJA temperatures and centennial turbidite thickness, ranked according to JJA temperatures and 100 year smoothed (ca. 570 BC - AD 120)..... 94

Figure 6.1 The Lake Seeberg catchment, the location of Lake Seeberg in Switzerland and Château-d'Oex monthly temperature and precipitation means from AD 1961 to AD 1990..... 106

Figure 6.2 The thermal regime of Lake Seeberg from thermistors located 12.5 m, 8.5 m, 6.5 m, 3.5 m and 1 m below the water surface..... 107

Figure 6.3 Water chemistry measurements (Conductivity, pH, Total Cation Hardness and Total Anion Hardness) from Lake Seeberg taken in 7/2008, 10/2008, 7/2009, 8/2009 and 10/2009.....	108
Figure 6.4 Average reflectance spectrum overlain by the second derivative and calculation of the Trough ₅₉₀₋₆₂₀	111
Figure 6.5 (a.) ²¹⁰ Pb _{total} , ²²⁶ Ra, ²¹⁰ Pb _{unsupported} , ¹³⁷ Cs and Spheroidal Carbonaceous Particles (SCPs) per gram of dry sediment, (b.) two potential age-depth models for the calibration period with references for the chronological markers denoted with white diamonds.....	116
Figure 6.6 (a.) examples of reflectance spectra from ca. AD 1955 - AD 2005, (b.) examples of reflectance spectra from ca. AD 1878 to AD 1955, (c.) Trough ₅₉₀₋₆₄₀ (d.) Trough ₅₉₀₋₆₄₀ dR _{mean} , (e.) Trough ₆₅₀₋₇₀₀ , (f.) RABD _{660:670} , (g.) L*, (h.) a*, and (i.) b*.....	118
Figure 6.7 Spectrophotometer absorption results.....	119
Figure 6.8 Results of (a.) sedimentation rates, (b.) mass accumulation rates (MAR), (c.) biogenic silica concentrations (as %bSi or %bSiO ₂), (d.) biogenic silica fluxes, (e.) median grain sizes (D ₅₀), (f.) loss-on-ignition at 550°C (as %LOI ₅₅₀ or %C _{org}), (g.) loss-on-ignition at 950°C (as %LOI ₉₅₀ or %CaCO ₃), (h.) percent autochthonous sedimentation (%AUTO; estimated from %bSiO ₂ , %C _{org} and %CaCO ₃), (i.) percent allochthonous sedimentation (%ALLO; estimated from 100% - %AUTO, plus %CaCO ₃).....	120
Figure 6.9 The impact of three, five and seven years of smoothing on r _{Pearson} , p _{corr} and Degrees of Freedom (DF) for %AUTO and MJJAS temperatures from Château-d'Oex.....	122
Figure 6.10 Three year smoothed %AUTO and three year smoothed MJJAS temperatures from Château-d'Oex.....	123

Tables

<i>Table 3.1</i> Laboratory methods applied to sediments from Lake Silvaplana and the freeze core from Lake Seeberg.....	32
<i>Table 3.2</i> Published reflectance algorithms used for the sediments of Lake Silvaplana.....	36
<i>Table 3.3</i> Published reflectance algorithms used for the sediments of Lake Seeberg.....	37
<i>Table 3.4</i> Custom reflectance algorithms used for the sediments of Lake Seeberg...	37
<i>Table 4.1</i> Calibrated AMS radiocarbon dates (Intcal04.14) from Lake Silvaplana used to constrain the floating varve chronology.....	61
<i>Table 4.2</i> Statistical characteristics of June-July-August (JJA) temperatures for the individual subsets and the entire reconstruction (ca. 570 BC - AD 120; AD 1177 - AD 1950) and instrumental temperatures (AD 1950 - AD 2000).....	69
<i>Table 5.1</i> Calibrated AMS radiocarbon dates (Intcal04.14) from Lake Silvaplana and sample characteristics. Sediment depth (m) with turbidites.....	88
<i>Table 6.1</i> Published reflectance algorithms used for the sediments of Lake Seeberg.....	111
<i>Table 6.2</i> Custom reflectance algorithms used for the sediments of Lake Seeberg.....	112

Abstract

Quantitative, high-resolution and long-term climate reconstructions are needed to determine the extent of natural climate variability during the late Holocene, to compare recent climate change to ‘naturally’ warm climates (e.g. the Roman Climate Optimum) and to interpret regional climate model projections for the 21st century. This is especially relevant for Central Europe and the Alps where regional climate models project enhanced inter-annual summer temperature variability and late summer - autumn extreme precipitation with continued warming.

Here, sediments from varved Lake Silvaplana (eastern Swiss Alps) were investigated as an archive of past climate. For sediments spanning ca. 570 BC - AD 120 (i.e. the late Iron Age to Roman Period transition), annually resolved June-July-August (JJA) temperatures were reconstructed from biogenic silica (bSi) fluxes (Type II regression; Standard Major Axis calibration-in-time) and chironomid assemblages. For sediments covering ca. 1450 BC – AD 420, mass accumulation rates (MAR) reconstructed glacier length changes in the catchment and approximated warm/dry and cool/wet climates. Turbidite frequencies and thicknesses (also ca. 1450 BC - AD 420) were a proxy for late summer - autumn palaeofloods.

Reconstructed JJA temperatures from ca. 570 BC - AD 120 were compared to JJA temperatures from the last millennium (reconstructed from the same sediment core but a different study, AD 1177 - AD 1950; instrumental from Sils Maria, AD 1950 - AD 2000). Inter-annual and decadal JJA temperature variability from ca. 570 BC - AD 120 exceeded values from the last millennium. However, multi-decadal and lower frequency variability were comparable. Warm and variable JJA temperatures were noted at the Late Iron Age - Roman Period transition (ca. 50 BC to AD 100 in this region) and a cold anomaly was recognized around 470 BC (Early - Late Iron Age). The warmest JJA temperatures occurred from ca. 570 BC - 351 BC (11.2°C) and the coolest were found from ca. AD 1351 - AD 1700 (8.8°C). Turbidites indicated eighty-five palaeofloods between ca. 1450 BC and AD 420. These were more frequent and thicker during cool/wet climate phases, as inferred from MAR.

Among reconstructed JJA temperatures (ca. 570 BC - AD 120), 130 analogues for the 21st century climate in the Alps were identified (i.e. 50 year windows with a warming trend and average JJA temperature exceeding AD 1950 - AD 2000 values from Sils Maria). During most of these analogues, the frequency and thickness of turbidites was less than the ca. 1450 BC - AD 420 50 year average.

Reconstructed JJA temperatures (ca. 570 BC - AD 120) and palaeofloods (ca. 1450 BC - AD 420) were used to explore regional climate model projections which suggest greater

inter-annual to decadal JJA temperature variability and more frequent extreme summer-to-autumn precipitation events in a warmer climate. Mean-Variability Change plots of reconstructed JJA temperatures (ca. 570 BC - AD 120) and reconstructed and instrumental JJA temperatures from the last millennium, revealed a strongly heteroscedastic behavior for mean JJA temperatures exceeding $\sim 9.8^{\circ}\text{C}$ in the Engadine (for reference, average Sils Maria JJA temperature from AD 1950 - AD 2000 = 9.8°C). This is consistent with regional climate models which project an increase in inter-annual temperature variability in Central Europe and the Alps with continued climate warming. Alternatively, the late summer - autumn palaeoflood record revealed a reduction in the frequency and magnitude of extreme summer-autumn precipitation events and floods in the eastern Swiss Alps with an increase in mean temperature. This suggests that late summer - autumn floods in this region might not increase under continued global warming.

Finally, we considered whether the calibration method developed for Lake Silvaplana which produced high-resolution quantitative temperature reconstructions from annually laminated sediments, could be applied in varved Lake Seeberg (limestone bedrock, north-western Swiss Alps). A calibration period chronology was established from ^{210}Pb and validated with ^{137}Cs and spheroidal carbonaceous particles. Up-to-annual measurements were made of sedimentation rates, MAR, bSi (concentrations and fluxes), reflectance from 380-730 nm, grain sizes and loss-on-ignition (550°C and 950°C). We estimated the percent of autochthonous sediments (%AUTO) and allochthonous sediments (%ALLO) from the results of loss-on-ignition and biogenic silica concentration.

Anomalous reflectance results were attributed to high water contents in the sediments. A steep increasing (long-term) trend in %AUTO after AD 1960 was significantly correlated to May-June-July-August-September (MJJAS) temperatures at Château-d'Oex. However, the possible influence of eutrophication on %AUTO should be further investigated. After three year smoothing, an MJJAS and %AUTO regression model had a root mean squared error of prediction (RMSEP) of 0.51°C , a reduction of error of 0.62 and a positive coefficient of efficiency of 0.03 (split-period approach; AD 1902 - AD 1960 and AD 1961 - AD 2004). For the entire calibration period (AD 1902 - AD 2004; $r_{\text{Pearson}}=0.76$, $p_{\text{corr}}<0.01$), the ten-fold cross-validated RMSEP decreased to 0.45°C .

The findings of this study offer insight into natural climate variability of the past in Central Europe and the Alps and the likelihood of regional climate model projections. Furthermore, they demonstrate the potential and limitations of varved sediments as an archive of past climate.

1. Introduction

a. Problem Framing

Global warming is a major challenge of our time and under discussion by science and media. The enhanced emission of greenhouse gases (carbon dioxide, methane, nitrous oxide and halocarbons) by human activities is expected to continue, resulting in a global average warming of ca. 0.2°C/decade to the mid 21st century (IPCC, 2007).

This warming is projected to be most pronounced over the land surface with spatially heterogeneous impacts. These impacts may include the flooding and erosion of coastal regions as sea levels rise, a reduction in snow cover and deeper thawing of permafrost (which will release additional carbon dioxide) in high latitude regions, and a reduction of precipitation in the subtropics (IPCC, 2007).

Regional climate models project that Central Europe and the Alps will become a ‘hot-spot’ of enhanced inter-annual summer temperature variability as land (i.e. soil moisture)-atmosphere feedbacks intensify (Schär et al., 2004; Scherrer et al., 2006; Seneviratne et al., 2006; Parey et al., 2010). A similar relationship between the mean and variability of temperatures was presented in the IPCC third assessment report (2001) (Figure 1.1).

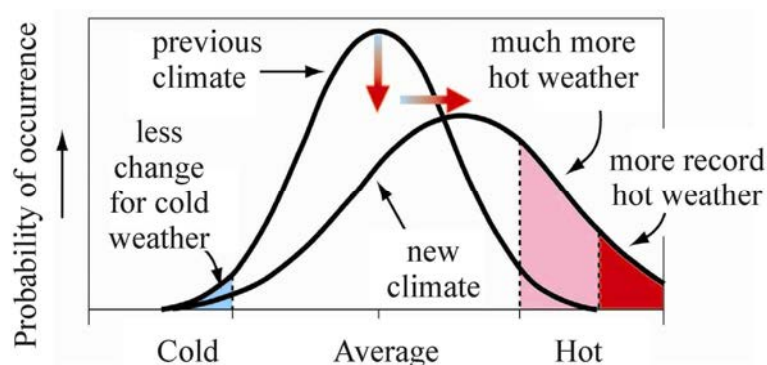


Figure 1.1 An increase in the mean and variability of temperatures (IPCC, 2001)

Other regional climate models project that Central Europe will have more extreme summer-autumn precipitation events and floods (Kundzewicz et al., 2005). This is because warmer temperatures enhance the moisture carrying capacity of the atmosphere which can cause cyclones to intensify (Kundzewicz et al., 2005). The impacts of warming will be particularly severe in Alpine regions where many ecosystems (e.g. lakes) are ultra-sensitive to changes in temperature (Thompson et al., 2005).

In response to these projections, mitigation and adaptation policies have become increasingly relevant (Stern, 2006). However, substantial uncertainties about future climate

change and natural climate variability (e.g. natural climate forcing and complex feedback mechanisms) remain. These uncertainties can be partly attributed to the lack of long-term observational (i.e. instrumental) climate data for many regions of the world. In Switzerland, home to a highly developed network of meteo-stations, temperature and precipitation data exist for only the last ca. 150 years (MeteoSchweiz, 2010).

Palaeoclimate records can provide additional information about natural climate variability preceding the instrumental period and reduce the uncertainties of regional climate model projections (Hegerl et al., 2006). For instance, the prolonged warm and dry conditions in Central Europe and the Alps during the Iron Age/Roman Period may serve as an analogue for 21st century climate. This could provide information about summer temperature variability and summer-autumn extreme precipitation during a generally warmer climate. These palaeoclimate records can be garnered through historical (documentary), tree ring, lake sediment, ice core, speleothem, palaeosol and geomorphic archives and offer different temporal resolutions and ranges (Figure 1.2).

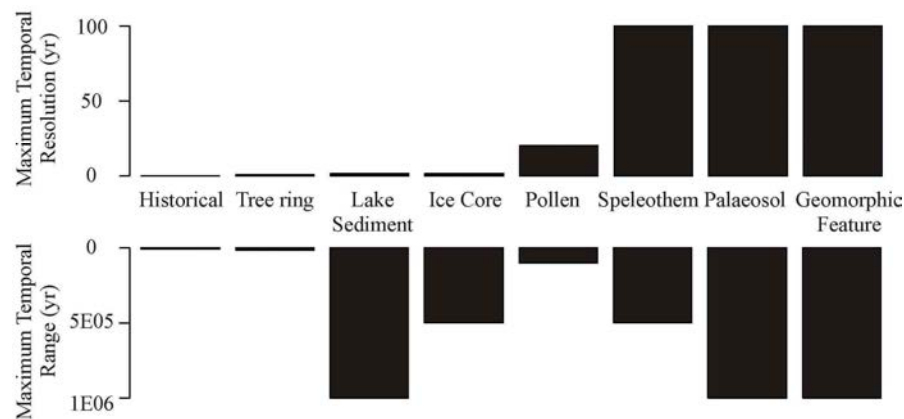


Figure 1.2 Typical palaeoclimate archives and their maximum temporal resolutions and ranges (adapted from Bradley and Eddy, 1991 and Bradley, 1999).

In particular, lake sediments can provide quantitative climate reconstructions at a high spatial resolution (e.g. relative to ice cores), a high temporal resolution (e.g. annual in varved sediments; Thomas and Briner, 2009) and a long temporal range (e.g. millennia; Zolitschka et al., 2000). Additionally, lake sediments have been shown to preserve low-frequency climate variability (Moberg et al., 2005).

The heterogeneous composition of lake sediments can provide multiple biological and non-biological climate proxies. Biological proxies (e.g. chironomids and chrysophyte stomatocysts) are typically converted into temperatures using transfer functions.

Alternatively, non-biological proxies can be transformed using a calibration-in-time (Grosjean et al., 2009; Trachsel et al., 2010a, b). Establishing a calibration-in-time depends on an accurate sedimentary chronology (and high-resolution sedimentary sampling) and a significant stable-in-time relationship between sedimentary variable (i.e. the proxy) and climate variable (e.g. temperature or precipitation) (Blass et al., 2007).

Palaeoclimate records from certain regions, such as the eastern Swiss Alps, are particularly valuable because, as evident in Figure 1.3, the June-July-August temperatures of this region are highly spatially correlated to western and central Europe and the northern Mediterranean (Trachsel et al., 2010a).

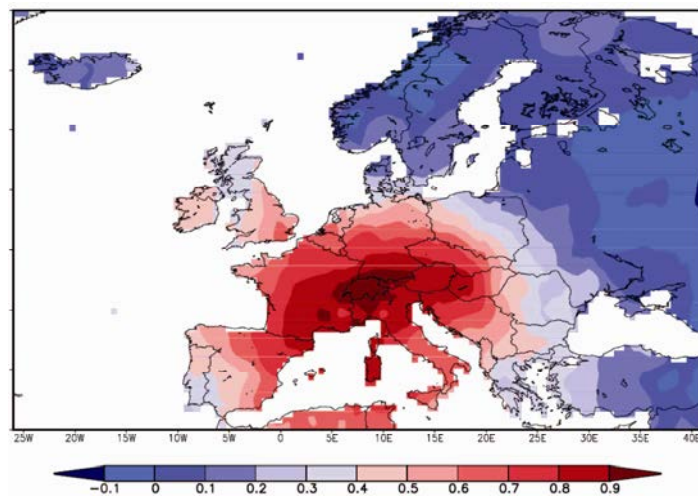


Figure 1.3 The spatial correlation of June-July-August temperatures from meteo-station Sils Maria to European meteo-stations with Pearson's r values indicated in color (Trachsel et al., 2010a).

b. Research Questions

Within the context of 1a, we have chosen to use the sediments of Lake Silvaplana (eastern Swiss Alps; ca. 570 BC - AD 120 or ca. 1450 BC - AD 420) and Lake Seeberg (north-western Swiss Alps; calibration period) to address four research questions:

1. *What was the extent of natural climate variability in Central Europe and the Alps during the late Holocene?*
2. *How did the climate from AD 1950 - AD 2000 in Central Europe and the Alps compare to 'naturally' warm climates such as the Roman Climate Optimum?*
3. *How realistic are the projections of regional climate models in the context of past climate in Central Europe and the Alps?*
4. *Can the calibration-in-time method which was effective in Lake Silvaplana be applied to other lakes?*

c. Outline

Following the introduction (Chapter 1), a brief description of the two sites (Lake Silvaplana and Lake Seeberg; Chapter 2) and a summary of the relevant data and methods (Chapter 3), we used the sediments of Lake Silvaplana to address the first three research questions in Chapters 4 and 5.

We elected to use sediments from Lake Silvaplana because they are annually laminated for the past 3300 years (Leemann and Niessen, 1994). This provides an accurate sedimentary chronology and facilitates high-resolution sampling. Additionally, the composition of sediments from Lake Silvaplana has been investigated in numerous studies and shown to be closely linked to changes in climate.

In Chapter 4, we present the results of an annually resolved June-July-August (JJA) temperature reconstruction (ca. 570 BC to AD 120) from biogenic silica (bSi) and chironomids in the sediments of Lake Silvaplana. This time period was chosen because lower resolution climate records suggest that it was warmer than the last millennium and could include analogues for the climate of the 21st century. Specifically, it includes a warmer (Early Iron Age), a cooler (Late Iron Age), and a moderate-to-warm (Roman Period) phase (Tinner et al., 2003).

This was compared to reconstructed JJA temperatures from AD 1177 to AD 1950 (the same sediment core, different study) and Sils Maria instrumental JJA temperatures from AD 1950 to AD 2000 to determine the extent of natural climate (in this case, JJA temperature) variability in Central Europe and the Alps between ca. 570 BC and AD 120 and to compare recent warming (i.e. AD 1950 - AD 2000) to the ‘naturally’ warm climate during the Roman Climate Optimum. Then, a Mean-Variability Change plot tested whether the projections of regional climate models (i.e. for an increase in summer temperature variability under continued climate warming in Central Europe and the Alps; Schär et al., 2004; Scherrer et al., 2006; Seneviratne et al., 2006; Parey et al., 2010) had precedents from ca. 570 BC to AD 120.

This chapter, under the title ‘*Quantitative inter-annual and decadal summer temperature variability ca. 570 BC - AD 120 (Iron Age - Roman Period) reconstructed from the varved sediments of Lake Silvaplana, Switzerland,*’ was accepted for publication by the Journal of Quaternary Science. Co-author Isabelle Larocque-Tobler provided all of the chironomid (and chironomid-derived July temperature) data, wrote the methods and results paragraphs regarding the chironomid (and chironomid-derived July temperature) data and produced Figure 4.4. Co-author Martin Grosjean provided the project concept, wrote the discussion paragraph on natural forcings, and assisted with the conclusion.

In Chapter 5, a complete record of palaeofloods was derived from turbidites and glacier activity (and associated climate phases) were inferred from mass accumulation rates (MAR) in sediments spanning ca. 1450 BC to AD 420. These records, in combination with the quantitative JJA temperature reconstruction of ca. 570 BC to AD 120 (Chapter 4), were used to investigate the behavior of floods (i.e. frequency and/or magnitude) under a wide range of climate variability. Specifically, we considered whether the frequency and magnitude of floods increased during warmer climates of ca. 1450 BC - AD 420. The findings of this study are important because regional climate models have projected an increase in extreme precipitation and floods in Central Europe and the Alps under continued global warming (Arnell and Liu, 2001; Kundzewicz et al., 2005). However, the relationship between recent floods (i.e. derived from instrumental and documentary records) and climate in Central Europe is inconclusive. This chapter, entitled '*Reconstructions of Late Holocene palaeofloods and glacier activity in the Upper Engadine, Switzerland (ca. 1450 BC - AD 420)*' was submitted for publication to the journal *Palaeogeography, Palaeoclimatology, Palaeoecology*. Co-authors Martin Grosjean and Lucien von Gunten provided discussion which improved the quality of this manuscript. Co-author Franz Gunther Kuglitsch provided the composite NCEP/NCAR reanalysis data and the description of the atmospheric patterns. Co-author Samuel Nussbaumer offered insight into the behavior of glaciers in the Swiss Alps.

The fourth research question, whether the calibration-in-time method that was effective in Lake Silvaplana is applicable in other varved lakes (e.g. Lake Seeberg), is considered in Chapter 6.

We investigated the sediments of Lake Seeberg because they have a different composition (i.e. organic-rich, higher carbonate content) than sediments from Lake Silvaplana. Lake Seeberg's sediments are varved for the last 2600 years (except for the upper ca. 15 cm; Hausmann et al., 2002) and their composition has been investigated by van der Knaap et al. (2000) for pollen, by Hausmann et al. (2002) for diatoms and mineralogy, and by Larocque-Tobler et al. (accepted; in which M. Stewart is a co-author) for chironomids. These studies have shown that sediments from Lake Seeberg are sensitive to changes in land-use and climate. Here, we used sediments spanning ca. AD 1878 to AD 2005 to determine: '*The potential of Lake Seeberg sediments as an archive of past climate.*' This chapter is in preparation for publication in the *Journal of Paleolimnology*. Co-author Martin Grosjean provided the project concept. Isabelle Larocque-Tobler, Franz Gunther Kuglitsch and Christian Kamenik provided discussion. Co-author Lucien von Gunten developed the ^{210}Pb models and transformed raw reflectance data into the $L^*a^*b^*$ space.

To conclude, Chapter 7 describes the main accomplishments of this thesis and suggests directions for future palaeoclimate studies.

References

- Arnell, N., Liu, C. 2001. Hydrology and water resources, In: McCarthy, J.J., Canziani, O.F., Leary, N.A., Dokken, D.J., White, K.S. (eds.), *Climate Change 2001: Impacts, Adaptation and Vulnerability. Contribution of Working Group II to the Third Assessment Report of the Intergovernmental Panel on Climate Change*. Cambridge: Cambridge University Press, Chapter 4.
- Blass, A., Grosjean, M., Troxler, A., Sturm, M. 2007. How stable are twentieth-century calibration models? A high-resolution summer temperature reconstruction for the eastern Swiss Alps back to AD 1580 derived from proglacial varved sediments. *The Holocene* 17: 51-63.
- Bradley, R.S., Eddy, J.A. 1991. Records of past global changes, In: Bradley, R.S. (ed.), *Global Changes of the Past*. Boulder: University Corporation for Atmospheric Research, 5-9.
- Bradley, R.S. (ed.) 1999. *Paleoclimatology: Reconstructing Climates of the Quaternary*, 2nd edition. International Geophysics Series vol. 64. Boston: Academic Press.
- Climate Change 2001: Synthesis report. A Contribution of Working Groups I, II, and III to the Third Assessment Report of the Intergovernmental Panel on Climate Change, Watson, R. and the Core Writing Team (eds.), Cambridge: Cambridge University Press.
- Grosjean, M., von Gunten, L., Trachsel, M., Kamenik, C. 2009. Calibration-in-time: Transforming biogeochemical lake sediment proxies into quantitative climate variables. *Pages News* 17 (3): 108-110.
- Hausmann, S., Lotter, A.F., van Leeuwen, J.F.N., Ohlendorf, C., Lemcke, G., Grönlund, E., Sturm, M. 2002. Interactions of climate and land-use documented in the varved sediments of Seebergsee in the Swiss Alps. *The Holocene* 12 (3): 279-289.
- Hegerl, G. C., Crowley, T. J., Hyde, W. T., Frame, D.J. 2006. Climate sensitivity constrained by temperature reconstructions over the past seven centuries. *Nature* 440: 1029-1032.
- Kundzewicz, Z.W., Ulbrich, U., Brücher, T., Graczyk, D., Krüger, A., Leckebusch, G.C., Menzel, L., Pińskwar, I., Radziejewski, M., Szwed, M. 2005. Summer Floods in Central Europe - Climate Change Track? *Natural Hazards* 36: 165-189.
- Larocque-Tobler, I., Quinlan, R., Stewart, M.M., Grosjean, M. (accepted) Chironomid-inferred temperature changes of the last century in Lake Seeberg (Seebergsee), Switzerland : assessment of two calibration methods. *Quaternary Science Reviews*.
- Leemann, A., Niessen, F. 1994. Holocene glacial activity and climatic variations in the Swiss Alps: reconstructing a continuous record from proglacial lake sediments. *The Holocene* 4: 259-268.
- MeteoSchweiz 2010. (http://www.meteoschweiz.admin.ch/web/de/klima/klima_heute_/jahresverlaeufo_nbcn/Segl_Maria.html)

Moberg, A., Sonechkin, D.M., Holmgren, K., Datsenko, N.M., Karlen, W. 2005. Highly variable northern hemisphere temperatures reconstructed from low- and high- resolution proxy data. *Nature* 433: 613-617.

Observations: Surface and Atmospheric Climate Change, In: Solomon, S., Qin, D., Manning, M., Chen, Z., Marquis, M.C., Averyt, K.B., Tignor, M., Miller, H.L. (eds.), *Climate Change 2007. The Physical Science Basis. Contribution of WG I to the Fourth Assessment Report of the Intergovernmental Panel on Climate Change*. Cambridge: Cambridge University Press.

Parey, S., Dacunha-Castelle, D., Huong Hoang, T.T. 2010. Mean and variance evolutions of the hot and cold temperatures in Europe. *Climate Dynamics* 34: 345-359.

Schär, C., Vidale, P.L., Lüthi, D., Frei, C., Häberli, C., Liniger, M.A., Appenzeller, C. 2004. The role of increasing temperature variability in European summer heatwaves. *Nature* 427: 332-336.

Scherrer, S.C., Appenzeller, C., Liniger, M.A. 2006. Temperature trends in Switzerland and Europe: Implications for climate normals. *International Journal of Climatology* 26: 565-580.

Seneviratne, S.I., Lüthi, D., Litschi, M., Schär, C. 2006. Land-atmosphere coupling and climate change in Europe. *Nature* 443: 205-209.

Stern, N. 2006. Short Executive Summary Stern Review Report on the Economics of Climate Change, pre-publication edition.

Thomas, E.K., Briner, J.P. 2009. Climate of the past millennium inferred from varved proglacial lake sediments on northeast Baffin Island, Arctic Canada. *Journal of Paleolimnology* 41 (1): 209-224.

Thompson, R., Kamenik, C., Schmidt, R. 2005. Ultra-sensitive Alpine lakes and climate change. *Journal of Limnology* 64: 139-152.

Tinner, W., Lotter, A.F., Ammann, B., Conedera, M., Hubschmid, P., van Leeuwen, J.F.N., Wehrli, M. 2003. Climatic change and contemporaneous land-use phases north and south of the Alps 2300 BC to 800 AD. *Quaternary Science Reviews* 22: 1447-1460.

Trachsel, M., Grosjean, M., Larocque-Tobler, I., Schwikowski, M., Blass, A., Sturm, M. 2010a. Quantitative summer temperature reconstruction derived from combined biogenic Si and chironomid record from varved sediments of Lake Silvaplana (south-eastern Swiss Alps) back to AD 1177. *Quaternary Science Reviews* 29 (19-20): 2719-2730.

Trachsel, M., Grosjean, M., Schnyder, D., Kamenik, C., Rein, B. 2010b. Scanning reflectance spectroscopy (380-730 nm): a novel method for quantitative high-resolution climate reconstructions from minerogenic lake sediments. *Journal of Paleolimnology* 44 (4): 979-994.

van der Knaap, W.O., van Leeuwen, J.F.N., Fankhauser, A., Ammann, B. 2000. Palynostratigraphy of the last centuries in Switzerland based on 23 lake and mire deposits: chronostratigraphic pollen markers, regional patterns, and local histories. *Review of Palaeobotany and Palynology* 108: 85-142.

Zolitschka, B., Brauer, A., Negendank, J. F. W., Stockhausen, H., Lang, A. 2000. Annually dated late Weichselian continental paleoclimate record from the Eifel, Germany. *Geology* 28: 783-786.

2. Study Site

a. Lake Silvaplana, Upper Engadine, Switzerland

Lake Silvaplana (1791 m a.s.l.) is situated in the Upper Engadine valley between Lake Sils and Lake Champfèr (Ohlendorf et al., 1997; Figure 2.1). The average depth of the lake is 47 m, the surface area is 2.7 km² and the volume is 127×10⁶ km³ (LIMNEX, 1994).

The catchment of Lake Silvaplana (175 km²) is underlain by the Lower Austroalpine Margna, the Upper Penninic Platta and the Lower Austroalpine Bernina. These are composed of granite, gneiss and carbonate (AdS, 2004; Blass, 2006). Additional details about the regional geology can be found in Ohlendorf (1999). Under the glaciated region of the catchment, bedrock is enriched in chlorite and mica (biotite and illite) (Ohlendorf, 1999; AdS, 2004; Trachsel et al., 2010b). In AD 1999, 5% of the catchment was glacier-covered (Kääb et al., 2002; Paul et al., 2002; Paul, 2007).

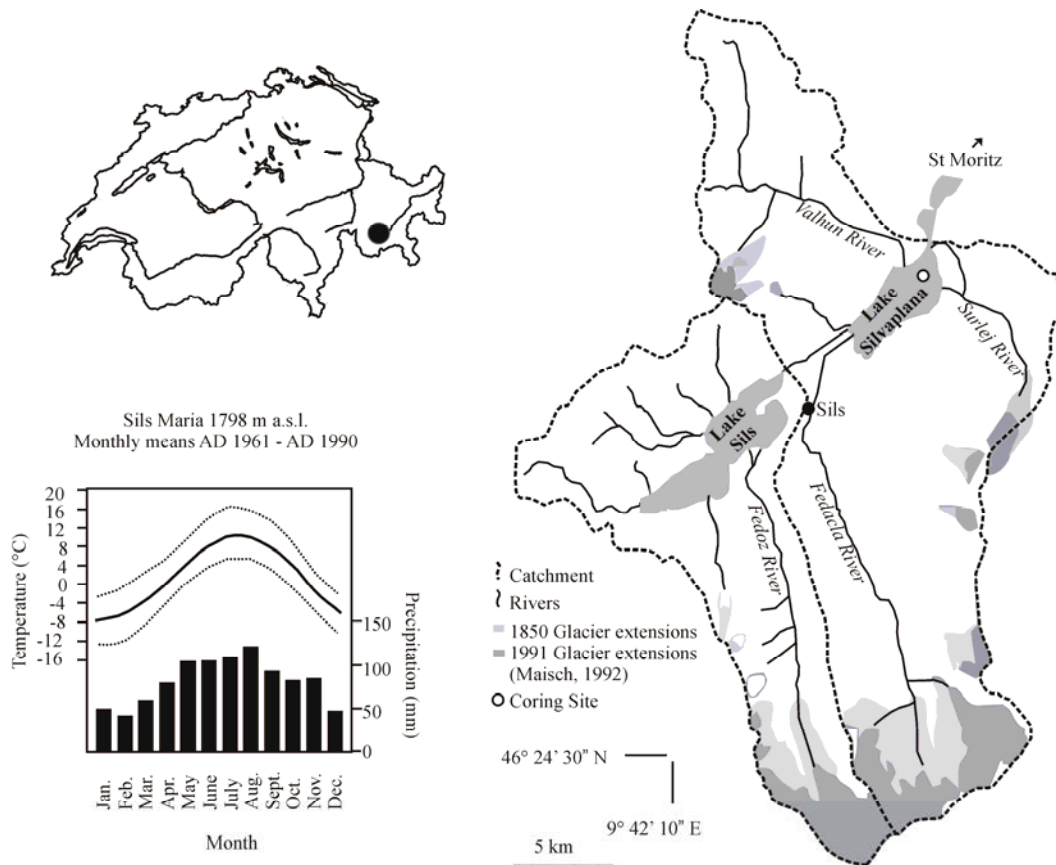


Figure 2.1 Characteristics of the Lake Silvaplana catchment (LIMNEX, 1994; Blass, 2006; right), the location of Lake Silvaplana in Switzerland (Mappad, 1996; upper left) and Sils Maria monthly temperature and precipitation means from AD 1961 to AD 1990 (MeteoSchweiz, 2010a; lower right).

The Inn, Fedacla, Valhun, and Surlej Rivers drain into Lake Silvaplana. Glacial melt-water (i.e. from the Fedacla River) and fluvial base flow are the most important purveyors of sediment (Blass et al., 2007a). Sediment trap data suggest that summer temperatures regulate sedimentation in distal regions of Lake Silvaplana at the monthly, seasonal and annual time scale (Blass et al., 2007a).

The lake mixes in May and November, has thermal stratification from June to October and has inverse thermal stratification below the ice cover from January to May (LIMNEX, 1994; Ohlendorf, 1999). According to water chemistry measurements taken over a year, the lake is oligotrophic and oxic with a pH of 7.8 (LIMNEX, 1994; Ohlendorf, 1999).

The region is dominated by a continental winter-dry climate with large fluctuations in monthly temperature and precipitation (MeteoSchweiz, 2010a). Temperature inversions enable cool and dry air to accumulate in the Engadine valley during the winter (Ohlendorf, 1999; MeteoSchweiz, 2010a). During the reference period (Sils Maria, AD 1961 - AD 1990), January temperatures averaged -7.2°C and February precipitation amounted to 42 mm (MeteoSchweiz, 2010a). Enhanced insolation and moist air from the Maloja Pass bring warm, windy and humid summers (Ohlendorf, 1999; MeteoSchweiz, 2010a). For the same reference period, July temperatures had a mean of 10.4°C and August precipitation reached 121 mm (MeteoSchweiz, 2010a).

This climate sustains diverse vegetation. Larch (*Larix decidua*) dominates the (sunny) western slopes of the Engadine valley whereas stone pine (*Pinus cembra*) is found on the (shady) eastern slopes (Ohlendorf, 1999). Spruce (*Picea abies*) is exclusively found in the region exposed to the 'Malojaschlange' belt of moist air (Ohlendorf, 1999). Current tree-line (the elevation supporting trees >5 m tall) is around 2410 m a.s.l. (Gobet et al., 2003). However, shrubs and herbs can be found above 3000 m a.s.l. (Ohlendorf, 1999). This region has been settled sporadically since the Mesolithic. During the Bronze Age, copper prospecting developed the Upper Engadine region (e.g. Oberhalbstein). By the Iron and Roman Age, active trading across Alpine passes favored settlements in the Lower Engadine (Gobet et al., 2003).

The varved sediments of Lake Silvaplana have been shown to be a viable archive of past climate. June-July-August (JJA) temperatures were reconstructed from biogenic silica (bSi) fluxes (AD 1580 - AD 1950; Blass et al., 2007b) and a combination of bSi and chironomids (AD 1177 - AD 1950; Trachsel et al., 2010a). Independently, chironomids were used to reconstruct July temperatures spanning ca. AD 1032 - AD 2001 (Larocque-Tobler et

al., 2010). Another biological proxy, chrysophyte stomatocysts, was used to reconstruct October to May temperatures from AD 1870 to AD 2004 (de Jong and Kamenik, accepted).

Mineral ratios in Lake Silvaplana sediments, shown by Ohlendorf (1999) to reflect glacial and non-glacial sediment sources, were the basis of temperature and precipitation reconstructions from AD 1580 to AD 1950 (Trachsel et al., 2008). In a novel application of scanning reflectance spectroscopy, reflectance-derived variables indicative of chlorite, illite and biotite were used to reconstruct June-July-August-September (JJAS) temperatures (AD 1177 - AD 1950; Trachsel et al., 2010b).

Finally, low-frequency mass accumulation rates (MAR) in Lake Silvaplana sediments have been shown to reflect glacier activity in the catchment (Leemann and Niessen, 1994; Ohlendorf et al., 1997; Blass, 2006; Blass et al., 2007a; Nussbaumer et al., accepted) and provide approximations of long-term changes in climate. Alternatively, turbidites spanning AD 1590 to AD 2000 have been attributed to historical floods (Blass, 2006; Caviezel, 2007).

b. Lake Seeberg, Bernese Oberland, Switzerland

Lake Seeberg (also known as Seebergsee; 1830 m a.s.l.) is located in the Bernese Oberland. The lake consists of two basins with maximum depths of 9 and 15.5 m and has a maximum volume of ca. $4.4 \times 10^4 \text{ km}^3$ (Hausmann et al., 2002) (Figure 2.2).

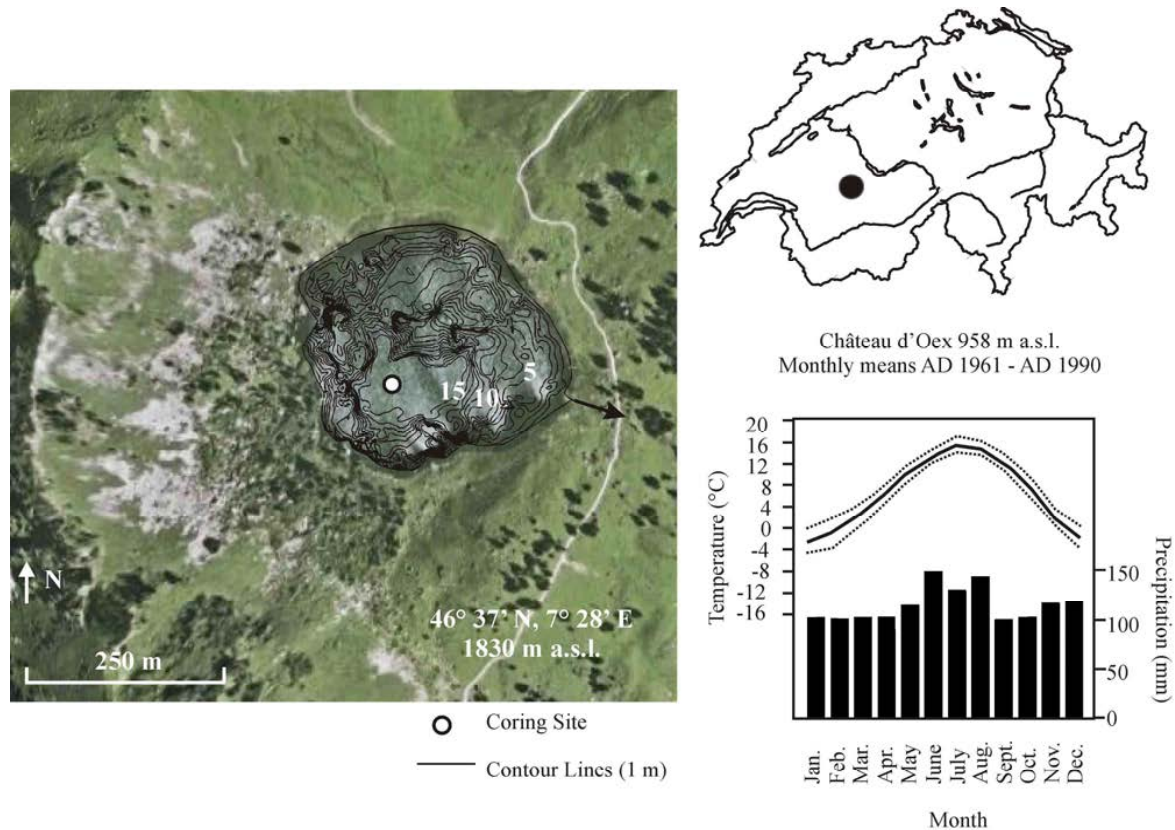


Figure 2.2 Characteristics of the Lake Seeberg catchment (modified from Hausmann et al., 2002; Google Earth, 2010; left), the position of Lake Seeberg in Switzerland (Mappad, 1996; upper right) and Château-d'Oex monthly temperature and precipitation means from AD 1961 to AD 1990 (MeteoSchweiz, 2010b; lower right).

This lake covers an area of 0.058 km^2 and drains a carbonate catchment of 0.23 km^2 . The catchment consists of 15% rocks, 26% screes and 45% bare ground (Guthruff et al., 1999). Soils along the east and south shore contain quartz, clays, plagioclase and K-feldspar, and limestone. At the southwest shore, a steep slope extends 200 m above the lake. Approximately 510 m beyond the lake, the outlet disappears in a doline (Hausmann et al., 2002).

The thermal regime of Lake Seeberg consists of mixing in June and November, thermal stratification between mid-June and late October and inverse thermal stratification under the ice cover from December to May. Diatom blooms follow each mixis (Hausmann et al., 2002). During the summer, blue and green algae are abundant and purple sulphur-

reducing bacteria are present in the deep and anoxic regions of the lake (Hausmann et al., 2002).

The climate of the Lake Seeberg region is classified as high-altitude temperate (Peel et al., 2007). At nearby meteo-station Château-d'Oex (958 m a.s.l.), average January temperatures were -2.7°C (reference period AD 1961 and AD 1990) and average July temperatures for the same reference period were 15°C (MeteoSchweiz, 2010b). Maximum precipitation occurred in June.

Present tree-line is located at the lake. Vegetation is dominated by Alpine meadows with occasional Norwegian spruce (*Picea abies*), green alder (*Alnus viridis*) and stone pine (*Pinus cembra*) (Hausmann et al., 2002). Water horsetail (*Equisetum fluviatile*) and sedges are found around the lake and the littoral zone contains slender-leaved pondtail (*Potamogeton filiformis*) (Hausmann et al., 2002).

The lake was hypertrophic between ca. AD 1350 and AD 1680 due to increased land-use in the catchment (Hausmann et al., 2002). Consistently, van der Knaap et al. (2000) found a transition from relatively high amounts of grass pollen in sediments from Lake Seeberg around AD 1500 to forest-indicating pollen by ca. AD 1650 - AD 1700. van der Knaap et al. (2000) also found evidence for increasing land-use between AD 1923 and AD 1996. In a recent study by Larocque-Tobler et al. (accepted), chironomids reconstructed the onset of anoxia after AD 1960.

References

- AdS 2004. Atlas der Schweiz - Interactive CD, version 2.0. Swiss Federal Office of Topography, Wabern.
- Blass, A. 2006. Sediments of two high-altitude Swiss lakes as high-resolution late Holocene paleoclimate archives. Inauguraldissertation der Philosophisch-naturwissenschaftlichen Fakultät der Universität Bern.
- Blass, A., Grosjean, M., Troxler, A., Sturm, M. 2007a. How stable are twentieth-century calibration models? A high-resolution summer temperature reconstruction for the eastern Swiss Alps back to AD 1580 derived from proglacial varved sediments. *The Holocene* 17: 51-63.
- Blass, A., Bigler, C., Grosjean, M., Sturm, M. 2007b. Decadal-scale autumn temperature reconstruction back to AD 1580 inferred from the varved sediments of Lake Silvaplana (southeastern Swiss Alps). *Quaternary Research* 68: 184-195.
- Caviezel, G. 2007. Hochwasser und ihre Bewältigung anhand des Beispiels Oberengadin 1750-1900. Master's thesis for the History Institute of the Universität Bern.
- de Jong, R., Kamenik, C. (accepted) Validation of a chrysophyte stomatocyst-based cold-season climate reconstruction from high-Alpine Lake Silvaplana. *Journal of Quaternary Science*.
- Gobet, E., Tinner, W., Hochuli, P.A., van Leeuwen, J.F.N., Ammann, B. 2003. Middle to Late Holocene vegetation history of the Upper Engadine (Swiss Alps): the role of man and fire. *Vegetation Historical Archaeobotany* 12: 143-163.
- Guthruf, J., Guthruf-Seilber, K., Zeh, M. 1999. Kleinseen im Kanton Bern. Bern: Paul Haupt AG.
- Hausmann, S., Lotter, A.F., van Leeuwen, J.F.N., Ohlendorf, C., Lemcke, G., Grönlund, E., Sturm, M. 2002. Interactions of climate and land-use documented in the varved sediments of Seebergsee in the Swiss Alps. *The Holocene* 12 (3): 279-289.
- Kääb, A., Paul, F., Maisch, M., Hoelzle, M., Haeberli, W. 2002. The new remote-sensing derived Swiss glacier inventory: II. First Results. *Annals of Glaciology* 34: 362-366.
- Larocque-Tobler, I., Grosjean, M., Heiri, O., Trachsel, M., Kamenik, C. 2010. Thousand years of climate change reconstructed from chironomid subfossils preserved in varved Lake Silvaplana, Engadine, Switzerland. *Quaternary Science Reviews* 29: 1940-1949.
- Larocque-Tobler, I., Quinlan, R., Stewart, M.M., Grosjean, M. (accepted) Chironomid-inferred temperature changes of the last century in Lake Seeberg (Seebergsee), Switzerland : assessment of two calibration methods. *Quaternary Science Reviews*.
- Leemann, A., Niessen, F. 1994. Holocene glacial activity and climatic variations in the Swiss Alps: reconstructing a continuous record from proglacial lake sediments. *The Holocene* 4: 259-268.

- LIMNEX 1994. Gewässerzustand und Gewässerschutzmassnahmen im Oberengadin. Bericht zuhanden des Amtes für Umweltschutz, Kanton Graubünden, 75 pp.
- Maisch, M. 1992. Die Gletscher Graubündens. Habil. Schrift Geographisches Institut Universität Zürich, Teil A und B Physische Geographie Vol. 33, 428 pp.
- Mappad Free Software 1996. <http://www.ngdc.noaa.gov/paleo/paleo.html>
- MeteoSchweiz 2010a. (http://www.meteoschweiz.admin.ch/web/de/klima/klima_heute/jahresverlaeuft_nbcn/Segl_Maria.html)
- MeteoSchweiz 2010b. (http://www.meteoschweiz.admin.ch/web/de/klima/klima_heute/Homogene_reihen.Par.0019.DownloadFile.ext.tmp/chateaudox.txt)
- Nussbaumer, S., Steinhilber, F., Trachsel, M., Breitenmoser, P., Beer, J., Blass, A., Grosjean, M., Hafner, A., Holzhauser, H., Wanner, H., Zumbühl, H. (accepted) Alpine climate during the Holocene: a comparison between records of glaciers, lake sediments and solar activity. *Journal of Quaternary Science*.
- Ohlendorf, C., Niessen F., Weissert, H. 1997. Glacial varve thickness and 127 years of instrumental climate data: A comparison. *Climatic Change* 36: 391-411.
- Ohlendorf, C. 1999. High Alpine lake sediments as chronicles for regional glacier and climate history in the Upper Engadine, southeastern Switzerland. Berichte aus der Geowissenschaft Shaker Verlag, Aachen, 203 pp.
- Paul, F. 2007. The new Swiss glacier inventory 2000 - application of remote sensing and GIS. Physische Geographie, Vol. 52. Geographisches Institut der Universität Zürich, Zürich, 210 pp.
- Paul F., Käab, A., Maisch, M., Kellenberger, T., Haeberli, W. 2002. The new remote-sensing derived Swiss glacier inventory: I. Methods. *Annals of Glaciology* 34: 355-361.
- Peel, M.C., Finlayson, B.L., McMahon, T.A. 2007. Updated world map of the Köppen-Geiger climate classification. *Hydrological Earth Systems Science* 11: 1633-1644.
- ‘Seebergsee.’ 43° 34’ 39.11” N, 7° 26’ 36.19” E. Google Earth. January 1, 1997. January 1, 2010.
- Trachsel, M., Eggenberger, U., Grosjean, M., Blass, A., Sturm, M. 2008. Mineralogy-based quantitative precipitation and temperature reconstructions from annually laminated lake sediments (Swiss Alps) since AD 1580. *Geophysical Research Letters* 35.
- Trachsel, M., Grosjean, M., Larocque-Tobler, I., Schwikowski, M., Blass, A., Sturm, M. 2010a. Quantitative summer temperature reconstruction derived from combined biogenic Si and chironomid record from varved sediments of Lake Silvaplana (south-eastern Swiss Alps) back to AD 1177. *Quaternary Science Reviews* 29 (19-20): 2719-2730.
- Trachsel, M., Grosjean, M., Schnyder, D., Kamenik, C., Rein, B. 2010b. Scanning reflectance spectroscopy (380-730 nm): a novel method for quantitative high-resolution climate reconstructions from minerogenic lake sediments. *Journal of Paleolimnology* 44 (4): 979-994.

van der Knaap, W.O., van Leeuwen, J.F.N., Fankhauser, A., Ammann, B. 2000. Palynostratigraphy of the last centuries in Switzerland based on 23 lake and mire deposits: chronostratigraphic pollen markers, regional patterns, and local histories. *Review of Palaeobotany and Palynology* 108: 85-142.

3. Data and Methods

a. Data

A long, continuous and homogenized record of instrumental meteorological data (e.g. Kuglitsch et al., 2009) is required to test the correlation between sediment composition and temperature (and/or precipitation), and to develop a calibration-in-time.

The nearest meteo-station to Lake Silvaplana meeting these requirements is Sils Maria (46° 26.3' N, 9° 45.9' E; 1798 m a.s.l.). This monthly homogenized record of temperature and precipitation spans from AD 1864 to present (MeteoSchweiz, 2010a).

The nearest meteo-station to Lake Seeberg which fulfils these requirements is Château-d'Oex (46° 28.6' N, 7° 8.5' E; 985 m a.s.l.; MeteoSchweiz, 2010b). Monthly homogenized instrumental temperature data are available from AD 1879 to present with occasional missing values for the earliest years. The total continuous temperature record covers from AD 1901 to present. The total continuous precipitation record spans from AD 1900 to present.

b. Field methods

Coring (Lake Silvaplana and Lake Seeberg)

A pair of parallel nine meter sediment UWITEC piston cores were recovered in three meter sections from the distal region of Lake Silvaplana (core names: SVP 06 2 and SVP 06 3) in the winter of 2005. The cores were delivered to the laboratory, split lengthwise and photographed (Nikon D80 digital camera 2300×1700 pixels; Appendix A). The core halves were wrapped in polyethylene film and stored at 4°C until sampling. In this thesis, only the lower six meters of the parallel cores are considered. Information about the composition of the upper three meters of sediments can be found in Blass et al. (2006, 2007a, b) and Trachsel et al. (2008, 2010a, b).

Also in the winter of 2005, a three meter Niederreiter freeze core (core name: SBS) and a ca. 1.5 meter UWITEC gravity core were extruded from the deepest basin of Lake Seeberg. All measurements (except for spectrophotometry) were conducted on the freeze core. Upon delivery to the laboratory, the freeze core was photographed (Nikon D80 digital camera 2300×1700 pixels; Appendix A), wrapped and stored at -10°C until sampling.

Thermistor data (Lake Seeberg)

Hourly thermistor data was collected from 12.5 m, 8.5 m, 6.5 m, 3.5 m and 1 m below the water surface to identify seasonal changes in lake circulation and thermal stratification. The

thermistors were attached to a mooring with a weight at the lake bed and a buoy at the water surface (Figure 3.1). The mooring was deployed to the deepest part of Lake Seeberg between July 2008 and October 2009. Thermistor data was downloaded using Minilog software in October 2008, July 2009, August 2009 and October 2009.

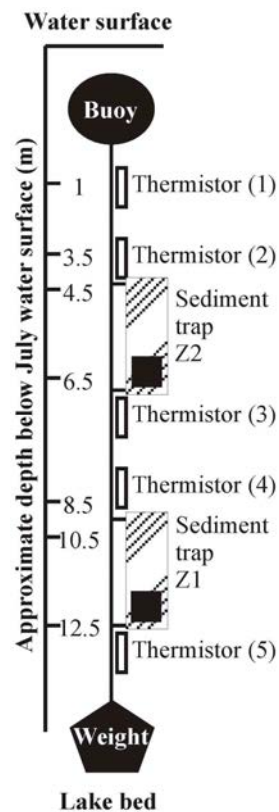


Figure 3.1 The mooring arrangement in Lake Seeberg

Sediment Traps (Lake Seeberg)

In addition to holding thermistors, the mooring had two cylindrical sediment traps (Z1 depth: 12.5 m - 10.5 m; Z2 depth: 6.5 m - 4.5 m). The sediment traps were periodically emptied and cleaned (October 2008, July 2009, August 2009 and October 2009), and their content was used to determine seasonal changes in biogenic silica (bSi) concentration, grain size and loss-on-ignition.

Water samples (Lake Seeberg)

Water samples and profiles provided a record of water chemistry and chemical stratification. Water samples were taken with a UWITEC instrument (13 m, 11 m, 10 m, 9 m, 7 m, 6 m, 5 m, 3 m, 2 m, 1 m below the water surface) near the mooring site (July 2008, October 2008,

July 2009, August 2009 and October 2009) and were tested in the laboratory for total cation hardness, total anion hardness and pH. Meanwhile, a Hydrolab M5 was used to obtain conductivity profiles.

Soil Samples (Lake Seeberg)

Soil samples were taken from the East and South shores of Lake Seeberg to identify potential sources of allochthonous sediments. Soil samples were tested for mineralogy (XRD), grain size and loss-on-ignition.

c. Laboratory methods

Core Inventory Silvaplana (SVP)															
Core	Section	Length (cm)	Wet Photos	Frozen Photos	Resin-Emb.			Thin Sections	Dating	Ref. Spec.	Sampled	bSi	Grain Size	LOI	Chirons (L. Laroque-Tobler)
					Blocks	Photos	Blocks								
SVP 06 2	IV	94	✓					Varve Cts	✓						
SVP 06 2	V	100	✓	✓					✓						
SVP 06 2	VI	93							✓						
SVP 06 2	VII	96	✓	✓		✓		Varve Cts	✓						
SVP 06 2	VIII - N/A														
SVP 06 2	IX	92	✓	✓					✓						
SVP 06 3	IV	96	✓				✓	Varve Cts							
SVP 06 3	V	98	✓	✓		✓		Varve Cts / ¹⁴ C	✓	✓	✓	✓	✓	✓	
SVP 06 3	VI	89	✓	✓		✓		Varve Cts / ¹⁴ C	✓	✓	✓	✓	✓	✓	
SVP 06 3	VII	96	✓	✓					✓						
SVP 06 3	VIII	99	✓	✓		✓		Varve Cts	✓						
SVP 06 3	IX	69	✓	✓		✓			✓						

Core Inventory Seebensee (SBS)															
Core	Section	Length (cm)	Wet Photos	Frozen Photos	Resin-Emb.			Thin Sections	Dating	Ref. Spec.	Sampled	bSi	Grain Size	LOI	Chirons (L. Laroque-Tobler)
					Blocks	Photos	Blocks								
SBS	1	55		✓			✓	²¹⁰ Pb/ ¹³⁷ Cs	✓	✓	✓	✓	✓	✓	
SBS	2	58		✓			✓		✓						
SBS	3	60		✓					✓						
SBS	4	62		✓					✓						
SBS	5	60		✓			✓		✓						

Table 3.1 Laboratory methods applied to sediments from Lake Silvaplana and the freeze core from Lake Seeborg

Chronology (Lake Silvaplana)

The chronology for the lower six meters of the Lake Silvaplana core was based on varve counts anchored with calibrated radiocarbon dates. The varve counts were floating (i.e. not continuous with the varve chronology to AD 1177 developed by Trachsel et al., 2010a) because of a turbidite at 275-300 cm depth (i.e. between AD 1177 and the section studied here). This turbidite had an erosive base which implies that varves may have been lost.

Varves were counted on resin-embedded blocks made according to the protocols of Lamoureux (1994) and Lotter and Lemcke (1999). Overlapping slabs (20×2 cm) of wet sediment were extracted from the core, flash frozen one-by-one with liquid nitrogen and freeze-dried overnight. Dried sediment slabs were arranged in aluminum trays and an epoxy resin (NSA, ERL, DER and DMAE) was decanted over the slabs. The resin was cured at 70°C overnight and the slabs were sent to GEOPREP (University of Basel, Switzerland) to be cut into blocks and polished.

The polished blocks were scanned at 1200 dpi. These scans were opened in ImageJ software (Abramoff et al., 2004) and the start of each varve was identified according to the Lake Silvaplana varve descriptions (i.e. a basal silt layer capped by a clay lamination) of Leemann and Niessen (1994). Varve counts were repeated three times and verified under a petrographic microscope. Marker horizons (i.e. turbidites) were used to combine varve counts from consecutive blocks and the three floating varve chronologies were fit through a turbidite at ~440 cm depth.

The floating varve chronology was constrained using calibrated accelerator mass spectrometry (AMS) radiocarbon dates. Radiocarbon dating is based on cosmic ray fluxes at the upper atmosphere catalyzing the collision of free neutrons with ^{14}N . This causes the displacement of protons from ^{14}N and formation of ^{14}C (Björck and Wohlfarth, 2001). ^{14}C is oxidized into $^{14}\text{CO}_2$ and circulates the atmosphere until it is up taken by plants and animals (i.e. via photosynthesis and the food-chain) and by oceans. The carbon which is integrated into the tissue of plants and animals is in equilibrium with its surroundings (e.g. the atmosphere, the ocean) until the organism dies and the uptake of CO_2 ceases (Björck and Wohlfarth, 2001). Radiocarbon measurements on this fossil organic matter are based on the decay of ^{14}C which has a half-life of 5568 years (Mook, 1986; Björck and Wohlfarth, 2001).

Terrestrial macrofossils (i.e. wood fragments and needles) were used for radiocarbon dating to avoid reservoir effects. This is because radiocarbon dates from (aquatic) organic carbon in bulk sediments in the upper three meters of sediments were anomalously old due to reservoir effects (M. Trachsel, unpublished data; Chapter 5; Stewart et al., submitted).

Macrofossils were only located in coarse-grained, organic-rich turbidite deposits which may have been reworked material. The type of terrestrial specimens was identified with assistance from P. Kaltenrieder. Specimens were cleaned with distilled water in a fine sieve, dried overnight at 105°C and sent to Poznań Radiocarbon Laboratory (T. Goslar; Poland). The radiocarbon dates were calibrated in Intcal04.14 (Reimer et al., 2004). Two of the six radiocarbon dates appeared to be anomalously old and were interpreted as being reworked material. The varve chronology which was most consistent with the four (acceptable) radiocarbon dates was elected to be the final chronology. Therefore, all ages presented here are calculated from an annually resolved but floating varve chronology anchored by calibrated radiocarbon dates (BC and AD).

Chronology (Lake Seeberg)

In Lake Seeberg, varves were counted on resin-embedded blocks (created using the same method as above) and thin sections (resin-embedded blocks thinned to 30 µm at GEOPREP, University of Basel, Switzerland) from the upper 25 cm of Lake Seeberg sediments (approximate calibration period). Consistent with the findings of Hausmann et al. (2002), varves could only be found lower (below ca. 15 cm) in the sediment core. Therefore, sediments from the calibration period were dated using radionuclides and spheroidal carbonaceous particles (SCPs).

Twenty-five consecutive sediment samples (0-25 cm; 6 cm³ each) were sent to EAWAG (Dubendorf) for ¹³⁷Cs (at 662 keV) and ²¹⁰Pb (at 46.5 keV) measurements. Peaks of ¹³⁷Cs signify fallout from thermo-nuclear tests (starting at ca. 1954 and peaking at ca. 1963) and the Chernobyl accident in AD 1986 (Appleby, 1997 and 2002). ²¹⁰Pb results from the decay of ²³⁸U into ²²⁶Ra and then ²²²Rn. ²²⁶Ra and ²¹⁰Pb_{total} are in disequilibrium because during the decay of ²²⁶Ra in soil, some of the gaseous isotope ²²²Rn escapes into the atmosphere via diffusion. The ²¹⁰Pb which forms (in situ) from the decay of ²²⁶Ra in soil is in equilibrium with ²²⁶Ra (= ²¹⁰Pb_{supported}). The ²¹⁰Pb which forms in the atmosphere is returned to the land, lakes and oceans through wet or dry deposition from the atmosphere (= ²¹⁰Pb_{unsupported}) (Appleby, 1997 and 2002). ²¹⁰Pb_{unsupported} reaches lake sediments through scavenging of ²¹⁰Pb_{unsupported} which is deposited on the lake, and from in wash from the catchment (Appleby, 1997 and 2002). To determine the amount of ²¹⁰Pb_{unsupported}, one must subtract ²²⁶Ra from ²¹⁰Pb_{total} at each level (Appleby, 1997 and 2002).

SCPs were counted on thirty-two consecutive sediment samples (0-29.5 cm) prepared according to the method used in Grob (2008). This involved digestion of organic matter with H₂O₂ (32%) and removal of calcite and iron oxides with HCl (10%).

SCPs indicate fossil fuel combustion which peaked in the Swiss Alps around AD 1977 +/-4 (Lotter et al., 2002). SCPs can be identified under magnification by their distinct shape (spheroidal; 3 dimensional), color (black), porosity, size (consistent within each lake, typically 5-10 µm) and fragility (Rose, 2001; Grob, 2008). Counts were converted to SCPs per gram of dried sediment.

The Constant Rate of Supply (CRS) model and the Sediment Isotope Tomography (SIT) model (both unconstrained and constrained with the peak of ¹³⁷Cs at ca. AD 1963) provided two possible age-depth models (Liu et al., 1991; Appleby, 2002; Carroll and Lerch, 2003). The model which was most consistent with independent stratigraphic markers such as the start of SCPs at ca. AD 1880 (Rose, 2001), the start of ¹³⁷Cs at ca. AD 1954, the AD 1963 peak of ¹³⁷Cs (Hausmann et al., 2002) and the AD 1977 +/- 4 SCP peak (Lotter et al., 2002), was elected the calibration period chronology. The calibration period chronology was consistently several centimeters offset from the Hausmann et al. (2002) age-depth model.

Scanning reflectance spectroscopy (Lake Silvaplana and Lake Seeberg) and spectrophotometry (Lake Seeberg)

Scanning reflectance spectroscopy was measured on a half of the sediment cores from Lake Silvaplana (unfrozen). For Lake Seeberg, a slab of frozen sediment (300×3×2 cm) was removed from the core and left to thaw. Reflectance was measured with a hand-held Gretag Macbeth Spectrolino (sensor aperture: 2.5 mm, spectral range: 380-730 nm, spectral resolution: 3 nm integrated to intervals of 10 nm bands, measurements at each 2 mm) (Trachsel et al., 2010b). This rapid, non-destructive and inexpensive method provides raw reflectance data which indicate changes in the composition (e.g. fossil pigments) of the sediments (Trachsel et al., 2010b).

A white ceramic reference piece composed of Barium Sulfate (BCA) was covered in polyethylene film and used to calibrate the Spectrolino (Rein and Sirocko, 2002). Then, the sediment core surface was scraped clean of oxidized sediment in the direction of laminations using a Swiss Army knife. This was challenging for the Lake Seeberg core due to the high water content of the sediments. The sediment surface was covered with a single layer of polyethylene film to prevent further oxidation and to keep the Spectrolino sensor clean (Rein

and Sirocko, 2002). A soft-bristle paint brush was used to gently expel any air bubbles caught between the sediment surface and the polyethylene film.

The raw reflectance data were divided by the reflectance of the BCA covered in polyethylene film (Rein and Sirocko, 2002). Then, the data were assigned years based on the age-depth model for the sediments and the associated depth of the Spectrolino data. For Lake Seeberg, this was only possible for the upper ca. 0-25 cm (i.e. the calibration period).

The average reflectance spectrum from Lake Silvaplana sediments dating ca. 1450 BC to AD 420 had the same reflectance minima (i.e. 480 nm and 690 nm) and maximum (580 nm) as the spectrum from AD 1177 to AD 1950 (Trachsel et al., 2010b; Figures 3.2a, b). According to Trachsel et al. (2010b), these reflectance features indicate changes in the mineral composition (i.e. biotite, illite and chlorite) of Lake Silvaplana sediments. High-frequency changes in the reflectance features (i.e. mineral composition) are related to glacial melt (i.e. summer temperatures) and runoff (Trachsel et al., 2010b). Low-frequency changes are influenced by glacier length variations in the catchment (Trachsel et al., 2010b). Therefore, the raw reflectance data from ca. 1450 BC to AD 420 were transformed using the published algorithms of Trachsel et al. (2010b; Table 3.2). These results can be found in Appendix C.

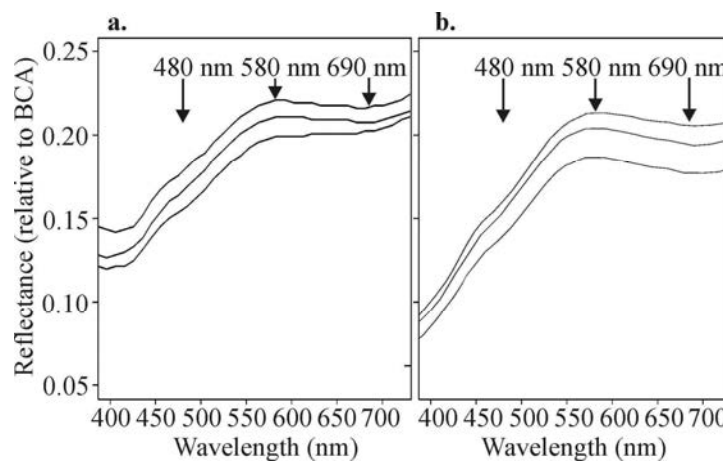


Figure 3.2 Reflectance spectra of sediments from several years between (a.) ca. 1450 BC and AD 420 and (b.) AD 1177 and AD 1950 (redrawn from Trachsel et al., 2010b)

Algorithm		
$R_{590}dR_{690}$	R_{590}/R_{690}	Biotite, Illite, Chlorite (USGS, 2007)
$R_{570}dR_{630}$	R_{570}/R_{630}	Biotite, Illite, Chlorite (Rein, 2003)
Min_{690}	$[(4 * R_{590} + 10 * R_{730}) / 14] R_{690}$	Chlorite (USGS, 2007)
$Trough_{590-730}$	$141 * R_{730} + [141 * (R_{590} - R_{730}) / 2] - (6 * R_{590} + 5 * R_{730}) - 10 * \sum_{600-720} R$	Chlorite (USGS, 2007)

Table 3.2 Published reflectance algorithms used for the sediments of Lake Silvaplana (Trachsel et al., 2010b)

Alternatively, this was the first time that scanning reflectance spectroscopy was applied to a sediment core from Lake Seeberg. To highlight changes in the slope of the spectrum, we overlaid the average reflectance spectrum with the 2nd derivative (Stephens et al., 2003). This revealed a trough spanning R₅₉₀ to R₆₄₀ and a trough from R₆₄₀ to R₇₂₀ (Table 3.3; Figure 3.3).

Two published algorithms were used to describe the trough from R₆₄₀ to R₇₂₀ and minima around 665 nm (Relative Absorption Band Depth, RABD).

Algorithm		
Trough ₆₅₀₋₇₀₀	$\frac{[(R_{650} * 51) + ((R_{700} - R_{650}) * 51) / 2] - \sum R_{650-700}}{R_{mean}}$	(Wolfé et al., 2006)
RABD _{660;670} dR _{mean}	$\frac{(((6 * R_{590} + 7 * R_{730}) / 13) R_{min(660;670)})}{R_{mean}}$	(Rein and Sirocko, 2002)

Table 3.3 Published reflectance algorithms used for the sediments of Lake Seeberg

Because no published algorithms describe the trough from R₅₉₀ to R₆₄₀, a custom algorithm was developed (Table 3.4). In an effort to account for changes in the water content of the sediments, the algorithm was divided by the average reflectance (R_{mean}; Balsam et al., 1998).

Algorithm	
Trough ₅₉₀₋₆₄₀	$[(R_{590} * 51) + ((R_{640} - R_{590}) * 51) / 2] - \sum R_{590-640}$
Trough ₅₉₀₋₆₄₀ dR _{mean}	$\frac{[(R_{590} * 51) + ((R_{640} - R_{590}) * 51) / 2] - \sum R_{590-640}}{R_{mean}}$

Table 3.4 Custom reflectance algorithms used for the sediments of Lake Seeberg

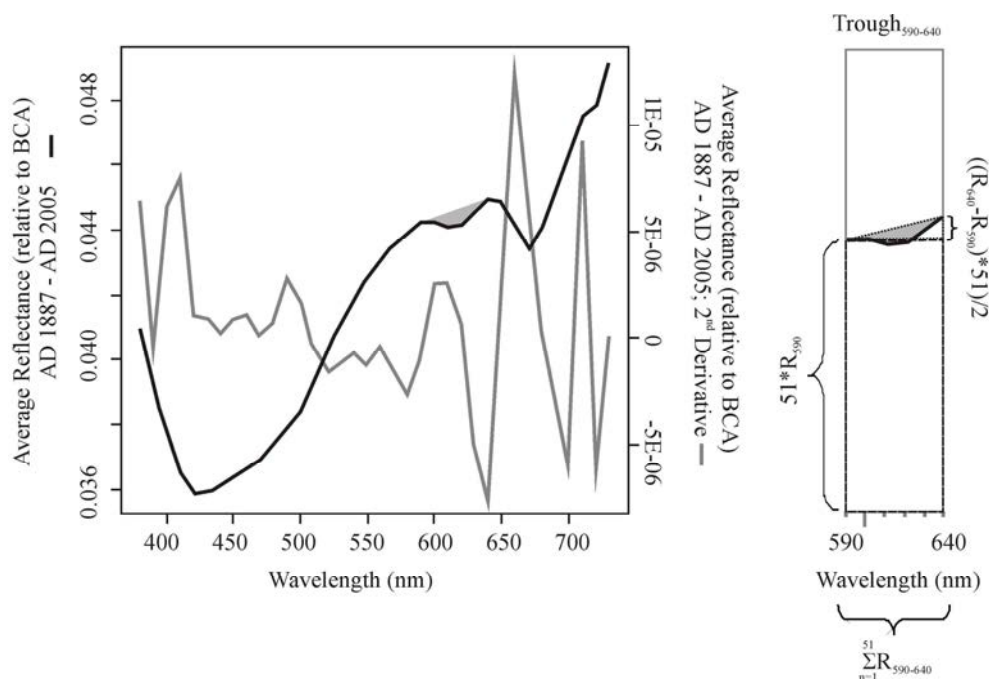


Figure 3.3 Calculation of the Trough₅₉₀₋₆₄₀

The two reflectance troughs in the Lake Seeberg sediments were further explored with spectrophotometry. Twelve ca. 1 cm³ sub-samples were taken from the Lake Seeberg gravity core (0-15 cm depth with sub-samples at 2, 4 and 14 cm excluded) and freeze-dried. For each sub-sample, 200 mg of sediment was placed in a 22 ml tube and extracted with acetone (Routh et al., 2009) in a 200 Dionex Accelerated Solvent Extractor (ASE). The sediment residue was flushed with 60% of the initial solvent volume (ca. 14 ml). The extracts were poured into 50 ml volumetric flasks to achieve equal concentrations.

Absorption spectra (330 nm to 800 nm; 1 nm resolution) were made on a Shimadzu Spectrophotometer UV-1800. The Spectrophotometer absorption results were corrected for acetone and glass flask effects with a reference. The corrected results (as percentages) were opened with UVProbe software. This revealed an absorption pattern consistent with the average reflectance spectrum of the Lake Seeberg freeze core. Specifically, there was an absorption maximum at 610 nm and at 665 nm.

According to Louda et al. (2002), reflectance minima (or absorption maxima) around 610 nm and 665 nm indicate chlorophyll degradation products. Thus, changes in these reflectance minima (or absorption maxima) could reflect variable organic contents.

Finally, the reflectance spectra of Lake Seeberg sediments was transformed into the L*a*b* color space according to Nederbragt et al. (2004) and Lindbloom (2011). The color of sediments can indicate changes in composition (e.g. mineralogy, grain size, pore water content or chemistry, organic content) related to the provenance or depositional environment (Andrews and Freeman, 1996). The raw reflectance spectra were converted into an XYZ coordinate system where Y indicates luminance (i.e. greyscale), and X and Z represent colors. The XYZ coordinate system was further transformed into L*a*b* which is closer to the human perception of color (Nederbragt et al., 2004).

L* values range from 0 (black) to 100 (white), indicating the lightness of sediments. In a study of marine sediments off the coast of eastern Canada, peaks in L* (i.e. lighter sediments) were correlated to higher amounts of detrital carbonate. Lower values of L* (i.e. darker sediments) were found for marine sediments with higher water contents (Andrews and Freeman, 1996).

Variations in a* and b* are typically more subtle than L* in sediments (Nederbragt and Thurow, 2004). a* reflects changes from green (negative values) to red (positive values). In marine sediments taken off of the coast of California, a* was positively correlated to total organic carbon (Nederbragt and Thurow, 2004). b* indicates changes from blue (negative) to yellow (positive). In sediments from Saanich Inlet (British Columbia, Canada), positive

values of b^* (more yellow) were attributed to diatom-rich laminations whereas negative values of b^* (more blue) were ascribed to detrital material (Debret et al., 2006).

Although $L^*a^*b^*$ has typically been applied to studies of marine (rather than lake) sediments, we assume that $L^*a^*b^*$ is equally sensitive to changes in the composition of lake sediments.

Mass Accumulation Rate (Lake Silvaplana and Lake Seeberg)

Mass accumulation rates (MAR) were calculated from varve thickness, dry sediment density and porosity using a modified version of the Berner (1971) and Niessen et al. (1992) method (i.e. organic carbon was not included in the calculation). In the sediments of Lake Silvaplana, high frequency peaks in MAR have been associated with glacio-nival melt (associated with summer temperatures) and precipitation (Blass et al., 2007a). Low-frequency shifts in MAR have been attributed to glacier length changes in the catchment (e.g. Leemann and Niessen, 1994; Ohlendorf et al., 1997; Blass et al., 2007a; Nussbaumer et al., accepted). In sediments from Lake Seeberg, MAR was not measured in previous studies. However, we suggest that it should be related to primary productivity (associated with summer temperatures and nutrient availability) and detrital inputs (related to precipitation).

Lake Silvaplana varve thicknesses were determined from the high-resolution scans of resin-embedded blocks. These scans were opened in ImageJ software and the start of each varve was digitally marked (Abramoff et al., 2004). An algorithm in ImageJ calculated the distance between each consecutive varve (i.e. varve thickness). Turbidites were identified as exceeding 2σ of the average varve thickness and/or having a coarser texture and different coloring than neighboring varves. These turbidites were excluded from MAR calculations. Alternatively, Lake Seeberg sedimentation rates were approximated through linear interpolation between age-depth model points. For both Lake Silvaplana and Lake Seeberg, the dry density of sediment was estimated at 2.65 g/cm^3 (=quartz) whereas porosity was found from the water content, dry sediment density and pore water density (ca. 1 g/cm^3 ; Blass et al., 2007a).

Sub-sampling (Lake Silvaplana and Lake Seeberg)

The sediments of Lake Silvaplana (dating ca. 570 BC - AD 120) and of Lake Seeberg (dating ca. AD 1878 - AD 2005; ca. 0-25 cm) were sub-sampled at up-to-annual resolution. Half of the sediment core from Lake Silvaplana was flash-frozen using liquid nitrogen. On both the frozen sediment core half from Lake Silvaplana and half of the freeze core from Lake

Seeberg, thumb-tacks were inserted at approximately 10 year intervals according to the respective age-depth models. The frozen sediments were placed in a core holder lined with blocks of dry ice to prevent thawing of the sediment core during sub-sampling. A knife or a band saw was used to scrape approximately annual layers from the sediment cores (Blass, 2006).

Biogenic silica (Lake Silvaplana and Lake Seeberg)

Biogenic silica concentrations (%bSi) were measured on all of the Lake Silvaplana sub-samples (dating ca. 570 BC - AD 120), the Lake Seeberg sub-samples (dating ca. AD 1878 - AD 2005) and the Lake Seeberg sediment trap material according to the protocol of Ohlendorf and Sturm (2008). Biogenic silica indicates diatom productivity which can be influenced by climate and land-use (e.g. Blass et al., 2007b).

Approximately 150 mg of sediment per sub-sample was treated with 5 ml H₂O₂ (30%) to remove organic matter. After a week, the sediments were washed with distilled water and freeze-dried. The loss in weight following treatment with H₂O₂ (30%) was used as an estimate of organic content. The sediments were combined with 10 ml of 1 M NaOH matrix in tubes and placed in an ultrasonic bath. The tubes were capped, shook with a mini-shaker set to >2500/minute, and transferred to an oven (90°C) for one hour. These last three steps were repeated three times. The tubes were centrifuged to separate the supernatant from the sediment. 700 µl of the supernatant was combined with 70 µl 65% HNO₃ and Milli-Q-Water up to 14 ml. Measurements of %bSi were made on an inductively coupled plasma optical emission spectrometer (ICP-OES; Paul Scherrer Institute, Switzerland) and results were corrected for lithogenic silica (Al:Si ratio 2:1) (Ohlendorf and Sturm, 2008). %bSi was converted to bSi flux by multiplying by MAR. For Lake Seeberg, %bSi was also presented as %bSiO₂. This entailed multiplying the %bSi values by the sum of the relative atomic mass of Si (28) and O₂ (2*16).

Grain size (Lake Silvaplana and Lake Seeberg)

Laser particle size measurements were made on all of the Lake Silvaplana sub-samples dating ca. 570 BC - AD 120 (results can be found in Appendix C), the Lake Seeberg sub-samples dating ca. AD 1878 - AD 2005 and the Lake Seeberg sediment trap material following removal of organic matter with H₂O₂ (30%) and bSi with NaOH (1 M). These measurements were conducted on a Malvern Mastersizer Hydro 200S with three repetitions of each sample.

This method is based on the principle that there is an inverse relationship between angle a grain diffracts a beam of monochromatic light and the size of the grain (Singer et al., 1988). Changes in the size (e.g. median grain size) and distribution (e.g. sorting) of sediments can indicate changes in the catchment (e.g. glacier cover), climate (e.g. precipitation, temperature) and provenance of sediments. For instance, Blass et al. (2007a) found that in the low frequency, the sorting and grain sizes of sediments deposited in Lake Silvaplana was dependent on glacier extent and activity. In a separate study, Blass et al. (2008) attributed larger median grain sizes from AD 1880 - AD 2004 to precipitation events which followed explosive volcanic eruptions.

Chironomid head capsules (Lake Silvaplana and Lake Seeberg)

Chironomid head capsules were counted by I. Larocque-Tobler for Lake Silvaplana at annual resolution for four time windows (approximately 570 BC - 500 BC, 480 BC - 440 BC, 390 BC - 340 BC, and 30 BC - 0) and for Lake Seeberg at one centimeter resolution for the 20th century (Larocque-Tobler, accepted).

Loss-on-ignition (Lake Seeberg)

Sequential loss-on-ignition (LOI) provides an estimate of the organic carbon and calcium carbonate content of sediments. This method was applied to Lake Seeberg sediments dating ca. AD 1878 - AD 2005, sediment trap material and soil samples using a modified sequential loss-on-ignition method (LOI; Dean, 1974; Heiri et al., 2001).

Sediments were kept in an oven overnight at 105°C to remove excess moisture, homogenized with a mortar and pestle and transferred to pre-weighed crucibles. The dried sediments were weighed (=DW₁₀₅) before being placed in a furnace at 550°C. After an hour, the sediments were removed from the furnace and deposited in a desiccator containing blue silica crystals to prevent the sediments from up taking air moisture during cooling. When the sediments had cooled, they were reweighed (=DW₅₅₀). The sediments were returned to the furnace at 950°C. After an hour, the sediments were removed from the furnace and placed back in the desiccator containing blue silica crystals. When the sediments had cooled, they were reweighed (=DW₉₅₀).

The percent loss of weight between DW₁₀₅ and DW₅₅₀, %LOI₅₅₀, is composed of CH₂O. This was multiplied by the relative atomic mass of CH₂O (30) divided by the relative atomic mass of C (12) to find the percent of organic carbon (%C_{org}). The percent loss of weight between DW₅₅₀ and DW₉₅₀ consists of carbon dioxide (CO₂). DW₉₅₀ was multiplied by

the relative atomic mass of CaCO_3 (100.088) divided by the relative atomic mass of CO_2 (44.009) to find the percent of calcium carbonate ($\%\text{CaCO}_3$) (modified from Heiri et al., 2001).

Percent Autochthonous Sediments and Percent Allochthonous plus carbonate

The percent of autochthonous sediment ($\%\text{AUTO}$) was estimated from the sum of $\%\text{bSiO}_2$, $\%\text{C}_{\text{org}}$ and $\%\text{CaCO}_3$. The percent of autochthonous sediment was subtracted from 100% and combined with $\%\text{CaCO}_3$ as an estimate of detritus ($\%\text{ALLO}$) from the catchment. Because the origins of $\%\text{CaCO}_3$ are unknown (i.e. could be marl or detritus), it was included in both variables ($\%\text{AUTO}$ and $\%\text{ALLO}$). Consequently, both variables should be interpreted prudently.

X-Ray Diffraction (Lake Seeberg)

The mineralogy of soil samples from the eastern and southern shores of Lake Seeberg was determined from smear slides. This indicated the source area of material in the sediment core and sediment trap.

The soil was homogenized using an agate mortar and organic matter was removed with H_2O_2 (30%). The organic-free soil was flushed with distilled water, treated with several drops of ethylene glycol and transferred to slides using a pipette. Once the slides were dried, they were placed in a Philips PW 3710 and scans were made from 4° to 40° 2θ (0.02° interval).

d. Statistical Methods

Reconstruction Methods (Lake Silvaplana)

B_{Si} fluxes in the sediments of Lake Silvaplana (ca. 570 BC - AD 120) were converted to JJA temperatures with the Type II Standard Major Axis regression calibration-in-time from Trachsel et al. (2010a) (JJA Sils Maria: AD 1864 - AD 1949, $r=0.67$, $p_{\text{corr}}=0.03$). The JJA temperatures reconstructed from b_{Si} were combined with chironomid-inferred July temperatures from four time windows (approximately 570 BC - 500 BC, 480 BC - 440 BC, 390 BC - 340 BC, and 30 BC - 0; I. Larocque-Tobler). This involved scaling the chironomid temperatures from July to JJA by the average 20th century difference (Sils Maria=0.8°C; Trachsel et al., 2010a). Then, the difference between the average b_{Si} temperature and the average chironomid temperature was calculated for the overlapping time windows. The difference between the overlapping time windows was estimated through linear interpolation.

This provided an annual estimate of the difference between the bSi- and chironomid-inferred temperatures. These values were added to the annually resolved bSi temperatures. The final root mean squared error (RMSE) included the error from the chironomid transfer function, from the bSi reconstruction (ten-fold cross-validation), and combination of the two reconstructions (leave-one-out method).

Calibration Methods (Lake Seeberg)

Resulting data (sedimentation rates, MAR, bSi concentrations or bSiO₂, bSi fluxes, %LOI₅₅₀ or %C_{org}, %LOI₉₅₀ or %CaCO₃, %AUTO, %ALLO, and D₅₀) from Lake Seeberg were regressed against instrumental temperature and precipitation data from meteo-station Château-d'Oex (AD 1901 - AD 2005). Correlation coefficients (r_{Pearson}) and p values (corrected for autocorrelation; p_{corr}) were quantified using the method of Trenberth (1984). %AUTO and May-June-July-August-September (MJJAS) had the highest correlation and were filtered with three, five, and seven year running averages to determine the amount of smoothing which maximizes the correlation while preserving statistical significance.

Following smoothing of %AUTO and MJJAS temperatures, a calibration (AD 1961 AD 2004) and a verification period (AD 1902 - AD 1960) was established to test the quality of ordinary least squares (OLS) regression model (i.e. cross-validation split-periods; von Gunten et al., 2009). The calibration and verification periods were split at AD 1960 to determine the influence of the increasing trend (after AD 1960) on the correlation between %AUTO and MJJAS. The reduction of error (RE), coefficient of efficiency (CE) and the root mean squared error of prediction (RMSEP) were calculated according to Cook et al. (1994).

Additionally, an OLS model which represents the complete range of calibration period climate variability (i.e. the entire AD 1901 - AD 2005 period) was developed. A ten-fold cross-validation provided the reconstruction error (RMSEP; Venables and Ripley, 2002; Peters and Hothorn, 2009; R Development Core Team, 2009; Therneau and Lumley, 2009; Leisch and Dimitriadou, 2010; Therneau et al., 2010).

Analytical Methods

The results of sedimentary analyses and temperature reconstructions were evaluated using a series of statistical methods calculated with R Statistical Software (R Development Core Team, 2009). These methods included: tests of data distribution (e.g. Kolmogorov-Smirnov test; Kirkman, 1996), autocorrelation, correlation coefficients (r_{Pearson}) and p values (corrected for autocorrelation; p_{corr} ; Trenberth, 1984), cross-correlations, changepoint analysis (e.g.

hierarchical clustering or the method of Caussinus and Mestre, 2004), spectral analysis (i.e. Morlet Wavelet analysis; Torrence and Compo, 1998), linear trends (decadal, 30 year and centennial), frequencies (e.g. turbidites) and Mean-Variability Change (MVC) analysis.

References

- Abramoff, M.D., Magelhaes, P.J., Ram, S.J. 2004. Image processing with ImageJ. *Biophotonics International* 11 (7): 36-42.
- Andrews, J.T., Freeman, W. 1996. The Measurement of Sediment Color Using the Colortron Spectrophotometer. *Arctic and Alpine Research* 28 (4): 524-528.
- Appleby, P.G. 1997. Sediment records of fallout radionuclides and their application to studies of sediment-water interactions. *Water, Air and Soil Pollution* 99: 573-586.
- Appleby, P.G. 2002. Chronostratigraphic techniques in recent sediments, In: Last, W.M., Smol, J.P. (eds.), *Tracking Environmental Change Using Lake Sediments, Volume 1: Basin Analysis, Coring and Chronological Techniques*. The Netherlands: Kluwer Academic Publishers, 171-203.
- Balsam, W.L., Deaton, B.C., Damuth, J.E. 1998. The effects of water content on diffuse reflectance spectrophotometry studies of deep-sea sediment cores. *Marine Geology* 149: 177-189.
- Berner, R.A. 1971. *Principles of chemical sedimentology*. McGraw-Hill Book Company.
- Björck, S., Wohlfarth, B. 2001. ¹⁴C chronostratigraphic techniques in paleolimnology, In: Last, W. M., Smol, J.P. (eds.), *Tracking Environmental Change Using Lake Sediments. Volume 1: Basin Analysis, Coring, and Chronological Techniques*. The Netherlands: Kluwer Academic Publishers, 205-245.
- Blass, A. 2006. Sediments of two high-altitude Swiss lakes as high-resolution late Holocene paleoclimate archives. Inauguraldissertation der Philosophisch-naturwissenschaftlichen Fakultät der Universität Bern.
- Blass, A., Grosjean, M., Troxler, A., Sturm, M. 2007a. How stable are twentieth-century calibration models? A high-resolution summer temperature reconstruction for the eastern Swiss Alps back to AD 1580 derived from proglacial varved sediments. *The Holocene* 17: 51-63.
- Blass, A., Bigler, C., Grosjean, M., Sturm, M. 2007b. Decadal-scale autumn temperature reconstruction back to AD 1580 inferred from the varved sediments of Lake Silvaplana (southeastern Swiss Alps). *Quaternary Research* 68: 184-195.
- Carroll, J., Lerche, I. 2003. *Sedimentary processes: quantification using radionuclides*. Elsevier, Oxford.
- Caussinus, H., Mestre, O. 2004. Detection and correction of artificial shifts in climate series. *Applied Statistics* 53: 405-425.
- Cook, E.R., Briffa, K.R., Jones, P.D. 1994. Spatial regression methods in dendroclimatology—a review and comparison of 2 techniques. *International Journal of Climatology* 14: 379-402.
- Dean, W. E. Jr. 1974. Determination of carbonate and organic matter in calcareous sediments and sedimentary rocks by loss on ignition: Comparison with other methods. *Journal of Sedimentary Petrology* 44: 242-248.

- Debret, M., Desmet, M., Balsam, W., Copard, Y., Francus, P., Laj, C. 2006. Spectrophotometer analysis of Holocene sediments from an anoxic fjord: Saanich Inlet, British Columbia, Canada. *Marine Geology* 229: 15-28.
- Grob, P. 2008. Spheroidal carbonaceous particles SCPs als Indikatoren der Umweltbelastung und als Datierungsmethode junger Seesedimente. MSc Thesis. University of Bern, Bern.
- Hausmann, S., Lotter, A.F., van Leeuwen, J.F.N., Ohlendorf, C., Lemcke, G., Grönlund, E., Sturm, M. 2002. Interactions of climate and land-use documented in the varved sediments of Seebergsee in the Swiss Alps. *The Holocene* 12 (3): 279-289.
- Heiri, O., Lotter, A.F., Lemcke, G. 2001. Loss-on-ignition as a method for estimating organic and carbonate content of sediments: reproducibility and comparability of results. *Journal of Paleolimnology* 25: 101-110.
- Kirkman, T.W. 1996. Statistics to Use. <http://www.physics.csbsju.edu/stats/> (April 2010)
- Kuglitsch, F.G., Toreti, A., Xoplaki, E., Della-Marta, P.M., Luterbacher, J., Wanner, H. 2009. Homogenization of Daily Maximum Temperature Series in the Mediterranean. *Journal of Geophysical Research* 114.
- Lamoureux, S.F. 1994. Embedding unfrozen lake sediments for thin section preparation. *Journal of Paleolimnology* 10: 141-146.
- Larocque-Tobler, I., Quinlan, R., Stewart, M.M., Grosjean, M. (accepted) Chironomid-inferred temperature changes of the last century in Lake Seeberg (Seebergsee), Switzerland : assessment of two calibration methods. *Quaternary Science Reviews*.
- Leemann, A., Niessen, F. 1994. Holocene glacial activity and climatic variations in the Swiss Alps: reconstructing a continuous record from proglacial lake sediments. *The Holocene* 4: 259-268.
- Leisch, F., Dimitriadou, E. 2010. mlbench: Machine Learning Benchmark Problems. R package version 2.1-0.
- Lindbloom, B. 2011. Color calculators and spreadsheets. <http://www.brucelindbloom.com>
- Liu, J., Carroll, J.L., Lerche, I. 1991. A technique for disentangling temporal source and sediment variations from radioactive isotope measurements with depth. *Nuclear Geophysics* 5: 31-45.
- Lotter, A.F., Lemcke, G. 1999. Methods for preparing and counting biochemical varves. *Boreas* 28: 243-252.
- Lotter, A.F., Appleby, P.G., Bindler, R., Dearing, J.A., Grytnes, J.A., Hofmann, W., Kamenik, C., Lami, A., Livingstone, D.M., Ohlendorf, C., Rose, N., Sturm, M. 2002. The sediment record of the past 200 years in a Swiss high-alpine lake: Hagelseewli (2339 m a.s.l.). *Journal of Paleolimnology* 22: 111-127.
- Louda, J.W., Liu, L., Baker, E.W. 2002. Senescence- and death-related alteration of chlorophylls and carotenoids in marine phytoplankton. *Organic Geochemistry* 33: 1635-1653.

MeteoSchweiz 2010a. (http://www.meteoschweiz.admin.ch/web/de/klima/klima_heute/jahre_sverlaeufe_nbcn/Segl_Maria.html)

MeteoSchweiz 2010b. (http://www.meteoschweiz.admin.ch/web/de/klima/klima_heute/Homogene_reihen.Par.0019.DownloadFile.ext.tmp/chateaudox.txt)

Mook, W.G. 1986. Business meeting (Trondheim). *Radiocarbon* 28.

Nederbragt, A.J., Francus, P., Bollmann, J., Soreghan, M.J. 2004. Image Calibration, Filtering, and Processing, In: Francus, P. (ed.), Tracking Environmental Change Using Lake Sediments, Volume 7: Image Analysis, Sediments and Palaeoenvironments. The Netherlands: Springer, 35-58.

Nederbragt, A.J., Thurow, J.W. 2004. Digital sediment colour analysis as a method to obtain high resolution climate proxy records. In: Francus, P. (ed.), Tracking Environmental Change Using Lake Sediments, Volume 7: Image Analysis, Sediments and Palaeoenvironments. The Netherlands: Springer, 105-124.

Niessen, F., Wick, L., Bonani, G., Chondrogianni, C., Siegenthaler, C. 1992. Aquatic system response to climatic and human changes: productivity, bottom water oxygen status, and sapropel formation in Lake Lugano over the last 10,000 years. *Aquatic Sciences* 54: 257-276.

Nussbaumer, S., Steinhilber, F., Trachsel, M., Breitenmoser, P., Beer, J., Blass, A., Grosjean, M., Hafner, A., Holzhauser, H., Wanner, H., Zumbühl, H. (accepted) Alpine climate during the Holocene: a comparison between records of glaciers, lake sediments and solar activity. *Journal of Quaternary Science*.

Ohlendorf, C., Niessen, F., Weissert, H. 1997. Glacial varve thickness and 127 years of instrumental climate data: A comparison. *Climatic Change* 36: 391-411.

Ohlendorf, C., Sturm, M. 2008. A modified method for biogenic silica determination. *Journal of Paleolimnology* 39: 137-142.

Peters, A., Hothorn, T. 2009. ipred: Improved Predictors. R package version 0.8-8. <http://CRAN.R-project.org/package=ipred>

R Development Core Team 2009. R: A language and environment for statistical computing. R Foundation for Statistical Computing. Vienna, Austria. ISBN 3-900051-07-0, URL <http://www.R-project.org>.

Reimer, P.J., Baillie, M.G.L., Bard, E., Bayliss, A., Beck, J.W., Bertrand, C., Blackwell, P.G., Buck, C.E., Burr, G., Cutler, K.B., Damon, P.E., Edwards, R.L., Fairbanks, R.G., Friedrich, M., Guilderson, T.P., Hughen, K.A., Kromer, B., McCormac, F.G., Manning, S., Bronk Ramsey, C., Reimer, R.W., Remmele, S., Southon, J.R., Stuiver, M., Talamo, S., Taylor, F.W., van der Plicht, J., Weyhenmeyer, C.E. 2004. IntCal04 Terrestrial Radiocarbon Age Calibration, 0-26 cal kyr BP. *Radiocarbon* 46: 1029-1058.

Rein, B., Sirocko, F. 2002. In-situ reflectance spectroscopy - analyzing techniques for high-resolution pigment logging in sediment cores. *International Journal of Earth Science* 91: 950-954.

- Routh, J., Choudhary, P., Meyers, P.A., Kumar, B. 2008. A sediment record of recent nutrient loading and trophic state change in Lake Norrviken, Sweden. *Journal of Palaeolimnology* 42 (3): 325-341.
- Rein, B. 2003. In-situ Reflektionsspektroskopie und digitale Bildanalyse - Gewinnung hochauflösender Paläoumweltdaten mit fernerkundlichen Methoden. Habilitationsschrift, University of Mainz, Mainz.
- Rose, N.L. 2001. Fly-ash particles, In: Last, W.M., Smol, J.P (eds.), Tracking Environmental Change Using Lake Sediments, Volume 2: Physical and Chemical Techniques. The Netherlands: Kluwer Academic Publishers, 319-349.
- Singer, J.K., Anderson, J.B., Ledbetter, M.T., McCave, I.N., Jones, K.P.N, Wright, R. 1988. An assessment of analytical techniques for the size analysis of fine-grained sediments. *Journal of Sedimentary Petrology* 58(3): 534-543.
- Stephens, F.C., Louchard, E.M., Reid, R.P., Maffione, R.A. 2003. Effects of microalgal communities on reflectance spectra of carbonate sediments in subtidal optically shallow marine environments. *Limnology Oceanography* 42 (1, 2): 535-546.
- Stewart, M., Grosjean, M., Kuglitsch, F.G., Nussbaumer, S.U., von Gunten, L. (submitted) Reconstructions of Late Holocene palaeofloods and glacier activity in the Upper Engadine, Switzerland (ca. 1450 BC - AD 420). *Palaeogeography, Palaeoclimatology, Palaeoecology*.
- Therneau, T.M., Atkinson, B., Ripley, B. 2010. rpart: Recursive Partitioning. R package version 3.1-46. <http://CRAN.R-project.org/package=rpart>
- Therneau, T.M., Lumley, T. 2009. survival: Survival analysis, including penalised likelihood. R package version 2.35-8. <http://CRAN.R-project.org/package=survival>
- Torrence, C., Compo, G.P. 1998. A practical guide to wavelet analysis. *Bulletin of American Meteorological Society* 79: 61-78.
- Trachsel, M., Eggenberger, U., Grosjean, M., Blass, A., Sturm, M. 2008. Mineralogy-based quantitative precipitation and temperature reconstructions from annually laminated lake sediments (Swiss Alps) since AD 1580. *Geophysical Research Letters* 35.
- Trachsel, M., Grosjean, M., Larocque-Tobler, I., Schwikowski, M., Blass, A., Sturm, M. 2010a. Quantitative summer temperature reconstruction derived from combined biogenic Si and chironomid record from varved sediments of Lake Silvaplana (south-eastern Swiss Alps) back to AD 1177. *Quaternary Science Reviews* 29 (19-20): 2719-2730.
- Trachsel, M., Grosjean, M., Schnyder, D., Kamenik, C., Rein, B. 2010b. Scanning reflectance spectroscopy (380-730 nm): a novel method for quantitative high-resolution climate reconstructions from minerogenic lake sediments. *Journal of Paleolimnology* 44 (4): 979-994.
- Trenberth, K.E. 1984. Some effects of finite sample size and persistence on meteorological statistics. Part I: Autocorrelation. *Monthly Weather Review* 112: 2359-2368.
- USGS 2007. Digital Spectral Library, splib06a. <http://speclab.cr.usgs.gov/spectral-lib.html>

Venables, W.N., Ripley, B.D. 2002. *Modern Applied Statistics with S*. Fourth Edition. New York: Springer, ISBN 0-387-95457-0

von Gunten, L., Grosjean, M., Rein, B., Urrutia, R., Appleby, P. 2009. A quantitative high-resolution summer temperature reconstruction based on sedimentary pigments from Laguna Aculeo, central Chile, back to AD 850. *The Holocene* 19: 873-881.

Wolfe, A.P., Vinebrooke, R.D., Michelutti, N., Rivard, B., Das, B. 2006. Experimental calibration of lake-sediment spectra reflectance to chlorophyll a concentrations: methodology and paleolimnological validation. *Journal of Paleolimnology* 36: 91-100.

4. Quantitative inter-annual and decadal June-July-August temperature variability ca. 570 BC - AD 120 (Iron Age - Roman Period) reconstructed from the varved sediments of Lake Silvaplana, Switzerland

Stewart, M., Larocque-Tobler, I., Grosjean, M.
Journal of Quaternary Science, accepted

a. Abstract

Annually resolved June-July-August (JJA) temperatures from ca. 570 BC to AD 120 (+/-100 years; approximately 690 varve years) were quantified from biogenic silica and chironomids (Type II regression; Standard Major Axis calibration-in-time) preserved in the varved sediments of Lake Silvaplana, Switzerland. Using 30 year (climatology) moving averages and detrended standard deviations (Mean-Variability Change MVC), moving linear trends, changepoints and wavelets, reconstructed temperatures were partitioned into a warmer (+0.3°C; ca. 570 BC - 351 BC), cooler (-0.2°C; ca. 350 BC - 16 BC) and moderate period (+0.1°C; ca. 15 BC - AD 120) relative to the reconstruction average (10.9°C; reference AD 1950 - AD 2000=9.8°C). Warm and variable JJA temperatures at the Late Iron Age - Roman Period transition (approximately 50 BC to AD 100 in this region) and a cold anomaly around 470 BC (Early - Late Iron Age) were inferred. Inter-annual and decadal temperature variability was greater in ca. 570 BC - AD 120 than the last millennium whereas multi-decadal and lower frequency temperature variability were comparable as evident in wavelet plots. Using MVC plots of reconstructed JJA temperatures from ca. 570 BC - AD 120, we verified current trends and European climate model outputs for the 21st century which suggest increased inter-annual summer temperature variability and extremes in a generally warmer climate (heteroscedasticity; hotspot of variability). We compared these results to MVC plots of instrumental and reconstructed temperatures (from the same sediment core and proxies but a different study) from AD 1177 to AD 2000. Our reconstructed JJA temperatures from ca. 570 BC - AD 120 showed that inter-annual JJA temperature variability increased rapidly above a threshold of ~10°C mean JJA temperature. This increase accelerated with continued warming up to >11.5°C. We suggest that the Roman Period serves with respect to inter-annual variability as an analogue for warmer 21st century JJA temperatures in the Alps.

b. Introduction

Climate reconstructions are needed to determine the response of the climate system to natural and anthropogenic forcings. A concern is increased inter-annual summer temperature variability and extremes in a warmer climate as observed in the 20th century and as projected by Regional and Global Climate Models for the 21st century, particularly in Europe ('hotspot of variability'; Schär et al., 2004; Scherrer et al., 2006; Seneviratne et al., 2006; Parey et al., 2010 and references therein). Enhanced inter-annual summer temperature variability under warming is ascribed in part to the soil moisture - atmosphere feedback mechanism which may manifest during dry and warm summers. Depletion of soil moisture increases the Bowen Ratio (=Sensible Heat : Latent Heat), resulting in a non-linear rise in the transfer of land surface energy into sensible heat (Schär et al., 2004; Seneviratne et al., 2006). Implications include greater heatwave and drought frequency with grave regional impacts (Seneviratne et al., 2006; Fischer and Schär, 2010). The relationship between the 'mean' and 'variability' of temperature weakens in cooler or very warm climates (Parey et al., 2010). Until now, most studies of the relationship between mean and inter-annual variability of summer temperatures have been limited to reanalysis and instrumental periods and projected future climate conditions. Therefore, the range of temperature variability and the thresholds for heteroscedasticity are poorly constrained (Scherrer et al., 2006; Parey et al., 2010).

Lake sediments can provide up-to-annual and long-duration (multi-millennial) records of past climate. Prerequisites include the presence of an accurate chronology, a recognized climate signal in the sediments, a sufficiently long local homogenized instrumental record, and an appropriate statistical calibration model (Kuglitsch et al., 2009; Trachsel et al., 2010b).

Here, an annually resolved, ca. 690 varve year (570 BC - AD 120, +/-100 years) quantitative June-July-August (JJA) temperature reconstruction from biogenic silica and chironomids in the sediments of Lake Silvaplana (eastern Swiss Alps) was used to determine the persistence of the relationship between mean and inter-annual variability of summer temperatures during warmer periods in the past (i.e. the Iron Age - Roman Period). These results were compared to instrumental and reconstructed temperatures from AD 1177 - AD 2000 (also from biogenic silica and chironomids in the same sediment core but a different study; Trachsel et al., 2010a), including the late Medieval Climate Anomaly and the Little Ice Age. These two temperature reconstructions are not continuous due to a large turbidite (approx. 275-300 cm depth) above the sediment section from this study.

Sediments from Lake Silvaplana were investigated because they are annually laminated (varved) for the past 3300 years (Leemann and Niessen, 1994) and the composition

has been investigated in various studies (e.g. Leemann and Niessen, 1994; Ohlendorf, 1999; Blass et al., 2007a, b; Trachsel et al., 2010a, b). Biogenic silica in Lake Silvaplana is closely related to changes in regional climate to at least AD 1177 (Trachsel et al., 2010a). Specifically, the JJA temperature signal in biogenic silica flux (bSi) combined with chironomids has been shown to reconstruct a wide (inter-annual to millennial) range of climate variability (Trachsel et al., 2010a). Furthermore, JJA temperatures of this region are spatially correlated to western and central Europe and the northern Mediterranean (Trachsel et al., 2010a). We focus on ca. 570 BC to AD 120 because lower resolution climate records suggest that it was warmer than the last millennium, including a warmer (Early Iron Age; in Central Europe ‘Hallstatt’), a cooler (Late Iron Age; in Central Europe ‘La Tène’), and a moderate-to-warm Roman Period (Tinner et al., 2003). Alongside instrumental and reconstructed temperatures from the last millennium, we will investigate the relationship between the mean and inter-annual variability of JJA temperatures during generally warmer and cooler conditions and isolate the mean temperature threshold above which heteroscedasticity occurs.

We aim to answer: (1.) what is the relationship between the mean and inter-annual variability of reconstructed JJA temperatures for ca. 570 BC - AD 120? How does the relationship between the mean and inter-annual variability of reconstructed JJA temperatures for ca. 570 BC - AD 120 compare to JJA temperatures of AD 1177 - AD 2000 (including the late Medieval Climate Anomaly, the Little Ice Age and the present)? (2.) How does the pattern of decadal, multi-decadal and centennial JJA temperature variability and trends during the Iron Age and Roman Period compare to the last millennium and the present? (3.) Do prolonged trends or large anomalies in JJA temperatures coincide with changes in natural forcings?

c. Study site

Lake Silvaplana (1791 m a.s.l., between 46° 24' N, 9° 42' E and 46° 30' N, 9° 52' E), belongs to a chain of lakes (Sils, Silvaplana, Champfèr and St. Moritz) in the Upper Engadine valley of eastern Switzerland (Ohlendorf et al., 1997). Lake Silvaplana covers 2.7 km², has a capacity of 127×10⁶ m³ and has an average depth of 47 m (LIMNEX, 1994) (Figure 4.1).

The contributing watershed (175 km²) includes 6 km² (1998 status) of glacier cover, underlain by three major tectonic nappes: the Lower Austroalpine Margna, the Upper Penninic Platta and the Lower Austroalpine Bernina consisting of granite, gneiss and carbonate (AdS, 2004; Blass et al., 2007a). Four tributaries connect Lake Silvaplana to the

watershed including the Fedadla River (principal purveyor of suspended sediments) (Blass et al., 2007a). Inflowing water has an average residence time of eight months (LIMNEX, 1994).

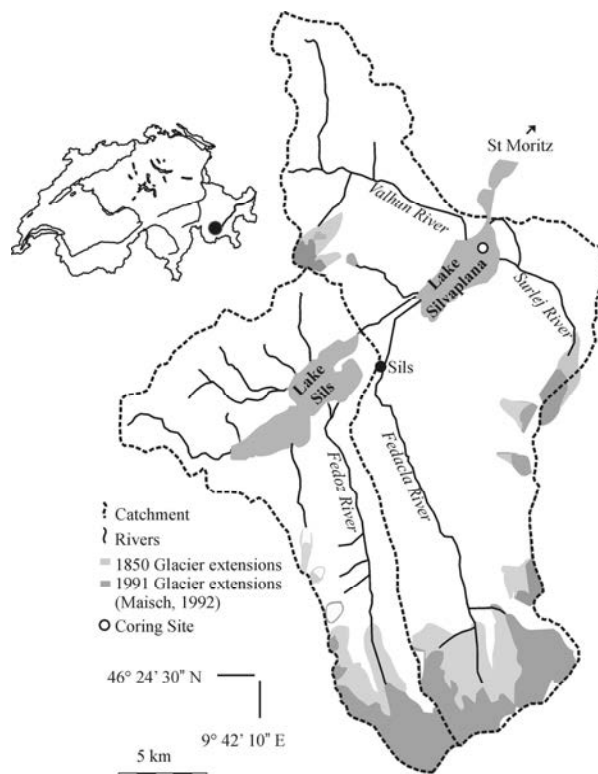


Figure 4.1 Site characteristics of Lake Silvaplana and the contributing watershed (right; modified from Blass et al., 2007a) and the location of Lake Silvaplana in Switzerland (left; Mappad, 1996).

The watershed is exposed to continental winter-dry conditions with large fluctuations in monthly temperature (MeteoSchweiz, 2010). Temperature inversions allow cool and dry air to accumulate in the Engadine valley during the winter which favors January to May ice-cover (Ohlendorf, 1999; MeteoSchweiz, 2010). Alternatively, warm and relatively moist and windy summers result from greater insolation and packages of moist air from the South (Ohlendorf, 1999; MeteoSchweiz, 2010).

Lake Silvaplana has a volume ratio (%_{epilimnion}/_{hypolimnion}) of 30/70. The lake overturns in May and November, is thermally stratified from June to October and inverse thermally stratified under the ice cover from January to May (LIMNEX, 1994; Ohlendorf, 1999). The lake is oligotrophic with sufficient oxygen in the hypolimnion (May, mid-July and end of summer) to be classified as oxic (LIMNEX, 1994; Ohlendorf, 1999).

Summer temperatures drive sedimentation in distal regions of Lake Silvaplana at the monthly, seasonal and annual time scale. Therefore, glacial melt-water and fluvial base flow are the most important purveyors of sediment (Blass et al., 2007a).

d. Methods

Sampling

We used the lower two thirds (300 cm to 900 cm) of a nine meter long UWITEC piston core recovered from the distal region of Lake Silvaplana in the winter of 2005 - 2006. The core was split lengthwise in the laboratory and photographed with a Nikon D80 digital camera (2300×1700 pixels; Appendix A). Half of the core was wrapped in polyethylene film and placed in storage at 4°C.

The other core half was frozen with liquid nitrogen, wrapped in polyethylene film and kept at -10°C until sub-sampling. Varves dating ca. 570 BC to AD 120 (360 cm to 465 cm) were identified on the frozen core from high-resolution (1200 dpi) scans of polished sediment blocks and digital photographs of the wet sediment core. Each varve was sub-sampled (i.e. scraped) from the frozen core using a knife.

All of the sub-samples were analyzed for mass accumulation rate (MAR), biogenic silica concentration (%bSi) and biogenic silica flux (bSi flux), whereas chironomids were counted in four discrete time windows at annual resolution (approximately 570 BC - 500 BC, 480 BC - 440 BC, 390 BC - 340 BC, and 30 BC - 0). The sampling design was chosen because Trachsel et al. (2010a) found that bSi flux had the highest skill for reconstructing multi- to sub-decadal JJA temperatures (i.e. ‘variability’) whereas the chironomid transfer function (Heiri et al., 2003; Larocque-Tobler et al., 2010) provided low (centennial) frequency July (scaled to JJA) temperature (i.e. ‘mean’). Combination of these two reconstructions captured both the variability and mean of JJA temperatures. This was most critical for the study of MVC behavior.

Dating

A floating chronology was established from varve counts on polished sediment blocks and constrained with four calibrated AMS radiocarbon dates. The varve chronology is not continuous to the present (Trachsel et al., 2010a) because of a turbidite with an erosive base at 275-300 cm depth (between AD 1177 and the section studied here). The number of varves removed by this turbidite is unknown.

To create polished sediment blocks, overlapping slabs (20×2 cm; Lamoureux, 1994; Lotter and Lemcke, 1999) of wet sediment were removed from the core, flash frozen with liquid nitrogen and freeze-dried overnight. The dried sediment slabs were arranged side-by-side in aluminum trays and a four component (NSA, ERL, DER and DMAE) epoxy resin (SPI) was poured over the slabs. The resin was cured in an oven (70°C) over 12 hours and the slabs were cut into blocks and polished at GEOPREP (University of Basel, Switzerland).

Polished sediment blocks were scanned (1200 dpi) and viewed in ImageJ software (Abramoff et al., 2004). Varves were identified from changes in lithology (see Results, Lithology) along three scan lines and marker horizons (i.e. turbidites) were used to combine varve counts from consecutive blocks.

Four terrestrial macrofossil-derived calibrated AMS radiocarbon dates were analyzed at the Poznań Radiocarbon Laboratory in Poland (Table 4.1). Terrestrial macrofossils (only found in turbidites) were used because radiocarbon dates of bulk sediments (including algal aquatic organic matter) in Lake Silvaplana are affected by reservoir effects. The macrofossils may be reworked material. Three macrofossil samples were taken from neighboring turbidites around 440 cm depth to test for internal consistency of the resulting radiocarbon dates (i.e. whether there was reworking). The radiocarbon dates should be interpreted as maximum ages. Following calibration of the four radiocarbon dates in Intcal04.14 (Reimer et al., 2004), the three floating varve chronologies were fit through a turbidite at ~440 cm depth. The varve chronology which was most consistent with the four radiocarbon dates was elected to be the final chronology. Therefore, all ages presented here are calculated from an annually resolved but floating varve chronology anchored by calibrated radiocarbon dates (BC and AD).

Sedimentological and biogeochemical analyses

Mass accumulation rates (MAR) were calculated from varve thickness, dry sediment density and porosity using a modified version of the Niessen et al. (1992) method (i.e. organic carbon was excluded from the calculation). Varve thickness was found from high-resolution (1200 dpi) scans of polished sediment blocks opened in ImageJ software (Abramoff et al., 2004). The transition from dark to light lamination was visually identified and digitally marked and an algorithm in ImageJ calculated the distance between each consecutive mark. Turbidites, identified as being $>2\sigma$ from the average varve thickness and/or having a different texture and coloring than neighboring varves, were excluded. The dry density of sediment was estimated at 2.65 g/cm³ (=quartz) (Blass et al., 2007a). Porosity was calculated from the water content,

dry sediment density and pore water density for each varve. Pore water density was estimated at 1 g/cm^3 .

Biogenic silica concentrations (%bSi) were measured according to the protocol of Ohlendorf and Sturm (2008). Approximately 150 mg of sediment per sub-sample was treated with 5 ml H_2O_2 (30%) to eliminate organic matter. The loss in weight before and after treatment with H_2O_2 (30%) was used as an estimate of organic matter. After a week, the sediments were cleaned with distilled water and freeze-dried. 10 ml of 1 M NaOH matrix was added to the organic-free sediments in plastic tubes and the tubes were placed in an ultrasonic bath. The tubes were capped, shook with a mini-shaker set to $>2500/\text{minute}$, and heated for one hour at 90°C . These last three steps were repeated three times. The tubes were centrifuged and 700 μl of the supernatant was pooled with 70 μl 65% HNO_3 and Milli-Q-Water. Measurements of %bSi were made by D. Fischer on an inductively coupled plasma optical emission spectrometer (ICP-OES; Paul Scherrer Institute, Switzerland) and results were corrected for lithogenic silica (Al:Si ratio 2:1) (Ohlendorf and Sturm, 2008).

Chironomid analysis

Chironomid head capsules were counted at annual resolution for four time windows (approximately 570 BC - 500 BC, 480 BC - 440 BC, 390 BC - 340 BC, and 30 BC - 0). These time windows were chosen based on changes recorded in the MAR and the bSi records. KOH 10% was added to the samples overnight then the samples were sieved in a 100 μm mesh. The residue remaining in the mesh was poured into a Bogorov counting tray and examined under a Leica Zoom 2000 binocular at 40X magnification. Each individual head capsule was hand-picked using a forceps and deposited in a drop of Hydromatrix on a microscope slide. The head capsules were identified at 400-1000X magnification using a Motic B3 Professional microscope. The identification followed Wiederholm (1983), Oliver and Roussel (1983), Larocque and Rolland (2006) and Brooks et al. (2007).

Statistical analysis

The product of MAR and %bSi (=bSi flux) was converted to JJA temperatures using the Type II regression (Standard Major Axis) calibration-in-time (JJA Sils Maria: AD 1864 - AD 1949, $r=0.67$, $p_{\text{corr}}=0.03$) developed by Trachsel et al. (2010a).

The program C2 was used to create the chironomid stratigraphy and ZONE was used for zonation (Juggins, 1991 and 2003). These zones were independent of the four studied periods suggesting an independent separation of chironomid assemblages. A transfer function

from the chironomid distribution in 101 lakes (Heiri et al., 2003; Heiri and Lotter, 2005; Bigler et al., 2006) was used to infer mean July air temperatures. The temperature gradient is 6°C. The transfer function was modified to fit Lake Silvaplana chironomid taxonomy (e.g. Tanypodinae were merged into two categories (*Pentaneurini* and *Procladius*) and all *Crictopus* were merged). This modified transfer function has a leave-one-out, cross-validated coefficient of determination (r^2) of 0.9, a root mean squared error of prediction (RMSEP) of 1.5°C, a maximum bias of 1.7°C, and was previously used to successfully reconstruct mean July air temperatures of the last 1000 years (Larocque-Tobler et al., 2010).

The inferred mean July temperatures resulting from the transfer function were scaled to JJA temperatures (for consistency with the bSi-inferred temperatures) by the average 20th century difference between measured mean July air temperature and measured mean JJA temperatures (Sils Maria=0.8°C; Trachsel et al., 2010a).

The bSi- and chironomid-inferred temperatures were combined by calculating the difference between the average bSi temperature and the average chironomid temperature for the four common time windows, extending this difference between the four windows through linear interpolation for an annual estimate of the difference between the bSi- and chironomid-inferred temperatures, and adding these differences to the annually resolved bSi temperatures. Combining bSi- and chironomid-inferred temperatures provided a robust JJA temperature reconstruction with skill in the inter-annual, decadal and centennial domains of climate variability (Trachsel et al., 2010a; Larocque-Tobler et al., 2010).

The root mean squared error (RMSE) of the combined JJA temperature reconstruction included the error from the bSi reconstruction (ten-fold cross-validation), the error from the chironomid transfer function, and combination of the two reconstructions (leave-one-out method).

To evaluate the annual JJA temperature reconstruction, a Kolmogorov-Smirnov test determined if the temperatures were normally distributed and whether parametric or non-parametric statistics should be applied (Kirkman, 1996). Then the mean, variance, and degree of autocorrelation were calculated to describe the series. Using 30 year moving averages (30 year m.a.), 30 year moving linear detrended standard deviations (30 year m. det. std. dev.), moving decadal to centennial linear trends, changepoint analysis (Constrained Hierarchical Clustering CHC and the method of Caussinus and Mestre C&M), and Morlet wavelet analysis, subsets of relatively homogeneous temperatures were identified (Caussinus and Mestre, 2004; Scherrer et al., 2006; Bunn, 2008 and in press; Juggins, 2009; von Gunten et al., 2009; R Development Core Team, 2009). Specifically, accumulations of changepoints

which coincide with 99th or 1st percentile trends (decadal, 30 year and/or centennial) were considered as possible transitions between subsets (i.e. periods of significant climatic change). We confirmed that the character of temperatures falling on either side of these possible transitions was distinct (i.e. in terms of variance) by running ANOVA (analysis of variance) on the three subsets following log transformation (to account for the distribution of the reconstructed temperatures) (Kirkman, 1996). Finally, a scatter-plot and linear model of 30 year m.a. versus 30 year m. det. std. dev. (Mean-Variability Change MVC) was created for the entire reconstruction and for the individual subsets to determine the relationship between mean JJA temperature and inter-annual JJA temperature variability under different climatic conditions (Scherrer et al., 2006).

Comparison to the last millennium record and instrumental data

To contextualize the inter-annual to centennial behavior of JJA temperatures in the reconstruction presented in this study, and to compare our warm-biased MVC plots to a generally cooler time window, annually resolved JJA temperatures [both instrumental and reconstructed from Lake Silvaplana sediments from AD 1177 - AD 1950 (using the same sediment core and proxies in another study) and exclusively instrumental from AD 1950 - AD 2000] were used for comparison (Trachsel et al., 2010a; MeteoSchweiz, 2010). First, a non-parametric (to account for the distribution of the reconstructed temperatures) Kolmogorov-Smirnov test determined whether the reconstructed temperatures from the Iron Age / Roman Period were statistically different from JJA temperatures between AD 1177 and AD 2000 (Kirkman, 1996). Then the mean, variance, and degree of autocorrelation were calculated to compare with values from ca. 570 BC - AD 120. Using the same statistical methods as for our reconstruction, three subsets were identified including one which roughly encapsulates the Little Ice Age (approximately AD 1600 - AD 1800 in the Northern Hemisphere; IPCC, 2001) and one which covers the later Medieval Climate Anomaly (approximately AD 1000 - AD 1400 in the Northern Hemisphere; IPCC, 2001). Finally, MVC plots for the entire AD 1177 - AD 2000 time series, for the three subsets of the Iron Age / Roman Period and for AD 1950 - AD 2000 were created to evaluate JJA temperature heteroscedasticity.

e. Results

Lithology

Sediments in the investigated section of the core had a basal silt layer (light colored, slightly coarser grained summer layer) with a clay cap (dark colored, slightly finer grained winter

layer; Figure 4.2). The average couplet thickness was 1.4 mm. This was consistent with the varve descriptions of Ohlendorf et al. (1997) and Blass et al. (2007a).

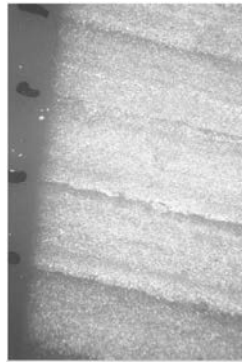


Figure 4.2 Core photo showing the lithology of Lake Silvaplana sediments (Blass, 2006).

Dating

Varve counts and radiocarbon dates provided a chronology that is accurate at the inter-annual scale from varve counting but floating within the accuracy of calibrated radiocarbon AMS dates (Table 4.1, Figure 4.3).

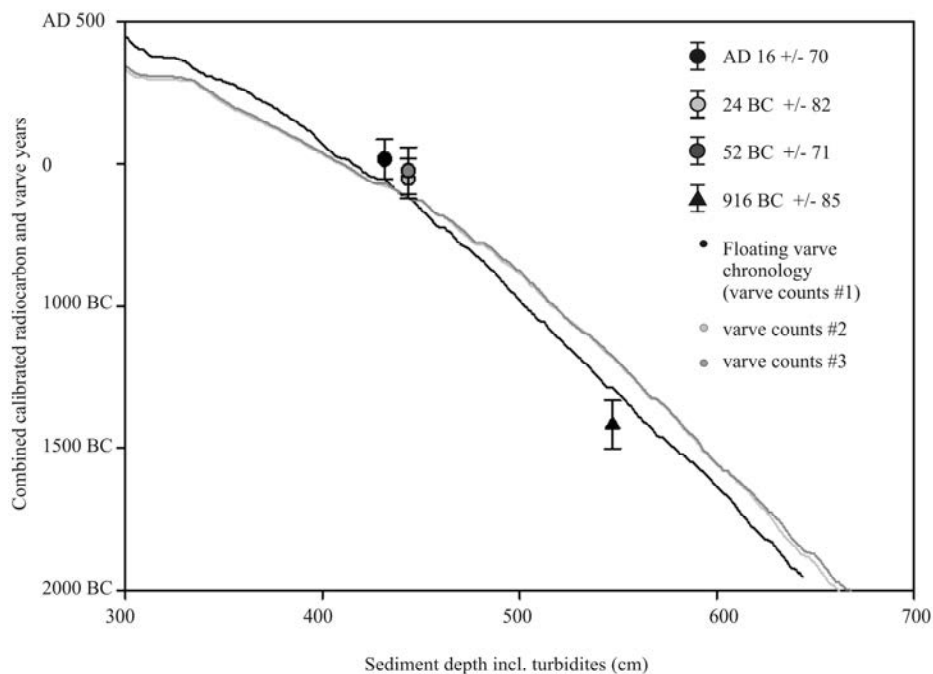


Figure 4.3 Age-depth model with the three series of varve counts.

When the three floating varve chronologies were anchored at the turbidite at ~440 cm, the maximum difference between the three series of varve counts was 120 years. 85

laminations were interpreted as possible turbidites. These were thicker ($>2\sigma$) than the average varve, had a coarse (i.e. sand) basal layer with increasingly fine grains towards the top of the deposit, and a high concentration of macrofossils.

The first three radiocarbon dates (Poz-28061, Poz-28062 and Poz-28064) had a difference in varve counts which was within the $\pm 2\sigma$ error range of the calibrated radiocarbon ages. This internal consistency suggested that there was no reworking of macrofossils within the sampled turbidites. The fourth radiocarbon date was taken from a turbidite with similar characteristics. The first series of varve counts fit through the four radiocarbon dates better than the other two series. The combination of these varve counts and the four radiocarbon dates suggested that the entire sediment section spanned approximately 1450 BC to AD 420 (± 100) of which 690 varve years (570 BC - AD 120, ± 100) are presented in this study (Figure 4.3).

Code (Poz-)	Sediment			Mass (mg)	^{14}C yr BP ($\pm 1\sigma$)	cal. ^{14}C age	cal. ^{14}C age		
	depth (cm)	Material	Context				1σ	2σ	range ($\pm 2\sigma$)
28061	~431 (387)*	Needles	Turbidite	5.4	1985 \pm 35	AD 16	35	70	54.5 BC - AD 85.5
28062	~443 (396)*	Needles	Turbidite	5	2020 \pm 30	24 BC	41	82	106 BC - AD 58
28064	~443 (396)*	Wood	Turbidite	72	2050 \pm 30	51.5 BC	35	71	122.5 BC - AD 19.5
30293	~546 (488)*	Needles	Turbidite	5	2765 \pm 35	916 BC	43	85	1001 BC - 831 BC

Table 4.1 Calibrated AMS radiocarbon dates (Intcal04.14) from Lake Silvaplana used to constrain the floating varve chronology. * Sediment depth [cm] without turbidites.

Chironomid assemblages and mean July air temperatures

A total of 208 samples spanning the four studied time windows between ca. 570 BC - AD 120 (see Methods, Chironomid analysis) and representing 41 taxa were analyzed. Of these taxa, 30 were present in more than two samples (Figure 4.4a). The most striking changes were the following: *Corynocera oliveri*-type (cold stenotherm), *Psectrocladius sordidellus*-group and *Protanypus* (cold stenotherm) were found only in sediments younger than ca. 440 BC whereas *Parakiefferiella* was found in sediment older than ca. 390 BC. *Limnophyes*, *Micropsectra insignilobus*-type, *Polypedilum*, *Tanytarsus lactesens*-type, *Paracladopelma*, *Brilla*, *Paratanytarsus* and *Tanytarsus mendax*-type were absent in zone 6 (older than ca. 535 BC). *Paratanytarsus* was recorded only during zone 3.

The mean July air temperature (MJAT) obtained from these assemblages is presented in Figure 4.4b. From ca. 570 BC to 550 BC, MJATs were warmer than the average (12°C). Values temporarily decreased around 550 BC - 525 BC but rebounded by 500 BC. Another

peak in MJAT was inferred between ca. 575 BC and 550 BC. In ca. 400 BC - 340 BC and ca. 24 BC - 0, MJATs oscillated around the average.

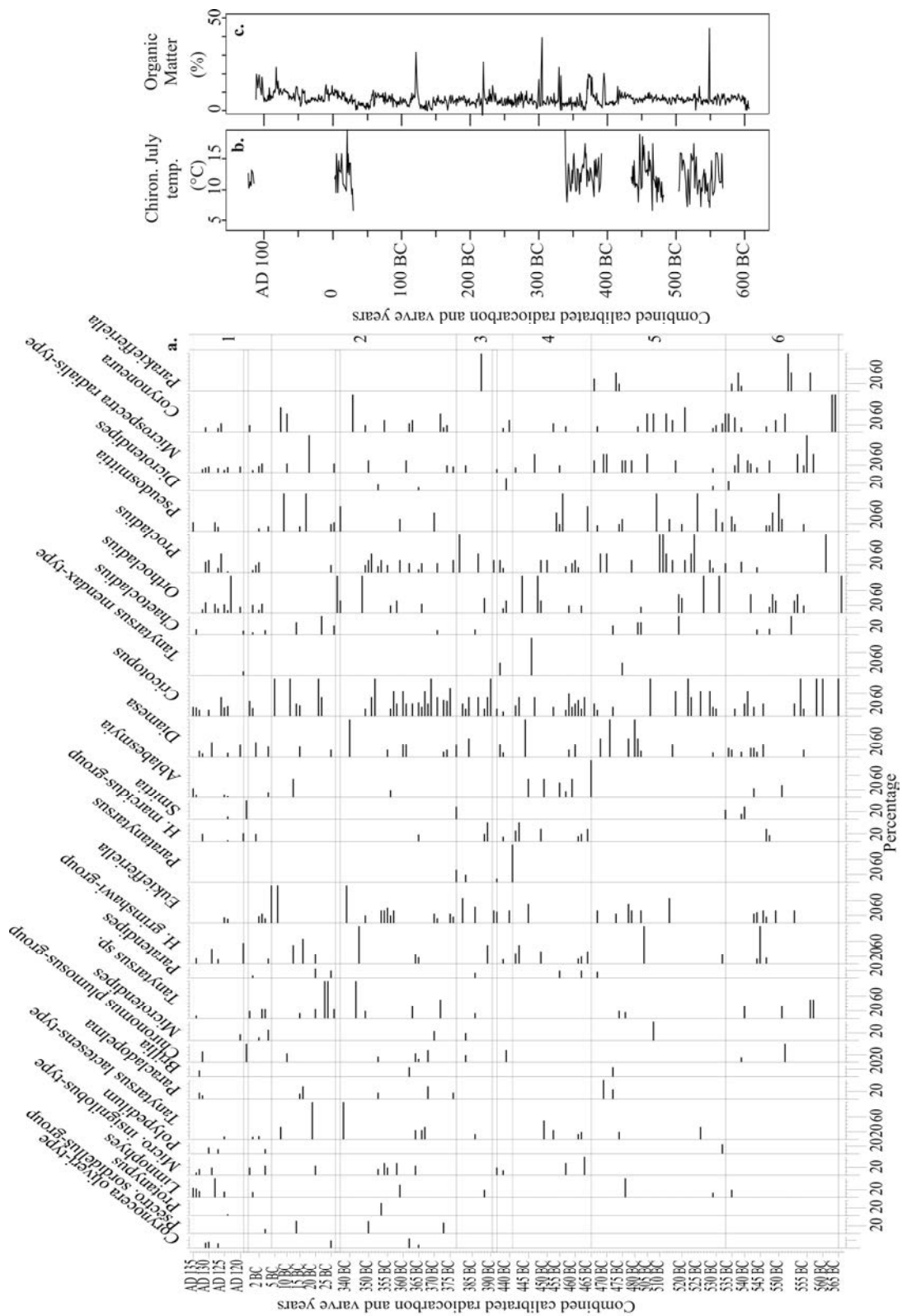


Figure 4.4 Results of (a.) chironomid assemblages, (b.) inferred mean July air temperatures (MJAT) and (c.) % organic matter (OM). For Figure 4.4a, percentages for each taxon are

represented. The black lines represent the zones created using the ZONE program (Juggins, 1991).

From ca. 30 BC to 0, MJATs were colder than the average. The MJAT variations were not related to changes in the organic matter (OM) percentages (i.e. peaks in MJAT were not always associated with increases or decreases of OM; Figure 4.4c).

Combined (bSi and chironomid) JJA temperature reconstruction ca. 570 BC - AD 120

Figures 4.5a-d show the annually resolved data for mass accumulation rates, bSi concentrations and bSi fluxes, and bSi-derived JJA temperatures. The bSi and chironomid JJA temperatures presented in Figures 4.5d and e were combined (Figure 4.5f). The RMSE of the combined reconstruction is 1.5°C which represents a 95% confidence interval of +/-3°C (Figures 4.5f, 4.6a, 4.6f).

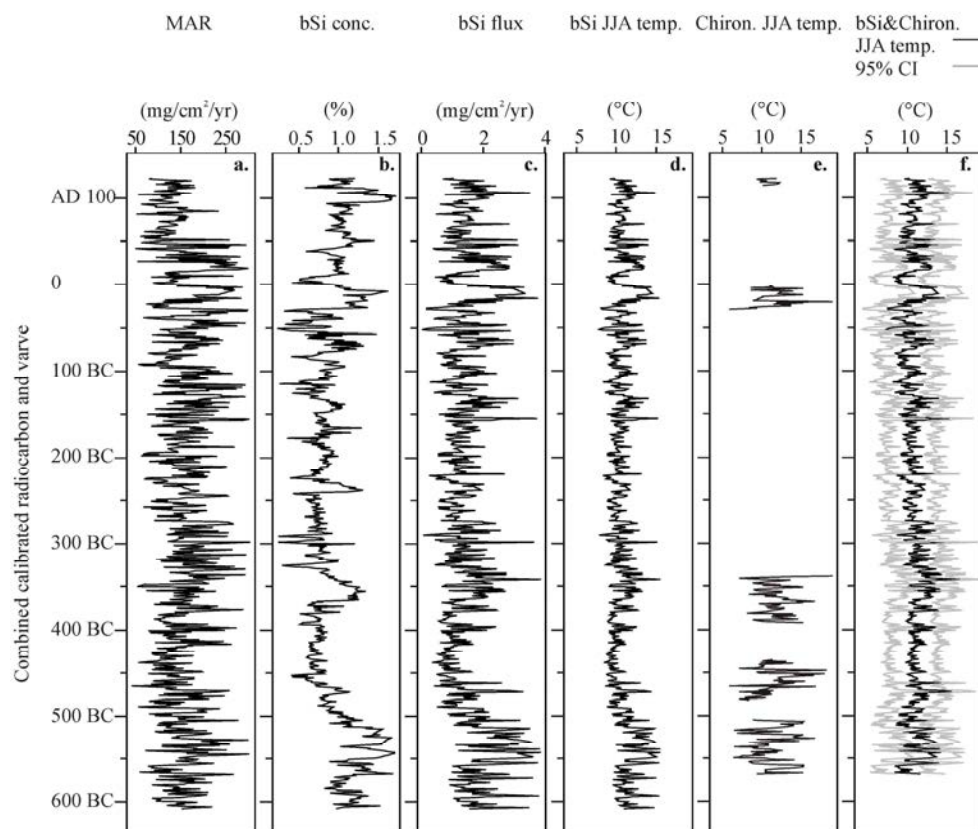


Figure 4.5 Results of (a.) mass accumulation rates (MAR), (b.) biogenic silica (bSi) concentrations, (c.) bSi fluxes, (d.) bSi June-July-August (JJA) temperature reconstruction, (e.) chironomid JJA temperature reconstruction (f.) combined bSi&chironomid JJA temperature reconstruction with the 95% confidence interval in grey.

The annually reconstructed JJA temperatures between ca. 570 BC and AD 120 were not normally distributed ($p < 0.01$), with a relatively high mean (10.9°C), a variance of 2°C , and an autocorrelation which was greatest at year 1 and decreased until year 10. Detailed analyses of 30 year m.a., 30 year m. det. std. dev., decadal to multi-decadal linear trends, changepoints and wavelets, reveal the presence of three relatively homogeneous periods of climate which were statistically distinct according to ANOVA ($p < 0.01$): a slightly warmer, a slightly cooler and a moderate period relative to the reconstruction average (Figures 4.6b, d, f, h, j, l and n, subsets A-C).

The first two hundred years of record (ca. 570 BC - 370 BC) had a rapid increase (warming) and then decrease (cooling) in the multi-decadal trends (30 year m.a. temperature) of JJA temperatures followed by a plateau at 11°C (Figures 4.6d and h). The 30 year m. det. std. dev. decreased from 1.9°C (ca. 570 BC - 540 BC) to the record minimum of 0.5°C (ca. 445 BC - 415 BC; Figure 4.6f). A changepoint around 557 BC (method C&M; Figure 4.6l) coincided with one of three very strong decadal JJA temperature warming trends (99th percentile; dark red in Figure 4.6h). Meanwhile, two very strong decadal JJA temperature cooling trends (1st percentile) were concurrent to the Early Iron Age to Late Iron Age transition. This was followed by a centennial warming trend and a shift from high power in all wavelet periods to minimal power between ca. 400 BC and 350 BC (Figure 4.7a).

Over the next hundred years (ca. 370 BC - 270 BC), the 30 year m.a. reached its record maximum (12.8°C , ca. 380 BC - 350 BC; Figure 4.6d), synchronous with a temporary increase in the inter-annual variability (30 year m. det. std. dev.) of JJA temperatures. Strong (99th percentile) decadal ($0.5^{\circ}\text{C}/\text{yr}$) and centennial ($0.02^{\circ}\text{C}/\text{yr}$) JJA warming trends were bordered by two changepoints, and there was an emergence of high power in the decadal to multi-decadal domains of variability (64 and 32-16 year periods; Figure 4.7a).

The maximum 30 year m.a. of JJA temperatures around 350 BC was followed by 300 years of cooling until the record minimum of 9.5°C (ca. 55 BC - 25 BC). There was also a decrease in the inter-annual JJA temperature variability until ca. 170 BC after which it rebounded. Decadal JJA temperature trends ranged from $\pm 0.3^{\circ}\text{C}/\text{yr}$ except for two decades with strong cooling ($-0.4^{\circ}\text{C}/\text{yr}$) around 150 BC and 130 BC. The latter coincided with a changepoint (method C&M). Multi-decadal trends remained moderate. Finally, we noted a transition from moderate-to-low power in wavelet periods 128, 64, 32 and 10-2 years (ca. 250 BC - 150 BC) to extremely low power (< 0.756) for all periods greater than 64 years, indicating exceptional climate stability (Figure 4.7a).

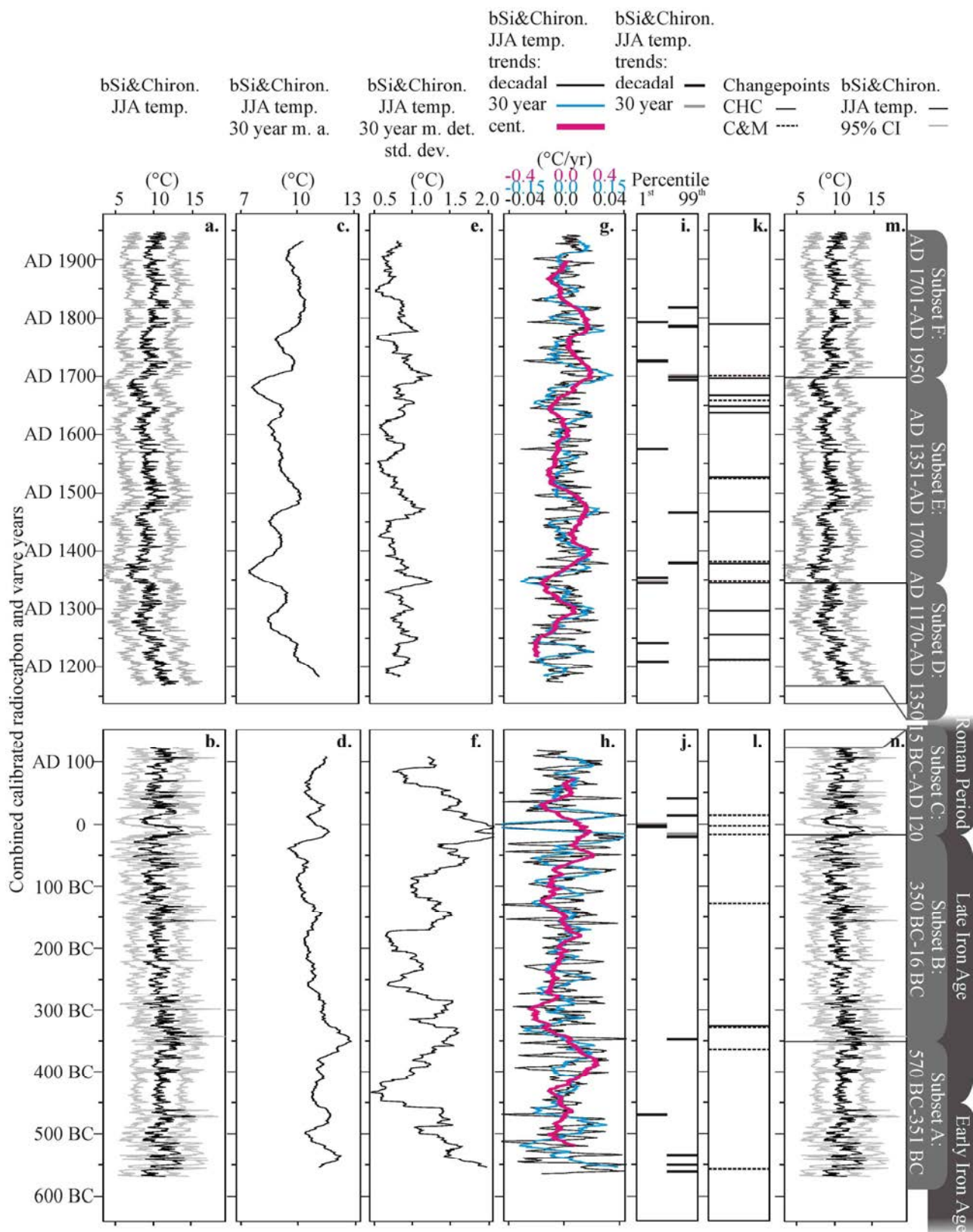


Figure 4.6 (a.) the biogenic silica (bSi) & chironomid June-July-August (JJA) temperature reconstruction from AD 1177 - AD 1950 with the 95% confidence interval in grey (Trachsel et al., 2010a), (b.) the bSi&chironomid JJA temperature reconstruction from ca. 570 BC - AD 120 with the 95% confidence interval in grey, (c.) the 30 year moving averages for the

bSi&chironomid JJA temperature reconstruction from AD 1177 - AD 1950, (d.) the 30 year moving averages for the bSi&chironomid JJA temperature reconstruction from ca. 570 BC - AD 120, (e.) the 30 year moving detrended standard deviations for the bSi&chironomid JJA temperature reconstruction from AD 1177 - AD 1950, (f.) the 30 year moving detrended standard deviations for the bSi&chironomid JJA temperature reconstruction from ca. 570 BC - AD 120, (g.) the decadal, 30 year and centennial trends for the bSi&chironomid JJA temperature reconstruction from AD 1177 - AD 1950, (h.) the decadal, 30 year and centennial trends for the bSi&chironomid JJA temperature reconstruction from ca. 570 BC - AD 120, (i.) the decadal and 30 year trends in the 1st and 99th percentile for the bSi&chironomid JJA temperature reconstruction from AD 1177 - AD 1950, (j.) the decadal and 30 year trends in the 1st and 99th percentile for the bSi&chironomid JJA temperature reconstruction from ca. 570 BC - AD 120, (k.) the changepoints for the bSi&chironomid JJA temperature reconstruction from AD 1177 - AD 1950, (l.) the changepoints for the bSi&chironomid JJA temperature reconstruction from ca. 570 BC - AD 120, (m.) subsets D, E, and F for the bSi&chironomid JJA temperature reconstruction from AD 1177 - AD 1950, (n.) subsets C, B and A for the bSi&chironomid JJA temperature reconstruction from ca. 570 BC - AD 120.

The final 200 years of the record were characterized by warming JJA temperatures up to 11.5°C (ca. 40 BC - 10 BC) followed by fluctuations between 11.5°C and 10.5°C. Inter-annual JJA temperature variability rose strongly until the record maximum (ca. 40 BC - 10 BC), and then decreased.

Decadal trends were variable from around 40 BC to AD 40 as shown by four decades with very strong cooling (1st percentile) and three decades with very strong warming (99th percentile). In many of these decades, changepoints were also found. One of the decades characterized by very strong JJA temperature warming and all of the decades with very strong cooling coincided with the Late Iron Age to Roman Period transition. We found high power in the 64-32 year periods with pulses of moderate-to-high power in the 16-8 year periods around 0 and AD 100 (Figure 4.7a).

According to these results, we propose three subsets of relatively homogeneous JJA temperature conditions (Table 4.2): subset A (ca. 570 BC - 351 BC, Early to Late Iron Age) was relatively warm. Inter-annual JJA temperature variability was very high around 570 BC and near 351 BC, separated by low inter-annual JJA temperature variability and cooler temperatures between ca. 460 BC and 400 BC. Decadal trends were pronounced. Subset B

(ca. 350 BC - 16 BC, Late Iron Age to Roman Period) had a JJA temperature cooling trend that was mostly pronounced in the long-term (centennial scale). Inter-annual JJA temperature variability fluctuated with a minimum between ca. 270 and 170 BC which coincided with a cooler climate. Few changepoints were found. The transition to subset C (ca. 15 BC – AD 120, start of Roman Period) coincided with rapid shifts between warming and cooling decadal JJA temperature trends. We observed very high but decreasing inter-annual JJA temperature variability and consistently high (multi-) decadal variability (with multiple changepoints). The JJA temperature approached the reconstruction average.

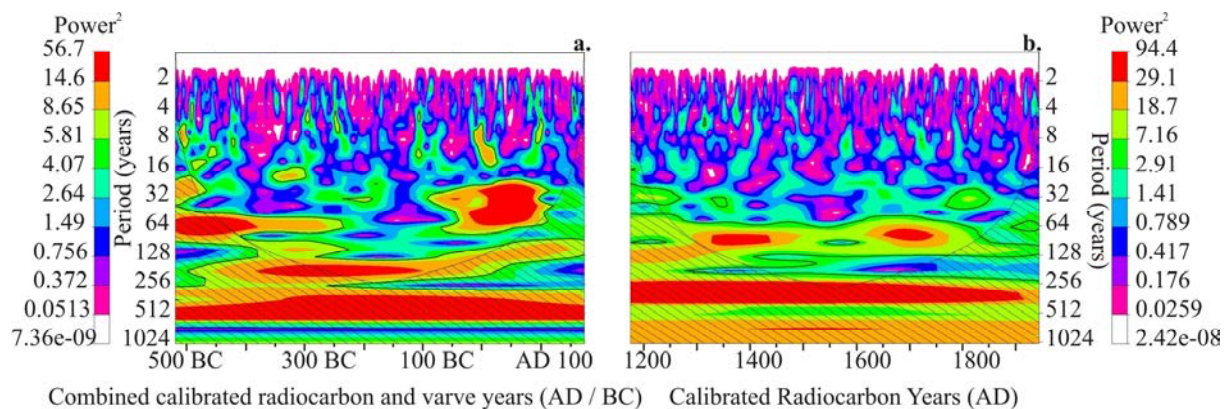


Figure 4.7 Morlet wavelets for (a.) the biogenic silica (*bSi*) & chironomid June-July-August (JJA) temperature reconstruction from ca. 570 BC - AD 120 and (b.) the *bSi*&chironomid JJA temperature reconstruction from AD 1177 - AD 1950 (Trachsel et al., 2010a).

Comparison to AD 1177- AD 2000

The character of the 570 BC - AD 120 (+/-100 year) reconstructed JJA temperatures fundamentally differed from AD 1177 - AD 2000. This was shown by a Kolmogorov-Smirnov test of statistical independence ($p < 0.01$), a reduced mean JJA temperature of 9.4°C (as opposed to 10.9°C in ca. 570 BC - AD 120), a strongly reduced inter-annual JJA temperature variability, much weaker decadal JJA temperature trends, and a longer duration of autocorrelation ($> \text{year } 29$) which suggests enhanced multi-decadal JJA temperature variability. The AD 1177 - AD 1950 record was partitioned into three periods of relatively homogeneous JJA temperatures (Table 4.2). Relative to the corresponding AD 1177 - AD 2000 values, subset D (AD 1177 - AD 1350; late Medieval Climate Optimum in the Lake Silvaplana region) had a moderate mean JJA temperature (9.7°C ; 0.2°C cooler than AD 1950 - AD 2000 and 1.2°C cooler than the Iron Age - Roman Period average), relatively low inter-annual JJA temperature variability, multiple changepoints and a strong multi-decadal to

centennial cooling (1st percentile). Subset E (AD 1350 - AD 1700) roughly coincided with the Little Ice Age, had a very low mean JJA temperature (8.8°C), a moderate variance (1.1°C), low inter-annual JJA temperature variability (compared to the Iron Age - Roman Period), a large number of changepoints, and a moderate number of very strong (multi-)decadal JJA temperature trends. Subset F (AD 1701 - AD 1950) had a relatively high mean JJA temperature (9.8°C; equally warm as AD 1950 - AD 2000; but 1.1°C cooler than the Iron Age - Roman Period average), a low variance (0.8°C), low (19th century) inter-annual JJA temperature variability, one changepoint, and strong (multi-)decadal cooling and warming trends.

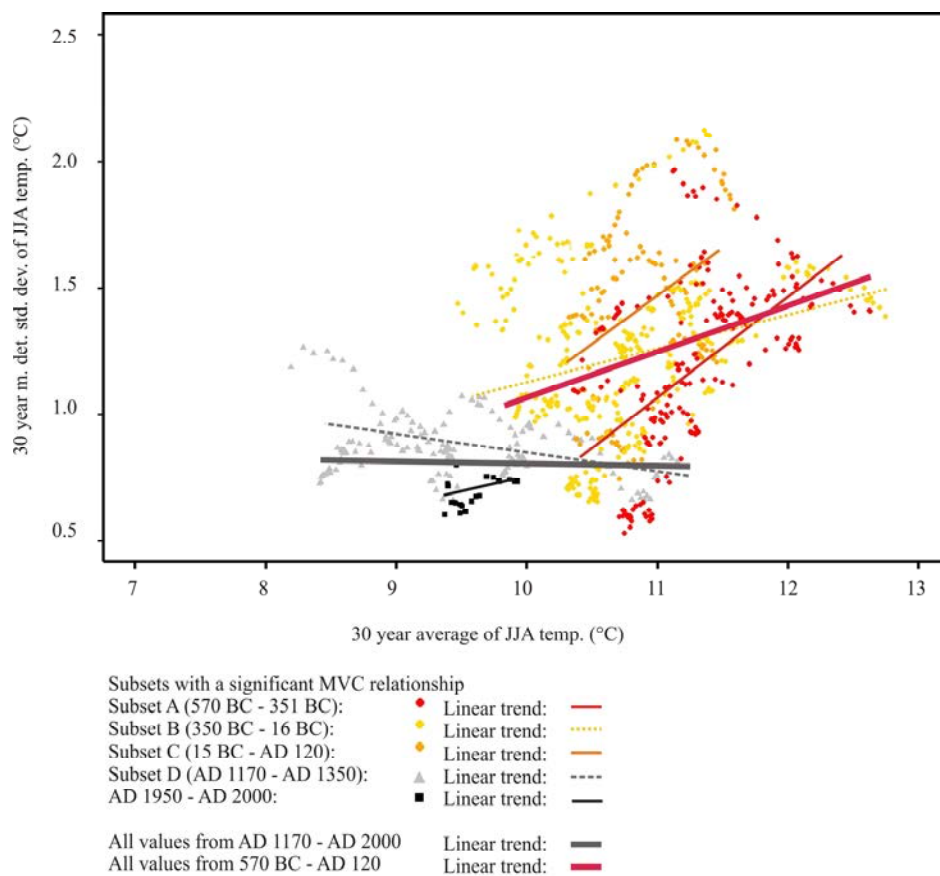


Figure 4.8 Mean-Variability Change (MVC) plot for the entire June-July-August (JJA) temperature reconstruction (ca. 570 BC - AD 120), for the entire combined reconstructed and instrumental temperature record (AD 1177 - AD 1950) and for subsets with a significant ($p < 0.05$) MVC relationship. Details provided in Table 4.2.

Figure 4.8 presents MVC plots for our entire Iron Age - Roman Period reconstruction (ca. 570 BC - AD 120), for reconstructed and instrumental temperatures (AD 1177 - AD 2000) and for the individual subsets with a significant relationship between mean and

variability of JJA temperatures. Positive relationships were found for the relatively warm Iron Age - Roman Period (ca. 570 BC - AD 120) and subsets A-C therein. The warmest subsets, A and C, showed the strongest increase in inter-annual JJA temperature variability with warming (Figure 4.8 and Table 4.2). Insignificant negative relationships were found for subsets E and F. Significant negative relationships belonged to subset D and the entire AD 1177 - AD 2000 record (mean JJA temperature=9.4°C). From Table 4.2 and Figure 4.8, we observed that the significant MVC relationships remained first constant and increased afterwards steeply with increasing mean JJA temperature (subsets B, C, A). This suggests that the mean JJA temperature threshold needed for heteroscedasticity was between 9.8°C and 10.7°C. As the mean JJA temperature continued to increase above this threshold, inter-annual temperature variability became increasingly sensitive.

Subset	Mean JJA Temperature (°C)	Variance JJA Temperature (°C)	Mean-Variability MVC relationships	Mult. r^2
Subset E AD 1351 - AD 1700	8.8	1.1	-0.02 .	0.01
All values from AD 1170 - AD 2000	9.4	1.3	-0.02 *	0.01
Subset D AD 1170 - AD 1350	9.7	1.5	-0.06 ***	0.12
AD 1950 - AD 2000	9.8	0.6	0.17 **	0.3
Subset F AD 1701 - AD 1950	9.8	0.8	-0.01	0
Subset B 350 BC - 16 BC	10.7	1.9	0.01	0.07
All values from 570 BC - AD 120	10.9	2	0.16 ***	0.08
Subset C 15 BC - AD 120	11	2.2	0.36 ***	0.13
Subset A 570 BC - 351 BC	11.24	1.9	0.39 ***	0.29

Table 4.2 Statistical characteristics of June-July-August (JJA) temperatures for the individual subsets and the entire reconstruction (ca. 570 BC - AD 120; AD 1177 - AD 1950) and instrumental temperatures (AD 1950 - AD 2000). The table is sorted by mean JJA temperatures. Positive Mean-Variability (MVC) relationships (slope of regression) are bold; significance levels of the MVC relationship are marked with: . ($p < 0.1$); * ($p < 0.05$); ** ($p < 0.01$), *** ($p < 0.001$)

Overall, JJA temperatures during the Iron Age - Roman Period were warmer and more variable than JJA temperatures from the last 800 years. However, multi-decadal and centennial trends were comparable as evident in Figure 4.7. Inter-annual JJA temperature variability and (multi-)decadal trends (both warming and cooling) seemed to be focused around specific periods (e.g. the early Roman Period). However, the late Iron Age was remarkably stable with low multi-decadal and centennial variability and gradual cooling. An equivalent for the extremely warm JJA temperatures in subset A (ca. 570 BC - 351 BC) was not found in AD 1177 - AD 2000. However, during the Iron Age - Roman Period, among 643

possible 50 year windows, we identified 130 precedents for the increasing linear trend ($0.02^{\circ}\text{C}/\text{yr}$, $p=0.02$) registered for AD 1950 - AD 2000. In all of these instances, the mean and variance of JJA temperatures exceeded the AD 1950 - AD 2000 values.

f. Discussion

The 570 BC - AD 120 (± 100 years) reconstruction benefited from a varve count and radiocarbon based chronology which afforded annually resolved data and precise 30 year floating chronologies. The uncertainty of the cumulative varve counts is approximately 100 years (18%). The absolute chronology (combined varve counts and radiocarbon dates) has an uncertainty of 100 to 150 years.

The reconstruction consisted of a calibrated and tested bi-proxy data set (bSi flux and chironomids) which provided quantitative JJA temperatures with skill in the inter-annual to centennial frequency domains of climate variability (Larocque-Tobler et al., 2010; Trachsel et al., 2010a). BSi flux provided a quantitative measure of diatom productivity which has been shown to be sensitive to warm season temperatures prior to eutrophication of the lake (post AD 1950; Blass et al., 2007b). Also, chironomids are sensitive to both water and air temperature as reflected in taxa assemblages (Larocque et al., 2009). Both proxies were previously used, independently and in combination, to successfully reconstruct JJA temperatures back to AD 1177 from the same sediment core (Larocque-Tobler et al., 2010; Trachsel et al., 2010a).

The quality of our ca. 570 BC - AD 120 JJA temperature reconstruction was limited by the chronological uncertainties of AMS radiocarbon dating (i.e. the calendar ages) and varve counts (i.e. the floating chronology). Varve identification came with the risk of missing or falsely identifying laminations related to the subjective nature of varve identification (Lamoureux and Bradley, 1996; Ojala, 2001). Therefore, a lamination which was identified as a turbidite for one scan line could have been interpreted as a series of varves on another scan line. This resulted in a maximum varve counting error of 120 years. However, the error of the 30 year floating chronology was negligible which was most relevant for the statistical analysis of climate variability and trends.

An additional source of error was imperfect varve-by-varve sampling and conversion of proxy data into temperatures. Detailed sedimentary analyses showed no changes in sedimentology which would lead us to question the integrity of the chronology and the relationship between our proxies (bSi and chironomids) and temperature (i.e. Figure 4.4c). Proxy series are not always able to capture seasonal variability (i.e. extremes) and a

calibration-in-time approach is not always reliable at capturing low-frequency (centennial) variability (Trachsel et al., 2010a). Therefore, the combination of a bSi flux derived JJA temperature reconstruction (calibration-in-time) with chironomid derived JJA temperature data (transfer function) for four time windows allowed a reconstruction of temperature variability in a wide spectrum of frequency domains. The resulting JJA record was more robust, particularly in the low-frequency domain, than an exclusively calibration-in-time based record inferred from bSi flux data. By adding interpolated differences (between JJA temperatures derived from bSi flux and chironomids) to the bSi temperatures, we risked creating artificial multi-centennial scale trends. However, this did not appear to be the case (Figures 4.6h and l) since changepoints do not generally fall into periods where chironomid-temperatures were used to anchor the bSi reconstruction (except for ca. 15 BC). Finally, the temperature reconstruction would have been improved by continuous chironomid data throughout the time series but the temporal demands of chironomid analysis limits the number of samples able to be analyzed in a reasonable amount of time.

Despite these caveats, the overall character of the ca. 570 BC - AD 120 temperature reconstruction agreed with contemporaneous lower-resolution climate records from the region. This suggests that the relationship between bSi flux and temperature, defined for the calibration period (AD 1864 - AD 1949) and stable-in-time back to AD 1177 (Trachsel et al., 2010a), persisted between ca. 570 BC and AD 120.

The mean temperature of the reconstruction was consistent with the chironomid-based July temperature reconstruction of Heiri et al. (2003) for 1550 BC - AD 950 (11.5-12°C). A high frequency and magnitude of droughts, related to these high temperatures, was reconstructed for 320 BC - AD 150 from N. Ireland peatlands (Swindles et al., 2010). The warmest subset A, coincided with warm spring temperatures at Oberer Landschitzsee and an increase in prehistoric farming North and South of the Alps (570 BC - 450 BC) and in the Upper and Lower Engadine (500 BC and 300 BC; 570 BC - 350 BC, respectively) (Zoller et al., 1996; Raba, 1996; Gobet et al., 2003; Tinner et al., 2003). Additionally, major alpine glaciers (the Great Aletsch glacier, the Gorner glacier and the Lower Grindelwald glacier) retreated around this time (Holzhauser et al., 2005). It also overlapped dry conditions at Walton Moss Bog, N. England (510 BC), and high chironomid-based July temperatures at Talkin Tarn, N. England (450 BC - 250 BC; Barber and Langdon, 2007). Finally, the reconstructed temperatures carry the signature of a major cooling event (two decadal linear trends in the 1st percentile) coincident to the Early Iron Age to Late Iron Age transition (ca. 450 BC; Figure 4.6h). The cooler subset B (roughly Late Iron Age; cf. La Tène) was

synchronous with a hiatus in land-use between 300 BC and 50 BC for the alpine region, probably related to a deteriorating climate (Zoller et al., 1996; Raba, 1996; Gobet et al., 2003; Tinner et al., 2003). The end of this subset, characterized by high climate variability (i.e. a series of decadal and 30 year linear trends in the 99th and 1st percentile and three changepoints), was concurrent to the Late Iron Age - Roman Period transition. After 50 BC, warmer JJA temperatures (i.e. subset C) were reconstructed for Oberer Landschitzsee (Schmidt et al., 2007). Plant macrofossils and dryness-indicating testate amoebae were found for this period in Walton Moss peat (Barber and Langdon, 2007). These conditions favored renewed land-use North and South of the Alps and in the Upper and Lower Engadine (Tinner et al., 2003; Zoller et al., 1996; Raba, 1996; Gobet et al., 2003).

(1.) What is the relationship between the mean and inter-annual variability of reconstructed JJA temperatures for 570 BC - AD 120 (+/- 100 years)?

A significant positive relationship between mean and variability (heteroscedasticity) of JJA temperatures above a certain lower threshold mean temperature (here between 9.8 and 10.7°C) was found. The slope of this relationship became steeper as the mean became progressively higher (i.e. slope for subset B << subset C < subset A). This is consistent with results from climate model experiments for European summers in the warmer 21st century and with theoretical considerations, and suggests that the mean JJA temperature threshold required for heteroscedasticity is around 9.8-10.7°C in the Engadine, Swiss Alps (mean of subset B) (Schär et al., 2004; Seneviratne et al., 2006; Parey et al., 2010). This is the temperature range that has been reached in the current decades and should persist during the first half of the 21st century according to future climate scenarios for the region. Our data demonstrate that the mean JJA temperatures during the warmest subset of our reconstruction (11.2°C, mean of subset A ca. 570 BC - 351 BC) have not yet transcended a second upper threshold above which consecutive very warm summers are predicated to reduce inter-annual temperature variability (Parey et al., 2010). Tentatively, we place this upper threshold to between 12°C and 13°C mean JJA temperature (Figure 4.8). However, the lower and the upper thresholds for inter-annual summer temperature heteroscedasticity (i.e. the probability density function of the soil moisture - atmosphere feedback) are also controlled by the seasonal rainfall and soil moisture regime. It is currently not known whether or not the Iron Age / Roman Period conditions are comparable to those of today and the 21st century.

(2.) *How does decadal, multi-decadal and centennial JJA temperature variability and trends during the Iron Age and Roman Period compare to the last millennium and the present?*

To contextualize the mean and variability of temperatures in the ca. 570 BC - AD 120 reconstruction, the JJA temperatures of AD 1177 - AD 2000 were considered. These were cooler and less variable at the inter-annual to (multi-)decadal scale (i.e. variance, 30 year m. det. std. dev. and number of multi-decadal trends in the 99th or 1st percentile) than temperatures from the Iron Age - Roman Period. However, JJA temperatures of AD 1177 - AD 2000 had more changepoints than their older counterpart and exhibited more pronounced centennial-scale temperature variability.

(3.) *Do prolonged trends of large amplitudes coincide with changes in known natural forcings?*

At millennial timescales, the behavior of Iron Age - Roman Period JJA temperatures relative to the last millennium can be attributed to orbital forcing. July insolation at 47°N was 4-6 W/m² higher between ca. 600 BC and AD 100 than during the last 800 years (Berger and Loutre, 1991). Furthermore, long-term orbital forcing exceeded shorter-term fluctuations of total solar irradiance by more than an order of magnitude during this time (Steinhilber et al., 2009). Although the grand solar minima of the last millennium (e.g. Wolf, Spörer, Maunder and Dalton Minima) are reflected in lower JJA temperatures (Trachsel et al., 2010a), there was no obvious response to changes in Total Solar Irradiance (TSI) during the Iron Age - Roman Period. Exceptions are the cool temperatures coinciding with a persistent strong negative TSI anomaly centered around 400 BC and warm JJA temperatures during the high TSI values of the late Early Iron Age (ca. 550 BC - 450 BC) and the Roman Period (subsets A and C).

g. Summary and Conclusions

Annually resolved (570 BC - AD 120, +/-100 years; Early Iron Age to Early Roman Period) quantitative June-July-August (JJA) temperatures were reconstructed from the varved sediments of Lake Silvaplana from biogenic silica flux (continuous, annually resolved, calibrated-in-time) and chironomids (four discrete windows, annually resolved, transfer function). Varve counts provided a floating chronology that was constrained by four AMS radiocarbon dates. The internal consistency and the highly precise annual resolution (within varve counting errors) of our data set were most relevant for the statistical analysis of inter-annual and decadal temperature variability and trends.

Temperatures reconstructed from ca. 570 BC - AD 120 were warmer than today (AD 1950 - AD 2000; 9.8°C) and the last millennium (from AD 1177 onwards, used here for comparison): the warmest period was reconstructed between ca. 570 BC - 351 BC (mean JJA temperature 11.2°C). We found moderately warm temperatures for the Roman Period (11°C, ca. 15 BC - AD 120) and less warm temperatures for the Late Iron Age (10.7°C, ca. 350 BC - 16 BC). The warmer summer conditions during the Iron Age - Roman Period compared to the last 800 years (MWP, LIA and present) were attributed to orbital forcing ($\Delta 4-6 \text{ W/m}^2$, July). The ca. 570 BC - AD 120 record agreed with other regional reconstructions.

Using the 570 BC - AD 120 (+/-100 years) temperature reconstruction, we assessed inter-annual to (multi-)decadal JJA temperature variability and trends during periods of warmer conditions in the past, which might serve as precedents for the future. Instrumental data, climate model experiments and theoretical considerations have suggested a strongly heteroscedastic behavior of summer temperatures in Central Europe and the Alps (increasing inter-annual temperature variability and extremes with increasing mean temperatures). According to Parey et al. (2010), there is a range of temperatures where heteroscedasticity is strongest. Under very cold and very warm conditions the link between mean and variability weakens. Our data showed that inter-annual to decadal temperature variability was strongly enhanced under warmer JJA of the Iron Age - Roman Period (compared to the last millennium). Conversely, multi-decadal temperature variability remained equivalent. Using Mean-Variability Change plots, a strongly heteroscedastic behavior was shown for mean JJA temperatures exceeding $\sim 9.8^\circ\text{C}$ (Engadine). This is the temperature that has been reached in the current decades. The upper mean JJA temperature limit, above which inter-annual temperature variability decreases again, was not captured by our reconstruction. According to our data it is above 11.2°C (i.e. the warmest period of our investigation, ca. 570 BC - 351 BC), tentatively between $12-13^\circ\text{C}$ (i.e. 2-3°C warmer than the current decades). These results agreed with the projections of regional climate models for the 21st century for Central Europe and the Alps and confirmed that at global scales, Central Europe will be a future global hotspot of warm season variability.

References

- Abramoff, M.D., Magelhaes, P.J., Ram, S.J. 2004. Image processing with ImageJ. *Biophotonics International* 11 (7): 36-42.
- AdS 2004. Atlas der Schweiz - Interactive CD, version 2.0. Swiss Federal Office of Topography, Wabern.
- Berger, A., Loutre, M.F. 1991. Insolation values for the climate of the last 10 million years. *Quaternary Sciences Reviews* 10: 297-317.
- Barber, K.E., Langdon, P.G. 2007. What drives the peat-based palaeoclimate record? A critical test using multi-proxy climate records from northern Britain. *Quaternary Science Reviews* 26: 3318-3327.
- Bigler, C., Heiri, O., Krskova, R., Lotter, A.F., Sturm, M. 2006. Distribution of diatoms, chironomids and Cladocera in surface sediments of thirty mountain lakes in south-eastern Switzerland. *Aquatic Sciences* 68: 154-171.
- Blass, A., Grosjean, M., Troxler, A., Sturm, M. 2007a. How stable are twentieth-century calibration models? A high-resolution summer temperature reconstruction for the eastern Swiss Alps back to AD 1580 derived from proglacial varved sediments. *The Holocene* 17: 51-63.
- Blass, A., Bigler, C., Grosjean, M., Sturm, M. 2007b. Decadal-scale autumn temperature reconstruction back to AD 1580 inferred from the varved sediments of Lake Silvaplana (southeastern Swiss Alps). *Quaternary Research* 68: 184-195.
- Brooks, S.J., Langdon, P.G., Heiri, O. 2007. The identification and use of Palaeartic Chironomidae larvae in palaeoecology. QRA Technical Guide No. 10, Quaternary Research Association, 276 pp.
- Bunn, A.G. 2008. A Dendrochronology Program Library in R (dplR). *Dendrochronologia* 26: 115-124.
- Bunn, A.G. In Press. Crossdating in R using the dplR library. *Dendrochronologia*.
- Caussinus, H., Mestre, O. 2004. Detection and correction of artificial shifts in climate series. *Applied Statistics* 53: 405-425.
- Fischer, E.M., Schär, C. 2010. Consistent geographical patterns of changes in high-impact European heatwaves. *Nature Geoscience* 3: 398-403.
- Gobet, E., Tinner, W., Hochuli, P.A., van Leeuwen, J.F.N., Ammann, B. 2003. Middle to Late Holocene vegetation history of the Upper Engadine (Swiss Alps): the role of man and fire. *Vegetation Historical Archaeobotany* 12: 143-163.
- Heiri, O., Lotter, A.F. 2005. Holocene and Lateglacial summer temperature reconstruction in the Swiss Alps based on fossil assemblages of aquatic organisms: a review. *Boreas* 34: 506-516.

- Heiri, O., Lotter, A.F., Hausmann, S., Kienast, F. 2003. A chironomid-based Holocene summer air temperature reconstruction from the Swiss Alps. *The Holocene* 13: 477-484.
- Holzhauser, H., Magny, M., Zumbühl, H.J. 2005. Glacier and lake-level variations in west-central Europe over the last 3500 years. *The Holocene* 15: 789-801.
- Intergovernmental Panel on Climate Change (IPCC) 2001. Climate Change 2001: The Scientific Basis. Cambridge University Press for the Intergovernmental Panel on Climate Change, Geneva.
- Juggins, S. 1991. ZONE, version 1.2. University of Newcastle, UK.
- Juggins, S. 2003. C2 data analysis, version 1.5.1. University of Newcastle, Newcastle, UK.
- Juggins, S. 2009. RIOJA: Analysis of Quaternary Science Data, version 0.5-6. <http://cran.rproject.org/web/packages/rioja/index.html>
- Kirkman, T.W. 1996. Statistics to Use. <http://www.physics.csbsju.edu/stats/> (April 2010)
- Kuglitsch, F.G., Toreti, A., Xoplaki, E., Della-Marta, P.M., Luterbacher, J., Wanner, H. 2009. Homogenization of Daily Maximum Temperature Series in the Mediterranean. *Journal of Geophysical Research* 114.
- Lamoureux, S.F. 1994. Embedding unfrozen lake sediments for thin section preparation. *Journal of Paleolimnology* 10: 141-146.
- Lamoureux, S., Bradley, R.S. 1996. A late Holocene varved sediment record of environmental change from northern Ellesmere Island, Canada. *Journal of Paleolimnology* 16: 239-255.
- Larocque, I., Rolland, N. 2006. Le guide visuel des chironomids sub-fossiles, du Québec à l'île d'Ellesmere, INRS rapport de Recherche R-900, ISBN 2-89146-440-3
- Larocque, I., Grosjean, M., Heiri, O., Bigler, C., Blass, A. 2009. Comparison between chironomid-inferred July temperatures and meteorological data AD 1850-2001 from varved Lake Silvaplana, Switzerland. *Journal of Paleolimnology* 41: 329-342.
- Larocque-Tobler, I., Grosjean, M., Heiri, O., Trachsel, M., Kamenik, C. 2010. Thousand years of climate change reconstructed from chironomid subfossils preserved in varved Lake Silvaplana, Engadine, Switzerland. *Quaternary Science Reviews* 29: 1940-1949.
- Leemann, A., Niessen, F. 1994. Holocene glacial activity and climatic variations in the Swiss Alps: reconstructing a continuous record from proglacial lake sediments. *The Holocene* 4: 259-268.
- LIMNEX 1994. Gewässerzustand und Gewässerschutzmassnahmen im OberEngadine. Bericht zuhanden des Amtes für Umweltschutz, Kanton Graubünden, 75 p.
- Lotter, A.F., Lemcke, G. 1999. Methods for preparing and counting biochemical varves. *Boreas* 28, 243-252.

Maisch, M. 1992. Die Gletscher Graubündens. Habil. Schrift Geographisches Institut Universität Zürich, Teil A und B Physische Geographie Vol. 33, 428 pp.

Mappad Free Software 1996. <http://www.ngdc.noaa.gov/paleo/paleo.html>

MeteoSchweiz 2010. (http://www.meteoschweiz.admin.ch/web/de/klima/klima_heute/jahresverlaeuft_nbcn/Segl_Maria.html)

Niessen, F., Wick, L., Bonani, G., Chondrogianni, C., Siegenthaler, C. 1992. Aquatic system response to climatic and human changes: productivity, bottom water oxygen status, and sapropel formation in Lake Lugano over the last 10,000 years. *Aquatic Sciences* 54, 257-276.

Ohlendorf, C., Niessen, F., Weissert, H. 1997. Glacial varve thickness and 127 years of instrumental climate data: A comparison. *Climatic Change* 36: 391-411.

Ohlendorf, C. 1999. High Alpine lake sediments as chronicles for regional glacier and climate history in the Upper Engadine, southeastern Switzerland. Berichte aus der Geowissenschaft Shaker Verlag, Aachen, 203 p.

Ohlendorf, C., Sturm, M. 2008. A modified method for biogenic silica determination. *Journal of Paleolimnology* 39, 137-142.

Ojala, A. 2001. Varved Lake Sediments in Southern and Central Finland: Long varve chronologies as a basis for Holocene palaeoenvironmental reconstructions. Academic Dissertation, Geological Survey of Finland, Espoo, 41 pp.

Oliver, D.R., Roussel, M.E. 1983. The insects and arachnids of Canada, part II. The genera of larval midges of Canada. Agriculture Canada, Publication 1746, 263 pp.

Parey, S., Dacunha-Castelle, D., Huong Hoang, TT. 2010. Mean and variance evolutions of the hot and cold temperatures in Europe. *Climate Dynamics* 34: 345-359.

Raba, A. 1996. Historische und landschaftsökologische Aspekte einer inneralpinen Terrassenlandschaft am Beispiel von Ramosch. Doctoral dissertation, Universität Basel.

R Development Core Team 2009. R: A language and environment for statistical computing. R Foundation for Statistical Computing. Vienna, Austria. ISBN 3-900051-07-0, URL <http://www.R-project.org>.

Reimer, P.J., Baillie, M.G.L., Bard, E., Bayliss, A., Beck, J.W., Bertrand, C., Blackwell, P.G., Buck, C.E., Burr, G., Cutler, K.B., Damon, P.E., Edwards, R.L., Fairbanks, R.G., Friedrich, M., Guilderson, T.P., Hughen, K.A., Kromer, B., McCormac, F.G., Manning, S., Bronk Ramsey, C., Reimer, R.W., Remmele, S., Southon, J.R., Stuiver, M., Talamo, S., Taylor, F.W., van der Plicht, J., Weyhenmeyer, C.E. 2004. IntCal04 Terrestrial Radiocarbon Age Calibration, 0-26 cal kyr BP. *Radiocarbon* 46: 1029-1058.

Schär, C., Vidale, P.L., Lüthi, D., Frei, C., Häberli, C., Liniger, M.A., Appenzeller, C. 2004. The role of increasing temperature variability in European summer heatwaves. *Nature* 427: 332-336.

- Scherrer, S.C., Appenzeller, C., Liniger, M.A. 2006. Temperature trends in Switzerland and Europe: Implications for climate normals. *International Journal of Climatology* 26: 565-580.
- Schmidt, R., Kamenik, C., Roth, M. 2007. Siliceous algae-based seasonal temperature inference and indicator pollen tracking ca. 4,000 years of climate/land-use dependency in the southern Austrian Alps. *Journal of Paleolimnology* 38: 541-554.
- Seneviratne, S.I., Lüthi, D., Litschi, M., Schär, C. 2006. Land-atmosphere coupling and climate change in Europe. *Nature* 443: 205-209.
- Steinhilber, F., Beer, J., Fröhlich, C. 2009. Total solar irradiance during the Holocene. *Geophysical Research Letters* 36.
- Swindles, G.T., Blundell, A., Roe, H.M., Hall, V.A. 2010. A 4500-year proxy climate record from peatlands in the North of Ireland: the identification of widespread summer 'drought phases'? *Quaternary Science Reviews* 29: 1577-1589.
- Tinner, W., Lotter, A.F., Ammann, B., Conedera, M., Hubschmid, P., van Leeuwen, J.F.N., Wehrli, M. 2003. Climatic change and contemporaneous land-use phases north and south of the Alps 2300 BC to 800 AD. *Quaternary Science Reviews* 22: 1447-1460.
- Trachsel, M., Grosjean, M., Larocque-Tobler, I., Schwikowski, M., Blass, A., Sturm, M. 2010a. Quantitative summer temperature reconstruction derived from combined biogenic Si and chironomid record from varved sediments of Lake Silvaplana (south-eastern Swiss Alps) back to AD 1177. *Quaternary Science Reviews* 29 (19-20): 2719-2730.
- Trachsel, M., Grosjean, M., Schnyder, D., Kamenik, C., Rein, B. 2010b. Scanning reflectance spectroscopy (380-730 nm): a novel method for quantitative high-resolution climate reconstructions from minerogenic lake sediments. *Journal of Paleolimnology* 44: 979-994.
- von Gunten, L., Grosjean, M., Rein, B., Urrutia, R., Appleby, P. 2009. A quantitative high-resolution summer temperature reconstruction based on sedimentary pigments from Laguna Aculeo, central Chile, back to AD 850. *The Holocene* 19: 873-881.
- Wiederholm, Y. 1983. Chironomidae of the Holarctic region. Part 1, Larvae. *Entomologica Scandinavia*, Supplement 19, 457 pp.
- Zoller, H., Erny-Rodman, C., Putschakunnel, P. 1996. The history of vegetation and land-use in the Lower Engadine (Switzerland): pollen record of the last 13,000 years. *Nationalpark Forschung in der Schweiz* 86. Zernez.

5. Reconstructions of Late Holocene palaeofloods and glacier activity in the Upper Engadine, Switzerland (ca. 1450 BC - AD 420)

Stewart, M., Grosjean, M., Kuglitsch, F.G., Nussbaumer, S.U., von Gunten, L.
Palaeogeography, Palaeoclimatology, Palaeoecology, Submitted

a. Abstract

The relationship between summer-autumn floods in Central Europe and climate warming is poorly constrained by instrumental and model data. To investigate this relationship, a complete record of palaeofloods, regional glacier lengths (and associated cool/wet and warm/dry climate phases) and regional glacier advances and retreats (and associated transitions between cool/wet and warm/dry climate phases) were derived from the varved sediments of Lake Silvaplana (ca. 1450 BC - AD 420; Upper Engadine, Switzerland). In combination, these records provide insight into the behavior of floods (i.e. frequency and magnitude) under a wide range of climate conditions.

Eighty-five palaeofloods were identified from turbidites in the sediments of Lake Silvaplana. Regional glacier lengths (and associated cool/wet and warm/dry climate phases) were inferred from centennial anomalies in low-frequency mass accumulation rates (MAR_{LP}). Regional glacier advances and retreats (and associated transitions between cool/wet and warm/dry climate phases) were inferred from centennial trends in MAR_{LP} . This is the first continuous record of glacier activity in the Lake Silvaplana catchment for this time period. These data agree with regional records of land-use, glacier activity and lake levels.

Thicker and more frequent turbidites were found during cool/wet phases of ca. 1450 BC to AD 420. However, no relationship to climate transitions was discerned. Consistently, June-July-August (JJA) temperatures dating ca. 570 BC - AD 120 were inversely correlated to the thickness and frequency of turbidites. The rate that turbidite thickness and frequency increased with cooler JJA temperatures was not linear. Finally, 130 analogues for 21st century climate in the Alps between ca. 570 BC - AD 120 (i.e. 50 year windows with a warming trend and average JJA temperature exceeding AD 1950 - AD 2000 values from Sils Maria) were considered. These revealed that turbidites were thinner and less frequent than between ca. 1450 BC - AD 420.

The findings of this study suggest that the frequency and magnitude of extreme summer-autumn precipitation events and floods in the eastern Swiss Alps might not increase under continued global warming.

b. Introduction

Continuous, high-resolution climate reconstructions are needed to place current warming into the context of past natural climate variability. One concern is the frequency and magnitude of summer-autumn floods in Central Europe under climate warming. Recent events have cost human lives and damaged infrastructure (Brázdil et al., 2002; Trenberth et al., 2007).

Changes in the frequency and magnitude of floods in Central Europe have been explored in instrumental hydrological time series (e.g. Mudelsee et al., 2003, 2004), historical data (e.g. Pfister et al., 2006; Schmoker-Fackel and Naef, 2010), natural proxies (e.g. Pauling et al., 2006; Debret et al., 2010) and regional climate models (e.g. Frei and Schär, 2001; Christensen and Christensen, 2003). Most instrumental (i.e. precipitation and river stage) time series only exist for the 20th century and have a sparse spatial distribution (Gimmi et al., 2007). Documentary data (i.e. written reports and flood marks) offer additional information. For instance, instrumental time series and weather diaries were used to reconstruct seasonal and annual precipitation in Bern, Switzerland back to AD 1760 (Gimmi et al., 2007). A flood history spanning AD 1750 to AD 1900 in the Engadine, Switzerland, was based on documentary sources (Caviezel, 2007). In Germany, historical data provided flood chronologies from the Pegnitz River until AD 1300 (Brázdil et al., 2002). A historical and instrumental flood record for the Elbe and Oder Rivers showed a decrease of winter floods but no significant trend for summer floods in the 20th century (Mudelsee et al., 2003, 2004). These findings for the Elbe and Oder Rivers are surprising because regional climate models (e.g. HIRHAM4 of E.U. PRUDENCE; Christensen and Christensen, 2003) project that future climate warming in Central Europe will bring more intense precipitation events (e.g. summer-autumn floods) (Arnell and Liu, 2001; Kundzewicz et al., 2005). This is attributed to an increase in the atmospheric concentration of water vapor during warm summers and the intensification of cyclones (Kundzewicz et al., 2005).

Lake sediments can provide additional information about the relationship between floods (i.e. frequency and magnitude) and climate on longer time scales than hydrological time series and historical data. This is because floods enhance the discharge of rivers and mobilize large sediment loads (Knighton, 1998). Where these rivers enter lakes, gravity flows ('turbidity currents') can develop (Sturm and Matter, 1978). Turbidity currents typically have a sediment concentration of 9% to 45% by volume (Bagnold, 1962; Mulder and Alexander, 2001). Within turbidity currents, sediments are suspended by fluid turbulence supplemented by grain-to-grain interaction (Bagnold, 1962; Mulder and Alexander, 2001). Flood-induced turbidity currents typically result in two sedimentary units. These turbidites (or 'inundites')

are composed of a thick lower deposit with a coarsening upwards grain size (i.e. inversely graded) which forms as flood conditions intensify and an upper deposit with a fining upwards (i.e. normally graded) grain size which forms as the flood wanes (Mulder and Alexander, 2001).

Turbidites have reconstructed extreme hydrological events in (e.g.) Lillooet Lake, British Columbia (Desloges and Gilbert, 1994) and Ape Lake, British Columbia (Gilbert and Desloges, 1987). In sediments from Lake Silvaplana spanning AD 1177 to AD 2000, most turbidites were attributed to historical floods (Blass, 2006; Caviezel, 2007; Trachsel et al., 2010). Furthermore, larger historical floods in the Upper Engadine (i.e. in AD 1828, AD 1834, AD 1951 and AD 1987) produced particularly thick turbidites (Blass, 2006).

Most of the historical floods in the Upper Engadine from AD 1177 to AD 2000 can be attributed to severe summer-autumn precipitation (Caviezel, 2007). For twelve severe summer-autumn precipitation events which formed turbidites in Lake Silvaplana between AD 1950 and AD 2000, a composite analysis using daily NCEP/NCAR reanalysis data of the mid-tropospheric geopotential height at 500 hPa (Z500) and Sea Level Pressure (SLP) revealed a distinct atmospheric pattern (Kalnay et al., 1996; Kistler et al., 2001). Strong negative anomalies of Z500 and SLP over western Europe and the western Mediterranean favored the advection of anomalous humid south-westerlies and convective precipitation over the western Alps (Kalnay et al., 1996; Kistler et al., 2001). Consistently, the weather station Sils Maria (Engadine, Switzerland) recorded from 32 to 91 mm of precipitation on these dates (MeteoSchweiz, 2010). Therefore, the frequency and thickness of turbidites should be a reliable proxy for the frequency and magnitude of palaeofloods, extreme summer-autumn precipitation and the associated synoptic-scale meteorological situation.

Regional glacier length and activity (i.e. advances and retreats) can be reconstructed from the low-frequency variability of mass accumulation rates (MAR) in the sediments of Lake Silvaplana. Leemann and Niessen (1994) found similarities between the low-frequency variability of MAR from Lake Silvaplana and advances and retreats of the Unterer Grindelwaldgletscher (Switzerland). Ohlendorf et al. (1997) found agreement between retreats of the Vadret da Morteratsch and the Vadret da Roseg (glaciers in the Upper Engadine, Switzerland) and low-frequency variability of MAR from Lake Silvaplana between AD 1864 and AD 1994. Following a similar logic, Blass et al. (2007) matched peaks of long-term MAR from Lake Silvaplana to fluctuations in the Unterer Grindelwaldgletscher (ca. AD 1570 - AD 1983) and the Vadret da Morteratsch (AD 1890 - AD 1990). Recently, Nussbaumer et al. (accepted) found consistencies between the square-root of low-frequency MAR ($MAR_{LP}^{1/2}$)

from Lake Silvaplana and the frontal position of the Unterer Grindelwaldgletscher, the Mer de Glace (France) and Vadret da Tschierva (Switzerland) from AD 1500 - AD 2000, and the Grosser Aletschgletscher (Switzerland) and the Gornergletscher (Switzerland) from AD 1177 - AD 2000. Because low-frequency MAR is related to glacier lengths in the Swiss Alps and glacier lengths are mainly driven by long-term changes in climate (e.g. Steiner et al., 2005), $MAR_{LP}^{1/2}$ provides an approximation of cool/wet climates (positive anomalies of $MAR_{LP}^{1/2}$), warm/dry climates (negative anomalies of $MAR_{LP}^{1/2}$), the transition from cool/wet to warm/dry climates (negative linear trends of $MAR_{LP}^{1/2}$) and the transition from warm/dry to cool/wet climates (positive linear trends of $MAR_{LP}^{1/2}$).

Finally, biogenic silica (bSi) flux and chironomids in the sediments of Lake Silvaplana successfully reconstructed June-July-August (JJA) temperatures from AD 1177 to AD 1950 (including the local expression of the late Medieval Climate Anomaly and the Little Ice Age; Trachsel et al., 2010) and from ca. 570 BC - AD 120 (including the local expression of the Iron Age and Roman Period; Stewart et al., accepted; Chapter 4).

Lake Silvaplana is an ideal archive to study palaeofloods because it has annually laminated (i.e. varved) sediments for the last 3300 years except for episodic turbidites (Leemann and Niessen, 1994). This provides an approximately annual chronology. Furthermore, the relationship between Lake Silvaplana sediments from the last millennium, floods, glacier activity, and summer temperatures is understood through previous studies (e.g. Leemann and Niessen, 1994; Ohlendorf, 1999; Blass et al., 2006; Trachsel et al., 2008). The time window ca. 1450 BC to AD 420 was chosen because in Central Europe it contains greater inter-annual JJA temperature variability than the last millennium (Stewart et al., accepted; Chapter 4). Therefore, it can provide information about the floods under a broad range of natural climate variability (e.g. including multiple analogues for a warmer 21st century).

In this paper, the following questions are investigated: (1.) What was the influence of long-term climate (i.e. cool/wet phases, warm/dry phases, cool/wet to warm/dry transitions and warm/dry to cool/wet transitions) on turbidite frequency and thickness in the sediments of Lake Silvaplana between ca. 1450 BC and AD 420? (2.) What was the influence of JJA temperatures on turbidite frequency and thickness in the sediments of Lake Silvaplana between ca. 570 BC and AD 120 (i.e. the years for which quantitative reconstructed JJA temperatures are available; Stewart et al., accepted; Chapter 4)? (3.) During windows with a trend and mean JJA temperature exceeding AD 1950 - AD 2000 (i.e. analogues for the

warmer 21st century), is turbidite frequency and thickness enhanced in the sediments of Lake Silvaplana?

c. Study site

Lake Silvaplana (1791 m a.s.l., between 46° 24' N, 9° 42' E and 46° 30' N, 9° 52' E) is located in the Upper Engadine valley of eastern Switzerland between Lakes Sils and Champfèr. Lake Silvaplana has a surface area of 2.7 km², a volume of 127×10⁶ m³ and a mean depth of 47 m (Figure 5.1; LIMNEX, 1994). Turnover occurs in May and November, stratification lasts from June to October and inverse thermal stratification (below ice cover) persists from January to May (LIMNEX, 1994; Ohlendorf, 1999).

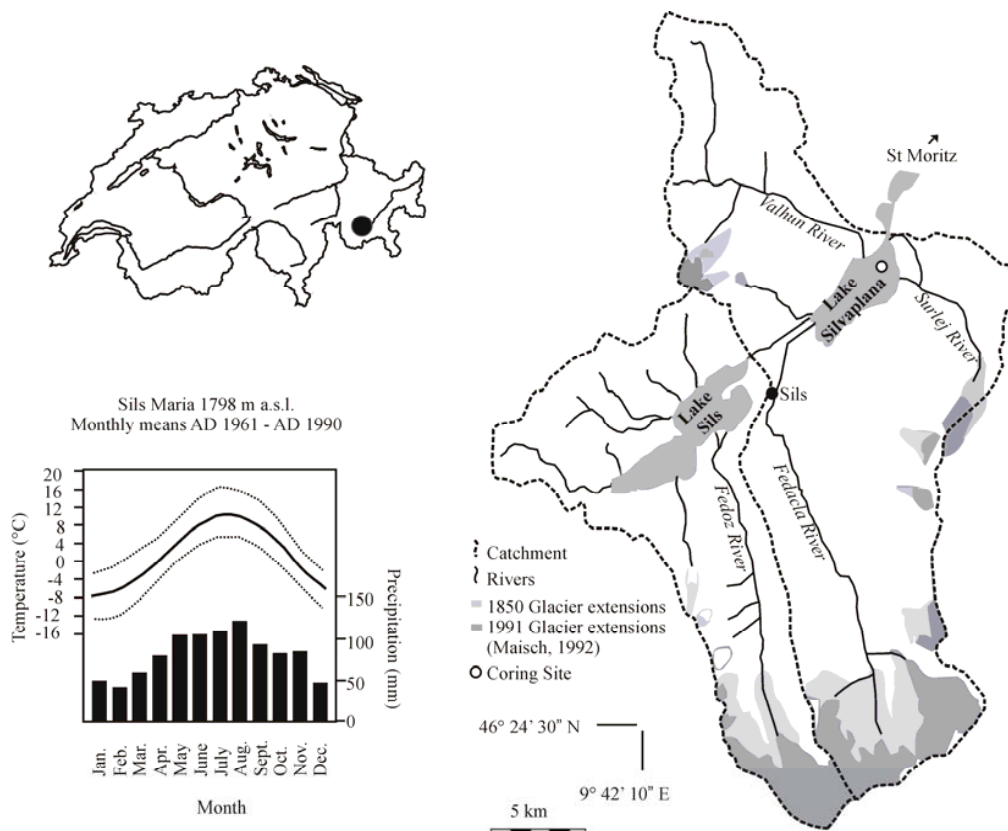


Figure 5.1 The Lake Silvaplana catchment including major fluvial systems, glacier cover and mean temperature and precipitation (Sils Maria; AD 1961 - AD 1990) (Mappad, 1996; Blass, 2006; MeteoSchweiz, 2010).

The catchment (175 km²) is underlain by three major tectonic nappes: the Lower Austroalpine Margna, the Upper Penninic Platta and the Lower Austroalpine Bernina

consisting of granite, gneiss and carbonate (AdS, 2004; Blass, 2006). As of 1999, 5% of the catchment was glacier-covered (Kääb et al., 2002; Paul et al., 2002; Paul, 2007).

Lake Silvaplana is connected to the catchment by the Inn River, the Fedaccla River, the Valhun and the Surlej Rivers (Blass, 2006). Inflowing water has an average residence time of eight months (LIMNEX, 1994).

A continental winter-dry climate dominates the region (MeteoSchweiz, 2010). In winter, temperature inversions favor the accumulation of cool and dry air in the Engadine valley, resulting in January to May ice-cover on the lake (Ohlendorf, 1999; MeteoSchweiz, 2010). Southerly moist air from over the Maloja Pass results in humid summers (Ohlendorf, 1999; MeteoSchweiz, 2010).

This climate favors larch (*Larix decidua*) and stone pine (*Pinus cembra*) vegetation in the catchment. Current tree-line (the elevation supporting trees >5 m tall) lies at 2410 m a.s.l. (Gobet et al., 2003). This region has sustained sporadic human settlements since the Mesolithic (e.g. artifacts from Valle Mesolcina date to 4850 BC). During the Bronze Age, copper prospecting expanded settlements near the Upper Engadine (e.g. Oberhalbstein). By the Iron and Roman Age, active trading across Alpine passes brought settlements to the Lower Engadine (Gobet et al., 2003).

d. Methods

Sampling

The lower six meters of a nine meter UWITEC piston core (winter, 2005) were investigated. The core was cut lengthwise and photographed (2300×1700 pixels). Half of the core was wrapped in polyethylene film and stored at 4°C until preparation of sediment blocks. The other half was flash-frozen with liquid nitrogen, covered in polyethylene film and preserved at -10°C until sub-sampling.

Dating

A turbidite with an erosive basal surface at 3 m depth (ca. AD 1177) prevented continuation of the varve chronology established for AD 1177 - AD 2000 (Trachsel et al., 2010; Stewart et al., accepted; Chapter 4). Therefore, three series of varve counts on polished sediment blocks were used to develop a floating varve chronology. For details regarding the construction of the polished sediment blocks the reader is directed to Stewart et al. (accepted; Chapter 4).

The three series of varve counts were combined with calibrated AMS radiocarbon dates (Poznań Radiocarbon Laboratory, Poland). Four radiocarbon dates from the (mostly

aquatic) organic carbon in bulk sediments (the upper sediment core; M. Trachsel, unpublished data) were subject to reservoir effects and consistently provided excessively old ages (i.e. ca. 7000 BC - 4000 BC; inset, Figure 5.3). This is likely related to carbonate bedrock in the catchment (Ohlendorf, 1999). Therefore, for this study, six radiocarbon dates were derived from terrestrial macrofossils. Turbidites were the only location where terrestrial macrofossils could be found and these materials could be reworked. Therefore, the radiocarbon dates from the terrestrial macrofossils are interpreted as maximum ages. To estimate the degree of reworking, the difference in calibrated radiocarbon dates and in varve counts from consecutive terrestrial macrofossils was evaluated.

Following calibration of the radiocarbon dates in Intcal04.14 (Reimer et al., 2004), the three varve chronologies were fit through a turbidite at ~4.4 m depth. The varve chronology which minimized the difference between varve counts and $\pm 2\sigma$ radiocarbon years is the final chronology. Therefore, all ages presented here are calculated from an annually resolved floating varve chronology anchored by calibrated radiocarbon dates (BC and AD). For more details, the reader is directed to Stewart et al. (accepted; Chapter 4).

Sedimentological analyses

Mass accumulation rates (MAR) were calculated from varve thickness, dry sediment density and porosity. The thickness of laminations was measured on the high-resolution (1200 dpi) scans of the polished sediment blocks with ImageJ software (Abramoff et al., 2004). Laminations exceeding 2σ of average varve thickness and/or having coarser grain sizes than surrounding sediments were interpreted as possible turbidites and excluded from MAR and varve counts.

Statistical analyses

Glacier length was reconstructed from the square-root of 100 year Loess low-pass filtered MAR ($MAR_{LP}^{1/2}$; Nussbaumer et al., accepted). The low-pass filter was set to a 100 year span to account for the time it takes larger glaciers in the Swiss Alps (e.g. the Grosser Aletschgletscher) to respond to long-term climate changes (i.e. temperature and/or precipitation). The square-root enabled comparison of glacier length changes to MAR (for additional detail consult Nussbaumer et al., accepted). Centennial anomalies (the difference between the 100 year average $MAR_{LP}^{1/2}$ and the record average) were used to estimate glacier high and low stands and therefore cool/wet and warm/dry climates, respectively. Centennial linear trends of $MAR_{LP}^{1/2}$ provided a record of glacier advances and retreats. These were used

to infer transitions between warm/dry and cool/wet climates or between cool/wet and warm/dry climates, respectively.

Centennial $MAR_{LP}^{1/2}$ anomalies and linear trends were compared to centennial turbidite frequencies and thicknesses. The records were ranked in descending order according to the $MAR_{LP}^{1/2}$ values (either anomalies or linear trends) and smoothed with a 100 year moving average. A Pearson correlation coefficient (r_{Pearson}) and p value (corrected for autocorrelation; p_{corr} ; Trenberth, 1984) was calculated to estimate the influence of long-term climate change (i.e. cool/wet or warm/dry phases, the transition from cool/wet to warm/dry phases and the transition from warm/dry to cool/wet phases) on turbidite frequency and thickness. These results were plotted and a linear regression tested whether the slope of the results were significantly different from zero.

June-July-August (JJA) temperatures from ca. 570 BC - AD 120 (quantitatively reconstructed from biogenic silica flux and chironomids; Stewart et al., accepted; Chapter 4) were used to compare centennial turbidite frequency and thickness to mean summer temperature. The data were ranked in descending order according to the centennial average JJA temperatures and smoothed with 100 year moving average. A Pearson correlation coefficient (r_{Pearson}) and p_{corr} were calculated to estimate the JJA temperature influence on turbidite frequency and thickness. These results were plotted and a linear regression tested whether the slope of the results were significantly different from zero.

To identify analogues for the warmer 21st century between ca. 1450 BC and AD 420, 50 year windows with warming trends and averages exceeding the AD 1950 - AD 2000 values were identified. The frequency and thickness of turbidites during these 50 year windows was compared to ca. 1450 BC - AD 420 averages.

Additional statistical methods include changepoint analysis (constrained hierarchical clustering; Juggins, 2009; R Development Core Team, 2009), cross-correlation analysis and calculation of average and standard deviation.

e. Results and Discussion

Lithology

Sediments throughout the section of interest consisted of a light-colored silt basal layer (summer) capped by a dark clay layer (winter). Couplets (average thickness: 1.4 mm) were consistent with the varve descriptions of Ohlendorf et al. (1997) and Blass et al. (2007). Varves were interrupted by 85 (average thickness: 8 mm) detrital-enriched and sandy deposits. In some cases, these were sufficiently thick that an inversely graded lower layer and

a normally graded upper layer were apparent. In other cases, these turbidites contained cross-laminations indicating a decreasing sediment load during waning of a flood (e.g. Mulder and Alexander, 2001). These 85 deposits were interpreted to be flood-induced turbidites ('inundites'; Figure 5.2).

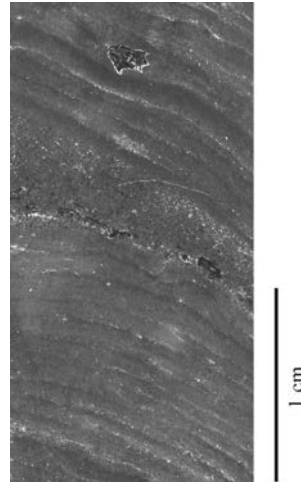


Figure 5.2 A high-resolution scan of a polished sediment block (approx. 5.77 m sediment depth) with a turbidite across the center. The base of each varve can be identified by the layers of lighter colored sediments.

Dating

Varve counts offered a chronology with inter-annual accuracy. The maximum difference between the varve counts, when fixed at a turbidite around 4.4 m, was 120 years. This difference could be related to falsely identifying laminations and the loss of varves through turbidity current erosion (Lamoureux and Bradley, 1996; Ojala, 2001).

Three calibrated radiocarbon dates (52 BC +/-71, 24 BC +/-82 and AD 16 +/-70; Table 5.1), taken from terrestrial macrofossils in two nearby turbidites, were internally consistent (i.e. the difference between the number of varves and number of calibrated radiocarbon years between the two turbidites was equivalent). This suggested that terrestrial macrofossils within these two sampled turbidites were not reworked. These three calibrated radiocarbon dates were also in accordance with calibrated radiocarbon date 916 BC +/-85. Alternatively, terrestrial-macrofossil derived calibrated radiocarbon dates 3493 BC +/-128 and 1213 BC +/-157 were anomalously old and were interpreted as reworked material (Wohlfarth et al., 1998). Therefore, only calibrated radiocarbon dates 916 BC +/-85, 52 BC +/-71, 24 BC +/-82 and AD 16 +/-70 were used in the final sediment chronology.

The first series of varve counts fit through the four accepted calibrated radiocarbon dates better than the other two series. These varve counts, combined with the four calibrated radiocarbon dates, suggested that the entire sediment section spanned approximately 1450 BC to AD 420 (+/-100) (Figure 5.3). For additional detail regarding the chronology, consult Stewart et al. (accepted; Chapter 4).

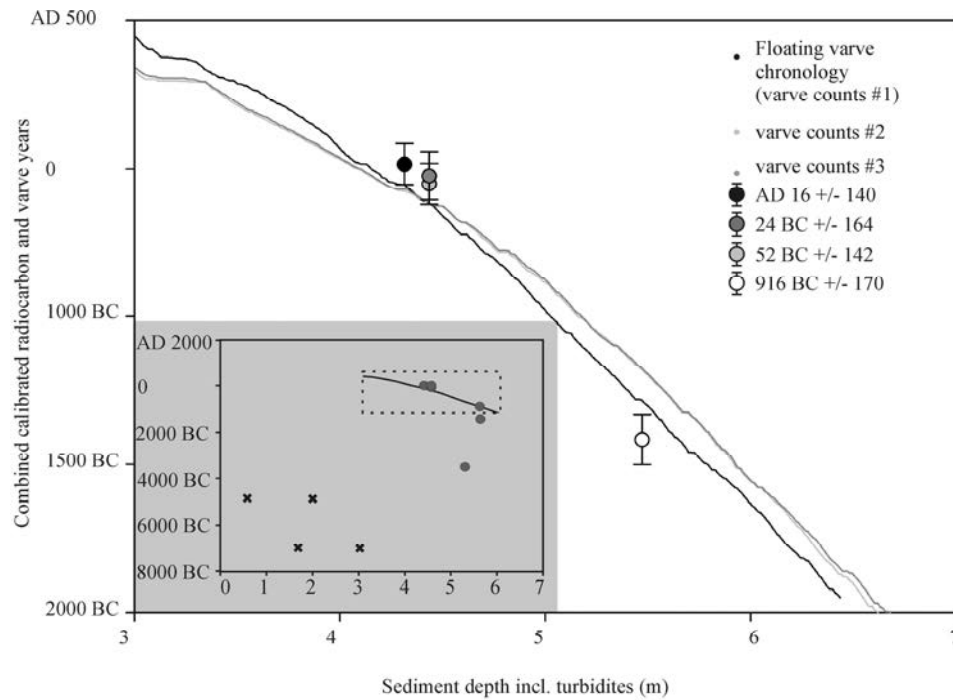


Figure 5.3 The age-depth model including the three series of varve counts and the four elected calibrated AMS radiocarbon dates with error bars denoting two standard deviations. The inset provides the complete record of calibrated radiocarbon ages. Grey circles represent terrestrial macrofossil-derived radiocarbon dates whereas black crosses signify the bulk sediment-derived radiocarbon dates (M. Trachsel, unpublished data).

Code Poz-	Depth in core (m)	Material	Context	Sample Mass (mg)	¹⁴ C age (+/- 1σ) BP	Cal. ¹⁴ C age (+/- 2σ) BC/AD
25246	~0.6	Bulk	Varves	16000	5950 +/- 60	4848 BC +/- 140
25245	~3.02	Bulk	Varves	58000	7890 +/- 40	6995 BC +/- 31
25243	~2.2	Bulk	Varves	14000	6000 +/- 40	4894 BC +/- 100
25242	~1.7	Bulk	Varves	8000	7860 +/- 50	6996 BC +/- 29
28061	~4.43	Needles	Turbidite	5.4	1985 +/- 35	AD 16 +/- 70
28062	~4.55	Needles	Turbidite	5	2020 +/- 30	52 BC +/- 71
28064	~4.55	Wood	Turbidite	7.2	2050 +/- 30	24 BC +/- 82
30292	~5.32	Needles	Turbidite	1	4665 +/- 35	3493 BC +/- 128
30293	~5.64	Needles	Turbidite	5	2765 +/- 35	916 BC +/- 85
30294	~5.64	Wood	Turbidite	4	2975 +/- 35	1213 BC +/- 157

Table 5.1 Calibrated AMS radiocarbon dates (Intcal04.14) from Lake Silvaplana and sample characteristics. Sediment depth (m) with turbidites.

Mass Accumulation Rate

MAR (ca. 1450 BC to AD 420; Figure 5.4a) averaged 169 mg/cm²/yr and had a standard deviation of 53 mg/cm²/yr. Changepoints in MAR were found around 380 BC, AD 50 and AD 130.

The MAR record was consistent with an independent MAR record also from the distal region of Lake Silvaplana (MAR_{LN}; Leemann and Niessen, 1994): following adjustment for a lag of 175 years (found through cross-correlation), there was a significant ($p < 0.01$) correlation between the two records and similar changepoints. This lag was consistent with the findings of Leemann and Niessen (1994) that the maximum difference between calibrated radiocarbon dates and varve counts in the MAR_{LN} chronology was 175 years.

As evident in Figure 5.4a, MAR was reduced between ca. 1450 BC and 900 BC with multi-decadal to centennial-scale oscillations. After 900 BC and until ca. 0, a millennial-scale increasing trend was super-imposed on these oscillations. After peaking at ~200 mg/cm²/yr at ca. 0, MAR decreased to 100 mg/cm²/yr where it remained until AD 100. This was followed by a rapid increase in MAR values. High MAR values persisted for the remainder of the record.

MAR-inferred phases of cool/wet and warm/dry phases (i.e. centennial anomalies in MAR_{LP}^{1/2}) and transitions between these phases (i.e. centennial trends in MAR_{LP}^{1/2}) were consistent with records of regional climate change from central european lake levels (Magny, 2004), the Grosser Aletschgletscher (Swiss Alps; Holzhauser et al., 2005), glaciers in the Grimsel region (Swiss Alps; Joerin et al., 2006), the Pasterze Glacier (Austrian Alps; Nicolussi and Patzelt, 2000), the Gepatschferner (Austrian Alps; Nicolussi and Patzelt, 2001), Oberer Landschitzsee (Austrian Alps; Schmidt et al., 2007) and Lake Le Bourget (French Alps; Debret et al., 2010) (Figures 5.4d-f).

Between ca. 1450 BC and 580 BC, negative centennial anomalies in MAR_{LP}^{1/2} suggested a warm/dry climate. An increasing centennial linear trend in MAR_{LP}^{1/2} from ca. 1340 BC coincided with elevated lake levels in Central Europe (Magny, 2004). This was followed by a decreasing centennial linear trend in MAR_{LP}^{1/2} after ca. 1250 BC which was consistent with a reduced length of the Grosser Aletschgletscher during the Bronze Age Optimum (Holzhauser et al., 2005). Another decreasing centennial linear trend in MAR_{LP}^{1/2} after ca. 1020 BC (partly overlapping with a dendroclimatology and GRIP inferred warm/dry phase; Tinner et al., 2003) coincided with a retreat of the Pasterze Glacier (Nicolussi and Patzelt, 2000), glaciers in the Grimsel region (Joerin et al., 2006) and the establishment of trees on the forefield of Gepatschferner (Nicolussi and Patzelt, 2001).

An increasing centennial linear trend in $MAR_{LP}^{1/2}$ after ca. 880 BC concurred with the flooding of lake-shore farmlands (Rychner et al., 1998; Tinner et al., 2003), higher lake levels in Central Europe (Magny, 2004), cool spring temperatures at Oberer Landschitzsee (Schmidt et al., 2007) and the Göschener cold phase I (approximately 1050 BC - 350 BC; Furrer, 2001). There were also two advances of the Grosser Aletschgletscher (Holzhauser et al., 2005).

Around 750 BC, a warming climate brought renewed farming north and south of the Alps and the transition from the Protogolasecca to Golasecca cultures (Tinner et al., 2003). Slightly warmer spring temperatures were also reconstructed from chrysophyte stomatocysts at Oberer Landschitzsee (Schmidt et al., 2007). This was reflected in negative $MAR_{LP}^{1/2}$ anomalies (ca. 750 BC - 666 BC).

Positive centennial anomalies of $MAR_{LP}^{1/2}$ around 580 BC to 400 BC coincided with elevated lake levels in Central Europe (Magny, 2004) and an extended Grosser Aletschgletscher (Holzhauser et al., 2005).

An increasing centennial linear trend in $MAR_{LP}^{1/2}$ from ca. 400 BC to 266 BC may be associated with the disappearance of farming locations in north and south of the Alps and in the Upper Engadine (Gobet et al., 2003). This was followed by brief decreasing centennial linear trend in $MAR_{LP}^{1/2}$ (ca. 265 BC - 166 BC) which coincided with a shift from the Golasecca to La Tène cultures (Tinner et al., 2003), a continued retreat of the Grosser Aletschgletscher (Holzhauser et al., 2005), reduced central european lake levels (Magny, 2004) and slightly warmer spring temperatures recorded by chrysophyte stomatocysts in Oberer Landschitzsee (Schmidt et al., 2007).

A shift to cooler conditions after ca. 210 BC was reflected in positive $MAR_{LP}^{1/2}$ anomalies (until approximately AD 50) and an increasing centennial linear trend in $MAR_{LP}^{1/2}$ from ca. 165 BC - 86 BC. This roughly coincided with an influx of glacial sediments in Lake Le Bourget (Debret et al., 2010).

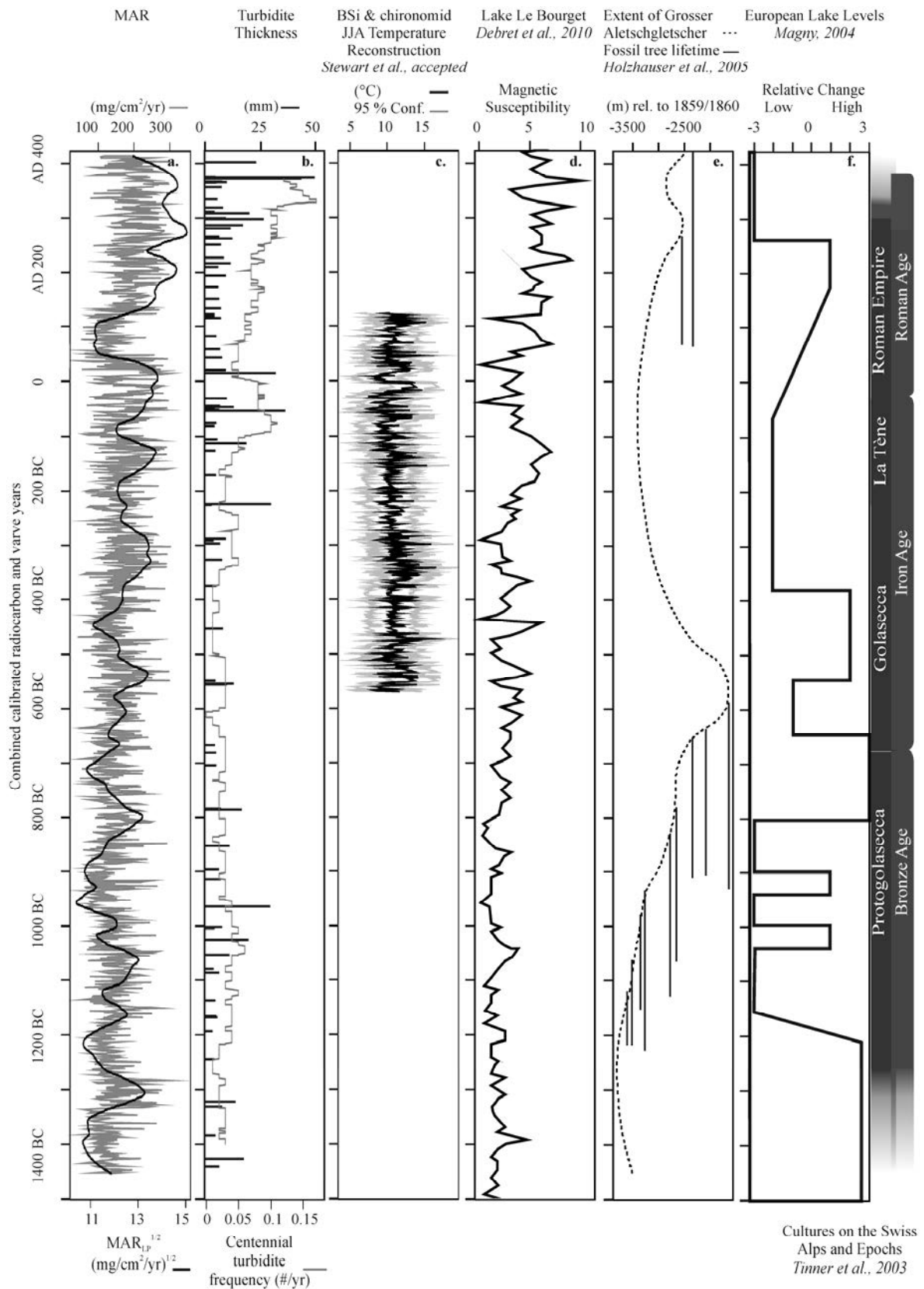


Figure 5.4 (a.) mass accumulation rates (MAR) overlain by $MAR_{LP}^{1/2}$, (b.) turbidite thicknesses and the centennial turbidite frequency, (c.) reconstructed June-July-August temperatures from biogenic silica (bSi) flux and chironomids (ca. 570 BC - AD 120) in the

sediments of Lake Silvaplana (Stewart et al., accepted; Chapter 4), (d.) the Lake Le Bourget magnetic susceptibility record (Debret et al., 2010), (e.) the Grosser Aletschgletscher extension curve (Holzhauser et al., 2005), (f.) lake level fluctuations in Central Europe (Magny, 2004). Cultures on the Alps and associated Epochs are presented alongside the aforementioned figures (Tinner et al., 2003).

Decreasing and increasing centennial linear trends in $MAR_{LP}^{1/2}$ occurred at ca. 85 BC to 31 BC and ca. 30 BC to AD 44, respectively. However, positive $MAR_{LP}^{1/2}$ anomalies persisted. Alternatively, negative $MAR_{LP}^{1/2}$ anomalies were associated with a glacier retreat from ca. AD 45 - AD 135 which was probably related to the Iron-Roman Age Optimum. Agriculture intensified north and south of the Alps and in the Upper and Lower Engadine, and roads were constructed over open passes (Gobet et al., 2003; Tinner et al., 2003). Furthermore, chrysophyte stomatocysts in Oberer Landschitzsee recorded positive spring temperature anomalies (Schmidt et al., 2007), the Grosser Aletschgletscher reached a minimum extent (Holzhauser et al., 2005), the Pasterze Glacier retreated (Nicolussi and Patzelt, 2000), there were two retreats of glaciers in the Grimsel region and a retreat of glaciers in the Bernina region (Joerin et al., 2006), and trees were established on the forefield of Gepatschferner (Nicolussi and Patzelt, 2001).

Around AD 136 to AD 335, increasing centennial linear trends in $MAR_{LP}^{1/2}$ occurred. At ca. AD 310, the maximum positive $MAR_{LP}^{1/2}$ anomaly from ca. 1450 BC - AD 420 was achieved. This roughly coincided with an advance of the Grosser Aletschgletscher (Holzhauser et al., 2005), a rise in lake levels in Central Europe (Magny, 2004) and increased glacial sediments in Lake Le Bourget (Debret et al., 2010).

Turbidite Thickness and Frequency

Turbidites (ca. 1450 BC to AD 420; Figure 5.4b) had an average thickness of 8 mm and a standard deviation of 9 mm.

The centennial frequency and thickness of turbidites was reduced for the first four hundred years of record ($\leq \sim 0.04$ per year and $\leq \sim 0.4$ mm per year, respectively; ca. 1450 BC - 1050 BC; Figure 5.4b). Both the centennial frequency and thickness was slightly elevated from ca. 1050 BC to 900 BC but returned to pre-1050 BC values from ca. 900 BC to 340 BC. Around 340 BC, turbidite frequencies up to 0.05 per year were reached. From approximately 95 BC to 65 BC, centennial turbidite frequencies were 0.1 per year. Concurrently, centennial turbidite thickness reached ~ 0.9 mm per year. Between ca. 65 BC and ca. 0, centennial

turbidite frequency decreased but centennial turbidite thickness exceeded 1 mm per year. Both centennial turbidite frequencies and thicknesses were slightly reduced from ca. 0 to AD 150. After AD 150, both values rose and reached the record (ca. 1450 BC - AD 420) maximum at ca. AD 330.

The influence of long-term climate (i.e. cool/wet phases, warm/dry phases, cool/wet to warm/dry transitions and warm/dry to cool/wet transitions) on turbidite frequency and thickness in the sediments of Lake Silvaplana between ca. 1450 BC and AD 420

In Figures 5.5a and b, MAR-inferred phases of cool/wet and warm/dry phases were compared to centennial turbidite frequency and centennial turbidite thickness. In Figures 5.5c and d, MAR-inferred transitions between cool/wet and warm/dry or between warm/dry and cool/wet phases were compared to centennial turbidite frequency and centennial turbidite thickness.

A significant positive correlation was found between $MAR_{LP}^{1/2}$ anomalies and turbidite frequency ($r_{\text{Pearson}} 0.86$ and $p_{\text{corr}} 0.01$) with a positive slope of the linear regression significantly different from zero. Negative $MAR_{LP}^{1/2}$ anomalies coincided with turbidite frequencies around 0.02 turbidites per year. During positive $MAR_{LP}^{1/2}$ anomalies, turbidite frequencies increased almost linearly up to ca. 0.12 turbidites per year.

A significant positive correlation was also found between $MAR_{LP}^{1/2}$ anomalies and turbidite thickness ($r_{\text{Pearson}} 0.85$ and $p_{\text{corr}} < 0.01$). The slope of the linear regression was positive and differed significantly from zero. Turbidite thicknesses were around 0.2 mm per year during negative $MAR_{LP}^{1/2}$ anomalies. As $MAR_{LP}^{1/2}$ anomalies became increasingly positive, turbidite thicknesses increased, reaching 1.2 mm/yr by $2.0 \text{ (mg/cm}^2\text{/yr)}^{1/2}$.

The rate of glacier advance or retreat had no significant correlation to turbidite frequency. Similarly, the rate of glacier advance or retreat had no significant correlation to turbidite thickness.

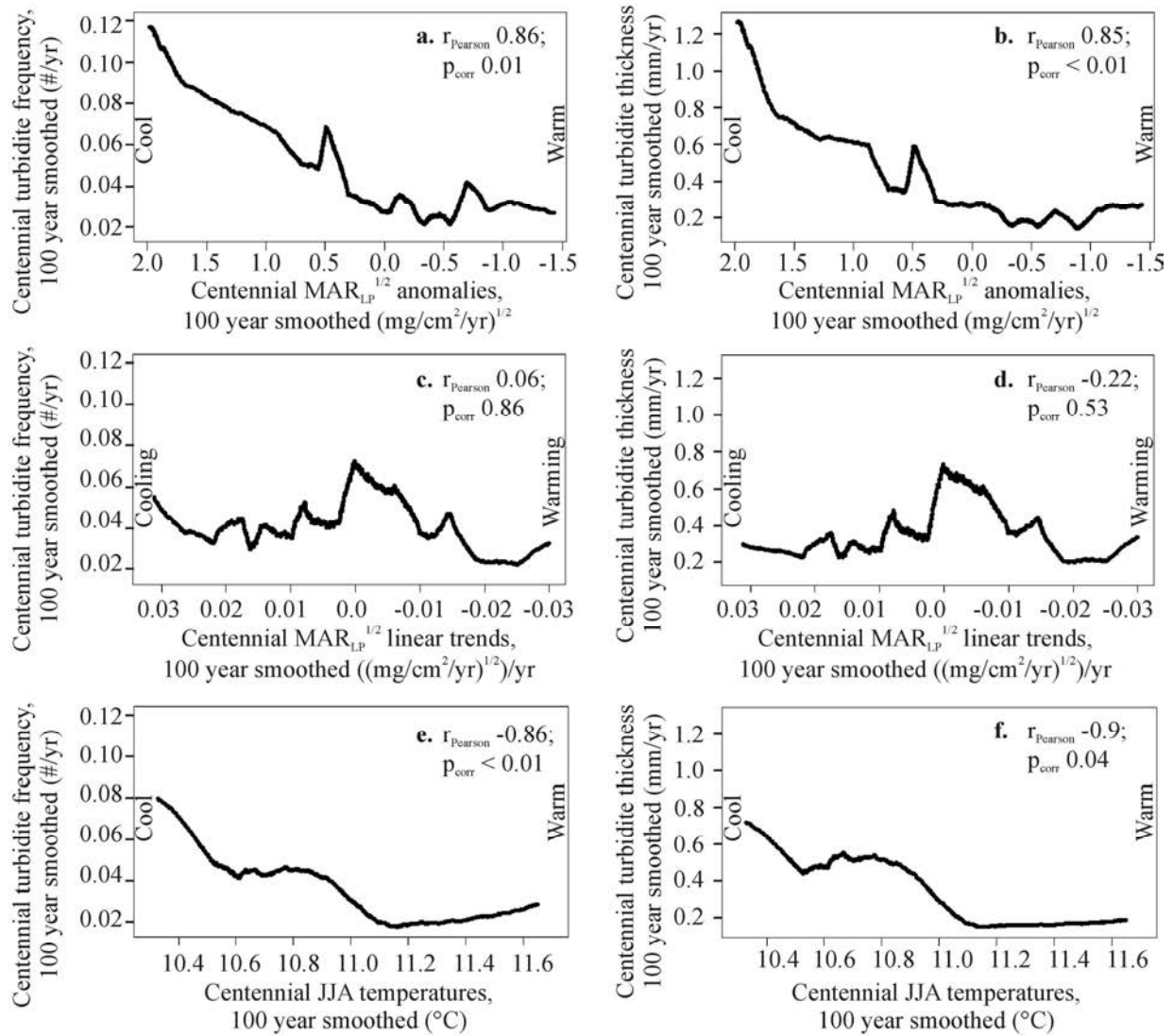


Figure 5.5 (a.) centennial anomalies in the square-root of low-frequency mass accumulation rates ($MAR_{LP}^{1/2}$) and centennial turbidite frequency, ranked according to $MAR_{LP}^{1/2}$ and 100 year smoothed (ca. 1450 BC - AD 420), (b.) centennial anomalies in $MAR_{LP}^{1/2}$ and centennial turbidite thickness, ranked according to $MAR_{LP}^{1/2}$ and 100 year smoothed (ca. 1450 BC - AD 420), (c.) centennial linear trends in $MAR_{LP}^{1/2}$ and centennial turbidite frequency, ranked according to $MAR_{LP}^{1/2}$ and 100 year smoothed (ca. 1450 BC - AD 420), (d.) centennial linear trends in $MAR_{LP}^{1/2}$ and centennial turbidite thickness, ranked according to $MAR_{LP}^{1/2}$ and 100 year smoothed (ca. 1450 BC - AD 420), (e.) centennial June-July-August (JJA) temperatures and centennial turbidite frequency, ranked according to JJA temperatures and 100 year smoothed (ca. 570 BC - AD 120), (f.) centennial JJA temperatures and centennial turbidite thickness, ranked according to JJA temperatures and 100 year smoothed (ca. 570 BC - AD 120).

The influence of JJA temperatures on turbidite frequency and thickness in the sediments of Lake Silvaplana between ca. 570 BC and AD 120

In Figures 5.5e and f, average centennial JJA temperatures were compared to centennial turbidite frequency and centennial turbidite thickness. This demonstrated a significant negative correlation between JJA temperatures and turbidite frequency ($r_{\text{Pearson}} -0.86$ and $p_{\text{corr}} < 0.01$) with a negative slope of the linear regression that differed significantly from zero.

The decrease in turbidite frequency with increased average centennial JJA temperature included several non-linearities. Turbidite frequency decreased with a warming climate until ca. 10.5°C. Turbidite frequency was unchanged from ca. 10.5°C to 10.9°C, and then decreased until 11.0°C. Above JJA temperatures of ca. 11.1°C, the turbidite frequency was unchanged.

A negative relationship was also found for JJA temperatures and turbidite thickness ($r_{\text{Pearson}} -0.9$ and $p_{\text{corr}} 0.04$). The negative slope of the linear regression significantly differed from zero. The decrease in turbidite thickness with increased JJA temperature was also interrupted by several non-linearities. From ca. 10.3°C to 10.5°C, the thickness of turbidites decreased. Turbidite thickness was unchanged from ca. 10.5°C to 10.9°C. After ca. 10.9°C, turbidite thickness decreased until 11.2°C.

The overall behavior of turbidites with changing JJA temperatures is consistent with the relationship between $\text{MAR}_{\text{LP}}^{1/2}$ anomalies and turbidites. This suggests that especially cool/wet phases during the investigated time window (ca. 1450 BC - AD 420) and phases of cool JJA temperatures during the window ca. 570 BC - AD 120 favored an increase in the frequency and magnitude of palaeofloods. However, these relationships are not linear.

Turbidite frequency and thickness in the sediments of Lake Silvaplana during windows with a trend and mean JJA temperature exceeding AD 1950 - AD 2000 (i.e. analogues for the warmer 21st century)

The relationship between turbidites and mean JJA temperatures was further investigated using 130 analogues (50 year windows) for a warmer 21st century in the Alps. These 50 year windows had an increasing trend and mean JJA temperature exceeding the Sils Maria AD 1950 - AD 2000 reference period (Sils Maria AD 1950 - AD 2000 JJA temperature trend=0.02°C/yr, $p=0.02$; average=9.8°C; MeteoSchweiz, 2010). Among these 130 windows, only 31 (24%) had a turbidite thickness and 35 (27%) had a turbidite frequency exceeding the ca. 1450 BC - AD 420 50 year averages (0.38 mm and 0.05 per year, respectively). Therefore,

the frequency and thickness of turbidites (i.e. the frequency and magnitude of palaeofloods) was not enhanced during warmer periods of ca. 570 BC - AD 120.

Finally, thicker and more frequent turbidites occurred in Lake Silvaplana during the 20th century (Sils Maria AD 1900 - AD 2000 JJA temperature average=9.7°C; Turbidite frequency=0.93 mm, Turbidite Thickness=0.2 per year) (Blass, 2006; MeteoSchweiz, 2010) than during the warmer ca. 570 BC - AD 120 (JJA temperature average=10.9°C; Stewart et al., accepted; Chapter 4). However, turbidite formation may have been influenced by hydrological engineering in the catchment in the 19th century (Gobet et al., 2003).

f. Conclusion

Future climate scenarios project an increase in the frequency and severity of summer-autumn floods in Central Europe in a warmer climate. However, model projections and flood records (i.e. historical and instrumental) of the recent past have yet to reach a consensus (e.g. Christensen and Christensen, 2003; Mudelsee et al., 2003).

Insight into the relationship between floods and climate, under a wide range of climate variability in Central Europe from ca. 1450 BC to AD 420, can be found in the sediments of Lake Silvaplana (Upper Engadine, Switzerland). The frequency and magnitude of local palaeofloods can be reconstructed from turbidite frequency and thickness, respectively. Long-term cool/wet and warm/dry climate phases can be reconstructed from anomalies in low-frequency mass accumulation rates (MAR). This is because low-frequency MAR reflects glacier lengths in the Swiss Alps and glacier lengths are a response to long-term climate conditions (e.g. Steiner et al., 2005). Transitions between cool/wet and warm/dry climate phases can be inferred from centennial trends in low-frequency MAR. Furthermore, quantitative absolute June-July-August (JJA) temperatures reconstructed from biogenic silica (bSi) flux and chironomids in the sediments of Lake Silvaplana are available from ca. 570 BC to AD 120 (Stewart et al., accepted; Chapter 4).

Comparison of turbidite frequency and thickness to MAR-inferred climate phases (ca. 1450 BC - AD 420) and JJA temperatures (ca. 570 BC - AD 120) suggests an increase in the frequency and magnitude of palaeofloods during cool/wet climates and windows of cooler JJA temperatures. Specifically, the frequency and thickness of turbidites were reduced during warm/dry climates of ca. 1450 BC to AD 420. Following the transition to cool/wet climates, the frequency and thickness of turbidites increased. However, no discernable relationship between the rate of transition from warm/dry to cool/wet climate and turbidite frequency or thickness could be found.

Increasing JJA temperatures from ca. 570 BC - AD 120 were matched by a decrease in the frequency and thickness of turbidites. However, the decrease was not linear. Finally, among 130 analogues (50 year windows) for warmer 21st century summers in the Alps, the average turbidite frequency and thickness was less than the ca. 1450 BC - AD 420 averages.

The findings of this study suggest that the frequency and magnitude of extreme summer-autumn precipitation events (i.e. flood events) and the associated atmospheric pattern in the eastern Swiss Alps was not enhanced during warmer (or drier) periods of ca. 1450 BC - AD 420. Therefore, evidence could not be found that summer-autumn floods would increase in the eastern Swiss Alps in a warmer climate of the 21st century. However, these findings need to be confirmed by independent (e.g. palaeoflood and modelling) studies.

References

- Abramoff, M.D., Magelhaes, P.J., Ram, S.J. 2004. Image Processing with ImageJ. *Biophotonics International* 11 (7): 36-42.
- AdS 2004. Atlas der Schweiz - Interactive CD, version 2.0. Swiss Federal Office of Topography, Wabern.
- Arnell, N., Liu, C. 2001. Hydrology and water resources, In: McCarthy, J.J., Canziani, O.F., Leary, N.A., Dokken, D.J., White, K.S. (eds.), *Climate Change 2001: Impacts, Adaptation and Vulnerability. Contribution of Working Group II to the Third Assessment Report of the Intergovernmental Panel on Climate Change*. Cambridge: Cambridge University Press, Chapter 4.
- Bagnold, R.A. 1962. Auto-suspension of transported sediment; turbidity currents. *Proceedings of the Royal Society of London* 265: 315-319.
- Blass, A. 2006. Sediments of two high-altitude Swiss lakes as high-resolution late Holocene paleoclimate archives. Inauguraldissertation der Philosophisch-naturwissenschaftlichen Fakultät der Universität Bern.
- Blass, A., Grosjean, M., Troxler, A., Sturm, M. 2007. How stable are twentieth-century calibration models? A high-resolution summer temperature reconstruction for the eastern Swiss Alps back to AD 1580 derived from proglacial varved sediments. *The Holocene* 17: 51-63.
- Brázdil, R., Glaser, R., Pfister, C., Stangl, H. 2002. Floods in Europe- A look into the Past. *Pages News* 10 (3): 21-23.
- Caviezel, G. 2007. Hochwasser und ihre Bewältigung anhand des Beispiels Oberengadin 1750-1900. Master's thesis for the History Institute of the Universität Bern.
- Christensen, J.H., Christensen, O.B. 2003. Climate modelling: Severe summertime flooding in Europe. *Nature* 421: 805-806.
- Debret, M., Chapron, E., Desmet, M., Rolland-Revel, M., Magand, O., Trentesaux, A., Bout-Roumazeille, V., Nomade, J., Arnaud, F. 2010. North western Alps Holocene paleohydrology recorded by flooding activity in Lake Le Bourget, France. *Quaternary Science Reviews* 29: 2185-2200.
- Desloges, J.R., Gilbert, R. 1994. The record of extreme hydrological and geomorphological events inferred from glaciolacustrine sediments, In: Olive, L.J., Loughran, R.J., Kesby, J.A. (eds.), *Variability in Stream Erosion and Sediment Transport*. International Association of Hydrological Sciences Publication No. 2 224, 133-142.
- Frei, C., Schär, C. 2001. Detection probability of trends in rare events: Theory and application to heavy precipitation in the Alpine region. *Journal of Climate* 14: 1568-1584.
- Furrer 2001. Alpine Vergletscherung vom letzten Hochglazial bis heute. Abhandlungen der Mathematisch-naturwissenschaftlichen Klasse, No. 3. Akademie der Wissenschaften und der Literatur, Mainz, 49 pp.

- Gilbert, R., Desloges, J.R. 1987. Sediments of ice-dammed, self-draining Ape Lake, British Columbia. *Canadian Journal of Earth Sciences* 24: 1735-1747.
- Gimmi, U., Luterbacher, J., Pfister, C., Wanner, H. 2007. A method to reconstruct long precipitation series using systematic descriptive observations in weather diaries: the example of the precipitation series for Bern, Switzerland (1760 - 2003). *Theoretical Applied Climatology* 87: 185 - 199.
- Gobet, E., Tinner, W., Hochuli, P.A., van Leeuwen, J.F.N., Ammann, B. 2003. Middle to Late Holocene vegetation history of the Upper Engadine (Swiss Alps): the role of man and fire. *Vegetation Historical Archaeobotany* 12: 143-163.
- Holzhauser, H., Magny, M., Zumbühl, H.J. 2005. Glacier and lake-level variations in west-central Europe over the last 3500 years. *The Holocene* 15 (6): 789-801.
- Joerin, U.E., Stocker, T.F., Schlüchter, C. 2006. Multicentury glacier fluctuations in the Swiss Alps during the Holocene. *The Holocene* 16 (5): 697-704.
- Juggins, S. 2009. RIOJA: Analysis of Quaternary Science Data, version 0.5-6. <http://cran.rproject.org/web/packages/rioja/index.html>
- Kääb, A., Paul, F., Maisch, M., Hoelzle, M., Haeberli, W. 2002. The new remote-sensing derived Swiss glacier inventory: II. First Results. *Annals of Glaciology* 34: 362 - 366.
- Kalnay, E., Kanamitsu, M., Kistler, R., Collins, W., Deaven, D., Gandin, L., Iredell, M., Saha, S., White, G., Woollen, J., Zhu, Y., Chelliah, M., Ebisuzaki, W., Higgins, W., Janowiak, J., Mo, K.C., Ropelewski, C., Wang, J., Leetmaa, A., Reynolds, R., Jenne, R., Joseph, D. 1996. The NMC/NCAR 40-Year Reanalysis Project. *Bulletin of American Meteorological Society* 77: 437-471.
- Kistler, R., Kalnay, E., Collins, W., Saha, S., White, G., Woollen, J., Chelliah, M., Ebisuzaki, W., Kanamitsu, M., Kousky, V., van den Dool, H., Jenne, R., Fiorino, M. 2001. The NCEP-NCAR 50-Year Reanalysis: Monthly Means CD-ROM and Documentation. *Bulletin of American Meteorological Society* 82: 247-267.
- Knighton, D., 1998. *Fluvial Forms and Processes: A new perspective*. London: Oxford University Press, 383 pp.
- Kundzewicz, Z.W., Ulbrich, U., Brücher, T., Graczyk, D., Krüger, A., Leckebusch, G.C., Menzel, L., Pińskwar, I., Radziejewski, M., Szwed, M. 2005. Summer Floods in Central Europe - Climate Change Track? *Natural Hazards* 36: 165-189.
- Lamoureux, S., Bradley, R.S. 1996. A late Holocene varved sediment record of environmental change from northern Ellesmere Island, Canada. *Journal of Paleolimnology* 16: 239-255.
- Leemann, A., Niessen, F. 1994. Holocene glacial activity and climatic variations in the Swiss Alps: reconstructing a continuous record from proglacial lake sediments. *The Holocene* 4: 259-268.

- LIMNEX 1994. Gewässerzustand und Gewässerschutzmassnahmen im Oberengadin. Bericht zuhanden des Amtes für Umweltschutz, Kanton Graubünden, 75 pp.
- Magny, M. 2004. Holocene climatic variability as reflected by mid-European lake-level fluctuations and its probable impact on prehistoric human settlements. *Quaternary International* 113: 65-79.
- Maisch, M. 1992. Die Gletscher Graubündens. Habil. Schrift Geographisches Institut Universität Zürich, Teil A und B Physische Geographie Vol. 33, 428 pp.
- Mappad Free Software 1996. <http://www.ngdc.noaa.gov/paleo/paleo.html>
- MeteoSchweiz 2010. http://www.meteoschweiz.admin.ch/web/de/klima/klima_heute_jahresverlaeufo_nbcn/Segl_Maria.html
- Mudelsee, M., Börngen, M., Tetzlaff, G., Grünewald, U. 2003. No upward trends in the occurrence of extreme floods in central Europe. *Nature* 425: 166-169.
- Mudelsee, M., Börngen, M., Tetzlaff, G., Grünewald, U. 2004. Extreme floods in central Europe over the past 500 years: Role of cyclone pathway "Zugstrasse Vb." *Journal of Geophysical Research* 109.
- Mulder, T., Alexander, J. 2001. The physical character of subaqueous sedimentary density flows and their deposits. *Sedimentology* 48: 269-299.
- Nicolussi, K., Patzelt, G. 2000. Discovery of early-Holocene wood and peat on the forefield of the Pasterze Glacier, Eastern Alps, Austria. *The Holocene* 10: 191-199.
- Nicolussi, K., Patzelt, G. 2001. Untersuchungen zur holozänen Gletscherentwicklung von Pasterze und Gepatschferner (Ostalpen). *Zeitschrift für Gletscherkunde und Glazialgeologie* 36: 1-87.
- Nussbaumer, S., Steinhilber, F., Trachsel, M., Breitenmoser, P., Beer, J., Blass, A., Grosjean, M., Hafner, A., Holzhauser, H., Wanner, H., Zumbühl, H. (accepted) Alpine climate during the Holocene: a comparison between records of glaciers, lake sediments and solar activity. *Journal of Quaternary Science*.
- Ohlendorf, C., Niessen, F., Weissert, H. 1997. Glacial varve thickness and 127 years of instrumental climate data: A comparison. *Climatic Change* 36: 391-411.
- Ohlendorf, C. 1999. High Alpine lake sediments as chronicles for regional glacier and climate history in the Upper Engadine, southeastern Switzerland. Berichte aus der Geowissenschaft Shaker Verlag, Aachen, 203 pp.
- Ojala, A. 2001. Varved Lake Sediments in Southern and Central Finland: Long varve chronologies as a basis for Holocene palaeoenvironmental reconstructions. Academic Dissertation, Geological Survey of Finland, Espoo, 41 pp.
- Paul, F. 2007. The new Swiss glacier inventory 2000 - application of remote sensing and GIS. Physische Geographie, Vol. 52. Geographisches Institut der Universität Zürich, Zürich, 210 pp.

- Paul F., Kääb, A., Maisch, M., Kellenberger, T., Haeberli, W. 2002. The new remote-sensing derived Swiss glacier inventory: I. Methods. *Annals of Glaciology* 34: 355-361.
- Pauling, A., Luterbacher, J., Casty, C., Wanner, H. 2006. Five hundred years of gridded high-resolution precipitation reconstructions over Europe and the connection to large-scale circulation. *Climate Dynamics* 26 (4): 387-405.
- Pfister, C., Weingartner, R., Luterbacher, J. 2006. Hydrological winter droughts over the last 450 years in the Upper Rhine basin: a methodological approach. *Hydrological Sciences Journal* 51 (5): 966-985.
- R Development Core Team 2009. R A language and environment for statistical computing. R Foundation for Statistical Computing. Vienna, Austria.
- Reimer, P.J., Baillie, M.G.L., Bard, E., Bayliss, A., Beck, J.W., Bertrand, C., Blackwell, P.G., Buck, C.E., Burr, G., Cutler, K.B., Damon, P.E., Edwards, R.L., Fairbanks, R.G., Friedrich, M., Guilderson, T.P., Hughen, K.A., Kromer, B., McCormac, F.G., Manning, S., Bronk Ramsey, C., Reimer, R.W., Remmele, S., Southon, J.R., Stuiver, M., Talamo, S., Taylor, F.W., van der Plicht, J., Weyhenmeyer, C.E. 2004. IntCal04 Terrestrial Radiocarbon Age Calibration, 0-26 cal kyr BP. *Radiocarbon* 46: 1029-1058.
- Rychner, V., Bolliger Schreyer, S., Carazzetti, R., David-Elbiali, M., Hafner, A., Hochuli, S., Janke, R., Rageth, J., Seifert, M. 1998. Geschichte und Kulturen der Bronzezeit in der Schweiz, In: Hochuli, S., Niffeler, U., Rychner, V. (eds.), Die Schweiz vom Paläolithikum bis zum frühen Mittelalter - Bronzezeit. Basel: Verlag Schweizerische Gesellschaft für Ur- und Frühgeschichte, 103-133.
- Schmidt, R., Kamenik, C., Roth, M. 2007. Siliceous algae-based seasonal temperature inference and indicator pollen tracking ca. 4,000 years of climate/land-use dependency in the southern Austrian Alps. *Journal of Paleolimnology* 38: 541-554.
- Schmocker-Fackel, P., Naef, F. 2010. Changes in flood frequencies in Switzerland since 1500. *Hydrology and Earth System Sciences* 14: 1581-1594.
- Steiner, D., Walter, A., Zumbühl, H.J. 2005. The application of a non-linear back-propagation neural network to study the mass balance of Grosse Aletschgletscher, Switzerland. *Journal of Glaciology* 51 (173): 313-323.
- Stewart, M., Larocque-Tobler, I., Grosjean, M. (accepted) Quantitative inter-annual and decadal summer temperature variability ca. 570 BC - AD 120 (Iron Age - Roman Period) reconstructed from the varved sediments of Lake Silvaplana, Switzerland. *Journal of Quaternary Science*.
- Sturm, M., Matter, A. 1978. Turbidites and varves in Lake Brienz (Switzerland): deposition of clastic detritus by density currents, In: Matter, A., Tucker, M.E. (eds.), Modern and Ancient Lake Sediments. Special Publications International Association of Sedimentologists. Oxford: Blackwell Scientific Publications, 147-168.
- Tinner, W., Lotter, A.F., Ammann, B., Conedera, M., Hubschmid, P., van Leeuwen, J.F.N., Wehrli, M. 2003. Climatic change and contemporaneous land-use phases north and south of the Alps 2300 BC to 800 AD. *Quaternary Science Reviews* 22: 1447-1460.

Trachsel, M., Eggenberger, U., Grosjean, M., Blass, A., Sturm, M. 2008. Mineralogy-based quantitative precipitation and temperature reconstructions from annually laminated lake sediments (Swiss Alps) since AD 1580. *Geophysical Research Letters* 35.

Trachsel, M., Grosjean, M., Larocque-Tobler, I., Schwikowski, M., Blass, A., Sturm, M. 2010. Quantitative summer temperature reconstruction derived from combined biogenic Si and chironomid record from varved sediments of Lake Silvaplana (south-eastern Swiss Alps) back to AD 1177. *Quaternary Science Reviews* 29 (19-20): 2719-2730.

Trenberth, K.E. 1984. Some effects of finite sample size and persistence on meteorological statistics. Part I: Autocorrelation. *Monthly Weather Review* 112: 2359-2368.

Trenberth, K.E., Jones P.D., Ambenje, P., Bojariu, R., Easterling, D., Klein Tank, A., Parker, D., Rahimzadeh, F., Renwick, J.A., Rusticucci, M., Soden, B., Zhai, P. 2007. Observations: Surface and Atmospheric Climate Change, In: Solomon, S., Qin, D., Manning, M., Chen, Z., Marquis, M.C., Averyt, K.B., Tignor, M., Miller, H.L. (eds.), *Climate Change 2007. The Physical Science Basis. Contribution of WG 1 to the Fourth Assessment Report of the Intergovernmental Panel on Climate Change*. Cambridge: Cambridge University Press.

Wohlfarth, B., Skog, G., Possnert, G., Homquist, B. 1998. Pitfalls in the AMS radiocarbon-dating of terrestrial macrofossils. *Journal of Quaternary Science* 13 (2): 137-145.

6. The potential of sediments from Lake Seeberg (Bernese Oberland, Switzerland) as an archive of past climate

Stewart, M., Grosjean, M., von Gunten, L., Kuglitsch, F.G., Larocque-Tobler, I., Kamenik, C. *Journal of Paleolimnology*, in preparation

a. Abstract

Long-term records of past climate are needed to contextualize recent climate change and to understand natural climate variability. However, instrumental records of past climate in Central Europe and the Swiss Alps rarely exceed the past 150 years. Fortunately, climate proxies can provide quantitative, high-resolution (up-to-annual) and long-duration (multi-millennial) reconstructions of past climate variability. Here, we evaluate the potential of recent sediments from Lake Seeberg (Bernese Oberland, Switzerland) as an archive of past climate. Up-to-annual measurements (ca. AD 1878 - AD 2005) were made of sedimentation rates, mass accumulation rates (MAR), biogenic silica (bSi), median grain size (D_{50}), loss-on-ignition (LOI) and scanning reflectance spectroscopy to assess their potential as climate proxies. Anomalous reflectance results were attributed to high water contents in the sediments and were not further explored as a climate proxy. We estimated the percent of autochthonous sediments (%AUTO) from the results of loss-on-ignition (%LOI₅₅₀ as %C_{org}, %LOI₉₅₀ as %CaCO₃) and biogenic silica concentration (%bSi as %bSiO₂). We estimated the percent of allochthonous sediments (%ALLO) from 100% - %AUTO, plus %CaCO₃. %CaCO₃ was included in both %AUTO and %ALLO because its origins in Lake Seeberg can be both autochthonous or allochthonous.

A steep increasing (long-term) trend after AD 1960 was found in sedimentary variables indicative of autochthonous productivity. A similar trend in warm-season (May-June-July-August-September; MJJAS) temperatures was found at nearby meteo-station Château-d'Oex. Consequently, we explored %AUTO as a proxy for MJJAS temperatures. With three year smoothing, an MJJAS and %AUTO regression model resulted in a root mean squared error of prediction (RMSEP) of 0.51°C, a reduction of error of 0.62 and a positive coefficient of efficiency of 0.03 (split-period approach). With the entire calibration period ($r_{\text{Pearson}}=0.76$, $p_{\text{corr}}<0.01$), the ten-fold cross-validated RMSEP decreased to 0.45°C.

These findings suggest that changes in autochthonous productivity in Lake Seeberg may be a reflection of warm season temperatures with the potential for reconstructing past MJJAS temperatures. However, the possible influence of eutrophication on %AUTO should be further investigated.

b. Introduction

Recent warming in Central Europe and the Alps (e.g. AD 1950 - AD 2000) has raised concerns about the response of the climate system to natural and anthropogenic forcings. For example, regional climate models project that Central Europe will be a 'hotspot' of increased inter-annual summer temperature variability and extremes under a generally warmer climate (Schär et al., 2004; Scherrer et al., 2006; Seneviratne et al., 2006; Parey et al., 2010). Other regional climate models suggest that continued climate warming will bring a higher frequency and magnitude of extreme precipitation and floods to Central Europe (Frei and Schär, 2001; Christensen and Christensen, 2003). However, many of these regional climate model projections have never been explored on long-term climate data because most meteo-stations in Central Europe have only been active for the past ca. 150 years (e.g. MeteoSchweiz, 2010).

Fortunately, long-term changes in the composition of lake sediments can provide quantitative, highly temporally resolved (up-to-annual) and long-duration (multi-millennial) reconstructions of natural climate variability in the past. This depends on an accurate sediment chronology, a recognized climate signal in the sediments, a long local homogenized instrumental record (e.g. Kuglitsch et al., 2009), and the appropriate choice of statistical calibration model (e.g. Esper et al., 2005; Trachsel et al., 2010a).

In high-altitude lakes which are not limited by nutrient availability or affected by extensive land-use (e.g. eutrophication; Blass et al., 2007b), elevated growing season temperatures have been shown to enhance primary productivity. This may be attributed to an extension of the growing season for photoautotrophs such as diatoms and chrysophytes (Smol, 1988; Battarbee, 2000; McKay et al., 2008).

Consequently, sedimentary indicators of primary productivity such as biogenic silica (bSi; a quantification of total diatom and chrysophyte abundance) have been used to reconstruct past temperatures. For example, bSi in the varved sediments of Lake Silvaplana, Switzerland, was used to reconstruct June-July-August (JJA) temperatures from AD 1177 - AD 1950 (Trachsel et al., 2010a) and from ca. 570 BC - AD 120 (Stewart et al., accepted; Chapter 4). In the sediments of Hallet Lake, Alaska, bSi was used to quantify JJA temperatures of the last two millennia (McKay et al., 2008).

The amount of chloropigments in organic-rich lake sediments may also be indicative of primary productivity (e.g. von Gunten et al., 2009). These pigments are related to photoautotroph abundance and can be measured rapidly and non-invasively with reflectance spectroscopy. For instance, Rein and Sirocko (2002) ascribed reflectance minima at 410 nm, 460 nm, 510 nm, 600-610 nm and 660-670 nm to diagenetic derivatives of chlorophyll.

Reflectance spectra from productive Lac La Biche (Alberta, Canada) revealed a reflectance trough centered at 675 nm in accordance with high-pressure liquid chromatography (HPLC) concentrations of chlorophyll-a and isomers (Wolfe et al., 2006). More recently, von Gunten et al. (2009) used the relative absorption band depth at 660-670 nm as an estimate of total sedimentary chlorin and the ratio of 660 nm to 670 nm as an indicator of pigment diagenesis in the highly organic sediments of Laguna Aculeo (Chile). Both of these variables had robust correlations to austral summer temperatures (December-January-February) (von Gunten et al., 2009).

Sediments from Lake Seeberg (Bernese Oberland, Switzerland) have vast potential as a climate archive. This is because Lake Seeberg sediments are biogenically varved (i.e. laminated with 2 diatom blooms per year) for the last ca. 2600 years except for the upper ca. 15 cm (Hausmann et al., 2002). Furthermore, the composition of Lake Seeberg sediments has been shown to be sensitive to both land-use and climate (van der Knaap et al., 2000; Hausmann et al., 2002; Larocque-Tobler et al., accepted).

Using calibration (i.e. instrumental) period sediments from Lake Seeberg, we investigate: (1.) How have recent sediments in Lake Seeberg changed? (2.) Can changes in sediments (i.e. in sedimentation rates, MAR, bSi, D₅₀, LOI, %AUTO and %ALLO) coinciding with the instrumental period (AD 1901 - AD 2005) be attributed to climate (temperature or precipitation) and be used to develop a calibration-in-time in order to reconstruct past climate?

c. Study site

Karstic Lake Seeberg (also known as Seebergsee; Bernese Oberland, Switzerland) contains two basins (9 m and 15.5 m) and has a maximum volume of ca. 4.4×10^{-4} km³. The catchment (0.23 km²; Figure 6.1) is covered by rocks, screes and bare ground (Guthruf et al., 1999). Soils along the eastern and southern shores are composed of quartz, clays, plagioclase and K-feldspar, and limestone. South-west of the lake, the land rises steeply. South-east of the lake, the outlet disappears in a doline.

Lake Seeberg is dimictic (mixings in June and November) and diatom blooms follow each mixis (Hausmann et al., 2002). Thermal stratification exists between mid-June and late October and inverse thermal stratification is found under the ice cover from December to May (Figure 6.2).

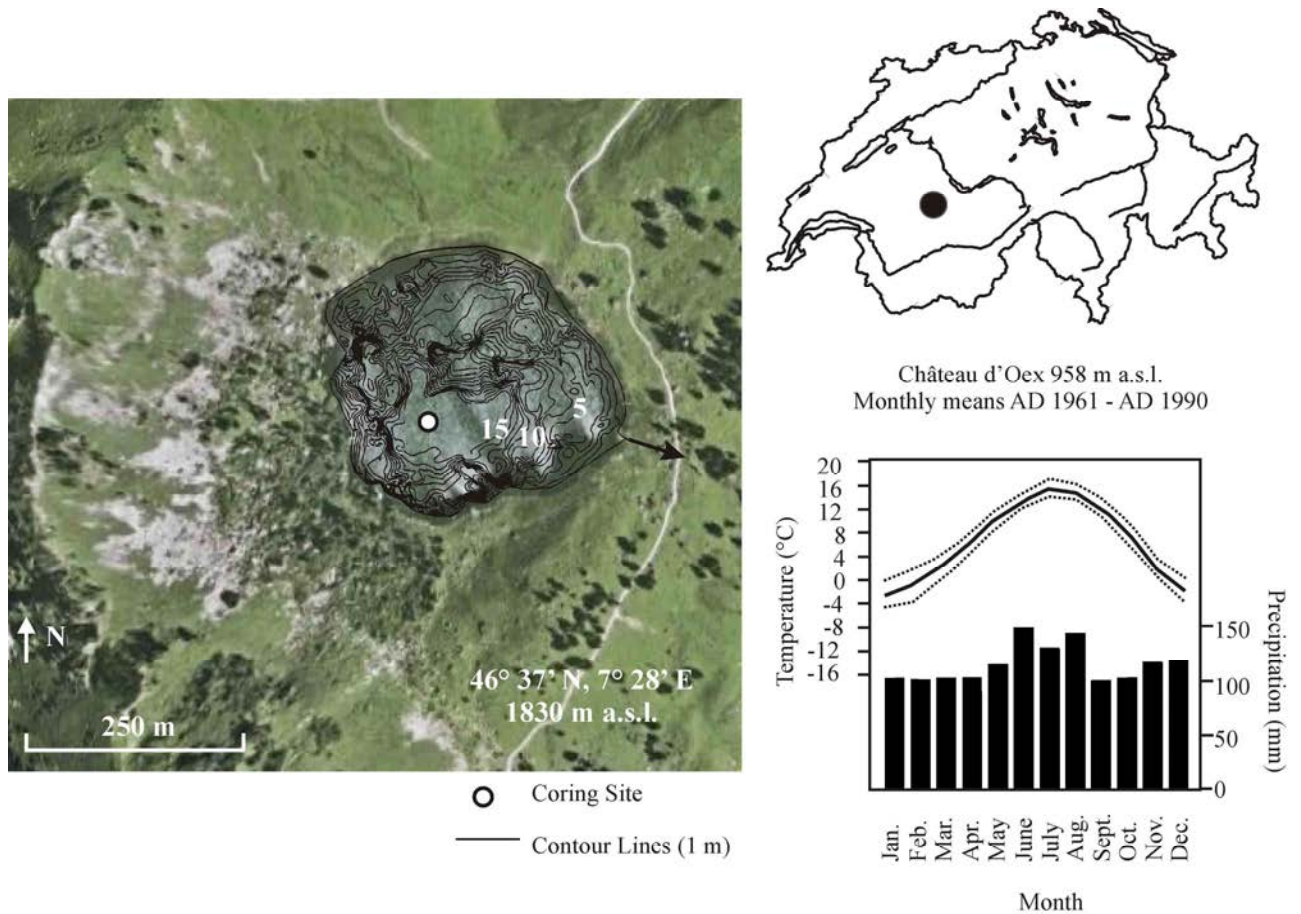


Figure 6.1 The Lake Seeberg catchment (modified from Hausmann et al., 2002; Google Earth, 2010; left), the location of Lake Seeberg in Switzerland (Mappad, 1996; upper right) and Château-d'Oex monthly temperature and precipitation means from AD 1961 to AD 1990 (MeteoSchweiz, 2010; lower right).

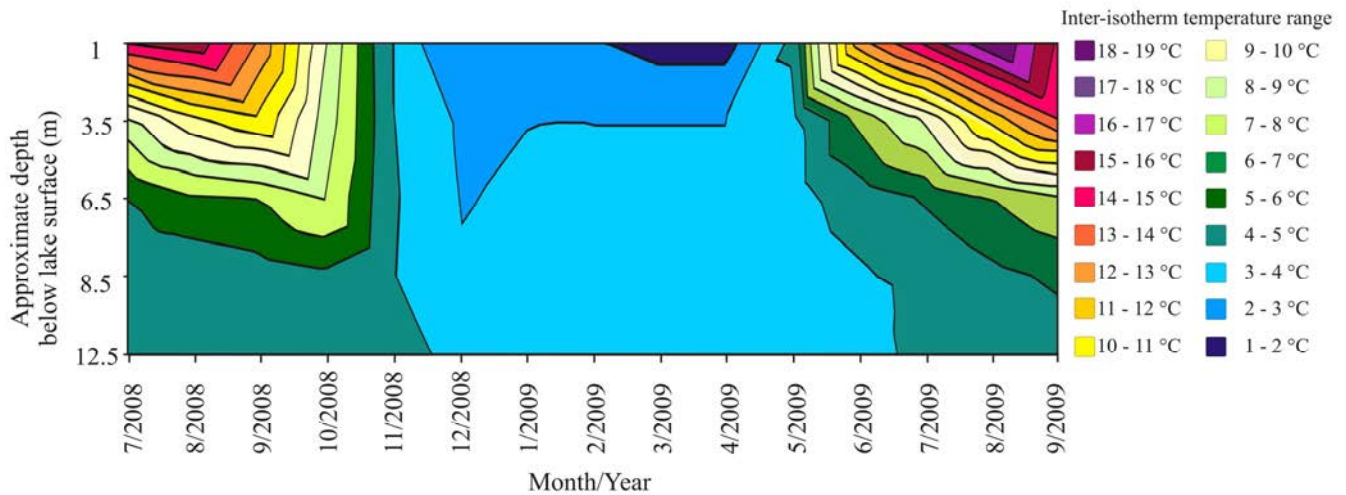


Figure 6.2 The thermal regime of Lake Seeberg from thermistors located 12.5 m, 8.5 m, 6.5 m, 3.5 m and 1 m below the water surface

Tree-line (the elevation supporting trees >5 m tall) is located at the lake. Vegetation consists of Alpine meadows with Norwegian spruce (*Picea abies*), green alder (*Alnus viridis*) and stone pine (*Pinus cembra*). Intensified land-use in the catchment from ca. AD 1350 to AD 1670 caused a hypertrophy of the lake (Hausmann et al., 2002). Currently, 14% of the catchment is used for cattle grazing (Guthruf et al., 1999).

The water chemistry of Lake Seeberg is seasonally and annually variable (Figure 6.3). In July 2008, profiles of conductivity, pH, total cation hardness and total anion hardness were approximately uniform with depth. Alternatively, in July 2009, a chemocline was observed around 7-8 meters below the lake surface. In August 2009, the chemocline reached depths of 11 meters, but reappeared at 7-8 meters below the lake surface in October. Sediment trap data can be found in Appendix D.

Blue-green algae are found in the lake during the summer and purple sulphur-reducing bacteria are present in the deep and anoxic regions of the lake (Hausmann et al., 2002 and personal observation).

The climate of the region is high-altitude temperate (Peel et al., 2007). At nearby meteo-station Château-d'Oex (958 m a.s.l.), January temperatures averaged -2.7°C (reference period=AD 1961 - AD 1990; MeteoSchweiz, 2010). During the same reference period, July temperatures at Château-d'Oex averaged 15°C and maximum precipitation occurred in June (MeteoSchweiz, 2010).

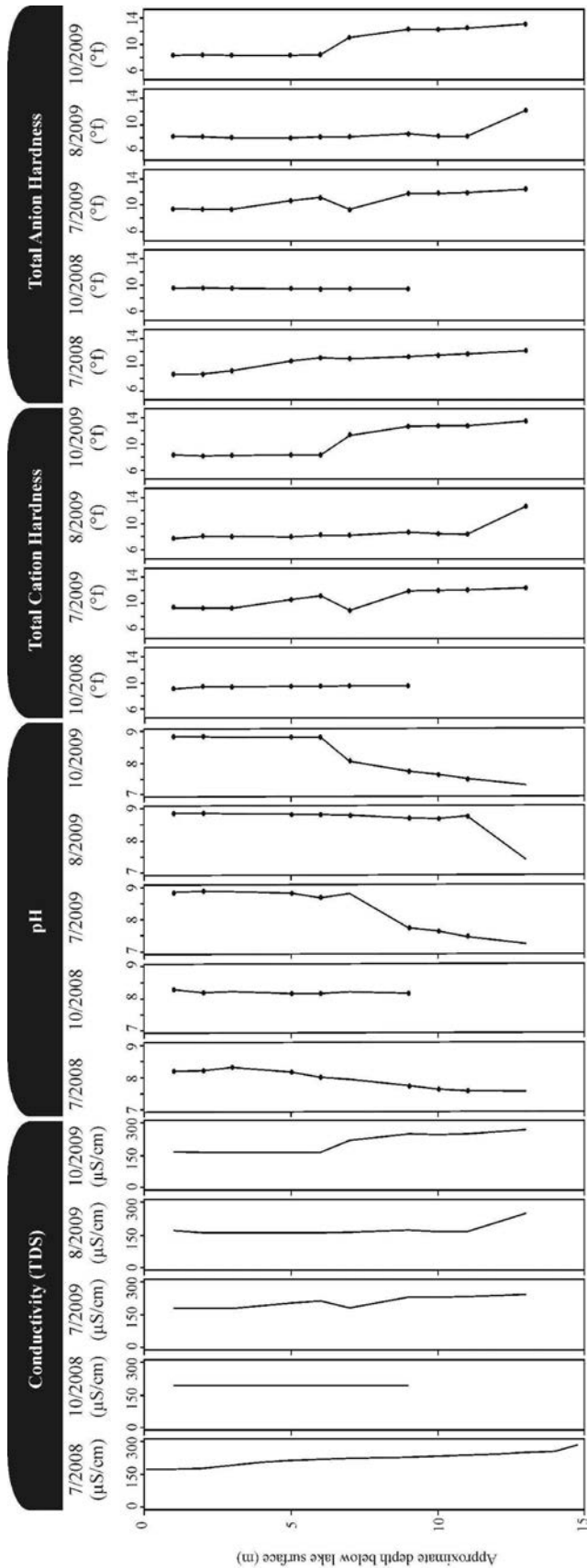


Figure 6.3 Water chemistry measurements (Conductivity, pH, Total Cation Hardness and Total Anion Hardness) from Lake Seeberg taken in 7/2008, 10/2008, 7/2009, 8/2009 and 10/2009.

d. Methods

Coring

A three meter Niederreiter freeze core was recovered from the deepest basin of Lake Seeberg in the winter of 2005. During the same field campaign, a supplementary UWITEC gravity core (ca. 1.5 m) was taken from this basin. All analyses except for spectrophotometry were conducted on the freeze core.

The freeze core was transported to the laboratory where it was photographed with a Nikon D80 digital camera (2300×1700 pixels; Appendix A). The core was wrapped in polyethylene film and stored at -10°C until sub-sampling. For this study, a focus is placed on recent sediments (i.e. sediments coinciding with the age-depth model; ca. AD 1878 - AD 2005; ca. 0-25 cm) and the Château-d'Oex instrumental period (AD 1901 - AD 2005).

Chronology

Varves were counted on resin-embedded blocks and thin sections from the upper 25 cm of the Lake Seeberg freeze core. Slabs of frozen sediment (20×2×1 cm) were created with a bone saw. The slabs were lyophilized, placed in aluminum trays and submerged in an epoxy resin composed of NSA, ERL, DER and DMAE (Lamoureux, 1994; Lotter and Lemcke, 1999). The resin was set overnight at 70°C and the slabs were cut into polished blocks and 30 µm thin sections at GEOPREP (University of Basel, Switzerland). The polished blocks and thin sections were scanned at 1200 dpi and viewed in ImageJ software (Abramoff et al., 2004).

As found by Hausmann et al. (2002), varves (i.e. couplets composed of dark organic and light carbonate laminations with ca. 2 diatom blooms per year) were only apparent below ca. 15 cm in the sediment core. Therefore, we used radionuclides and spheroidal carbonaceous particles (SCPs) to establish a chronology for the upper 25 cm of sediments.

EAWAG (Dubendorf) provided ^{210}Pb (at 46.5 keV) and ^{137}Cs (at 662 keV) values for twenty-five consecutive sediment samples (0-25 cm depth; 6 cm³ each). ^{210}Pb forms when ^{238}U decays into ^{226}Ra and then into ^{222}Rn . ^{226}Ra and $^{210}\text{Pb}_{\text{total}}$ are in disequilibrium because during the decay of ^{226}Ra in soil some of the gaseous isotope ^{222}Rn diffuses into the atmosphere. Alternatively, the ^{210}Pb which forms from the decay of ^{226}Ra in soil is in equilibrium with ^{226}Ra ($=^{210}\text{Pb}_{\text{supported}}$). $^{210}\text{Pb}_{\text{unsupported}}$ (i.e. the ^{210}Pb which forms in the atmosphere) is returned to the land, lakes and oceans through wet or dry deposition from the atmosphere (Appleby, 1997 and 2002). Most relevant for ^{210}Pb dating is the amount of $^{210}\text{Pb}_{\text{unsupported}}$. This is found by subtracting ^{226}Ra from $^{210}\text{Pb}_{\text{total}}$ at each level (Appleby, 1997

and 2002). ^{137}Cs indicates thermo-nuclear tests (starting at ca. 1954 and peaking at ca. 1963) and the Chernobyl accident in AD 1986 (Appleby, 1997 and 2002).

Spheroidal Carbonaceous Particles (SCPs) indicate fossil fuel combustion which reached an apex in the Swiss Alps around AD 1977 (Lotter et al., 2002). SCPs were counted on thirty-two consecutive sediment samples (0-29.5 cm) prepared according to the method used in Grob (2008). Organic matter was removed with hydrogen peroxide (32%) and carbonates and iron oxides were eliminated with hydrochloric acid (10%). SCPs were distinguished under magnification by shape (spheroidal), color (black), porosity, size (ca. 5-10 μm) and fragility (Rose, 2001; Grob, 2008). SCP counts were converted to SCPs per gram of dried sediment.

The results of ^{210}Pb measurements were put in the Constant Rate of Supply (CRS) model and the Sediment Isotope Tomography (SIT) model (Liu et al., 1991; Appleby, 2002; Carroll and Lerch, 2003). We elected the model which was most consistent with independent stratigraphic markers to be the final calibration period chronology [e.g. the introduction of ^{137}Cs (ca. AD 1954; Appleby, 1997 and 2002), the peak of ^{137}Cs (ca. AD 1963; Appleby, 1997 and 2002; Hausmann et al., 2002), the appearance of SCPs (ca. AD 1880 in the Swiss Alps; Rose, 2001) and the peak of SCPs (ca. AD 1977 \pm 4 in the Swiss Alps; Lotter et al., 2002)].

Scanning Reflectance Spectroscopy and Spectrophotometry

Scanning reflectance spectroscopy was conducted on thawed sediments from the Lake Seeberg freeze-core with a hand-held Gretag Macbeth Spectrolino (sensor aperture: 2.5 mm, spectral range: 380-730 nm, resolution: 3 nm integrated to 10 nm bands, measurements at 2 mm intervals) (Trachsel et al., 2010b).

First, we calibrated the Spectrolino against a white ceramic reference piece (Barium Sulfate; BCA) in polyethylene film (Rein and Sirocko, 2002). Then, we used a knife to remove oxidized sediments from the surface. The high water content of the sediments (ca. AD 1878 - AD 2005 average=95%) made it difficult to remove the oxidized surface without disturbing the lower sediment. The sediment surface was wrapped in polyethylene film to prevent further oxidation and to protect the Spectrolino sensor (Rein and Sirocko, 2002). Air bubbles were gently expelled with a soft-bristle brush.

The raw reflectance data were divided by the reflectance of the polyethylene-covered BCA (Rein and Sirocko, 2002). The reflectance data were assigned years based on the depths of the age-depth model.

To interpret the reflectance spectroscopy results, the average reflectance spectrum was plotted and overlain with the second derivative (Stephens et al., 2003). This highlighted changes in the slope of the spectrum including two reflectance troughs (from R₅₉₀ to R₆₄₀ and from R₆₄₀ to R₇₂₀) (Figure 6.4).

We used two published algorithms to describe the trough from R₆₄₀ to R₇₂₀ and the minimum (Relative Absorption Band Depth, RABD) around 665 nm (Table 6.1).

Algorithm		
Trough ₆₅₀₋₇₀₀	$\frac{[(R_{650} * 51) + ((R_{700} - R_{650}) * 51) / 2] - \sum R_{650-700}}{R_{\text{mean}}}$	(Wolfe et al., 2006)
RABD _{660:670} dR _{mean}	$\frac{(((6 * R_{590} + 7 * R_{730}) / 13) R_{\text{min}(660,670)})}{R_{\text{mean}}}$	(Rein and Sirocko, 2002)

Table 6.1 Published reflectance algorithms used for the sediments of Lake Seeberg

However, no published algorithms could be found which describe the trough from R₅₉₀ to R₆₄₀. Therefore, we adapted the Trough₆₅₀₋₇₀₀ equation from Wolfe et al. (2006) (Table 6.2). In an effort to account for changes in the water content of the sediments, the algorithm was divided by the average reflectance (R_{mean}; Balsam et al., 1998).

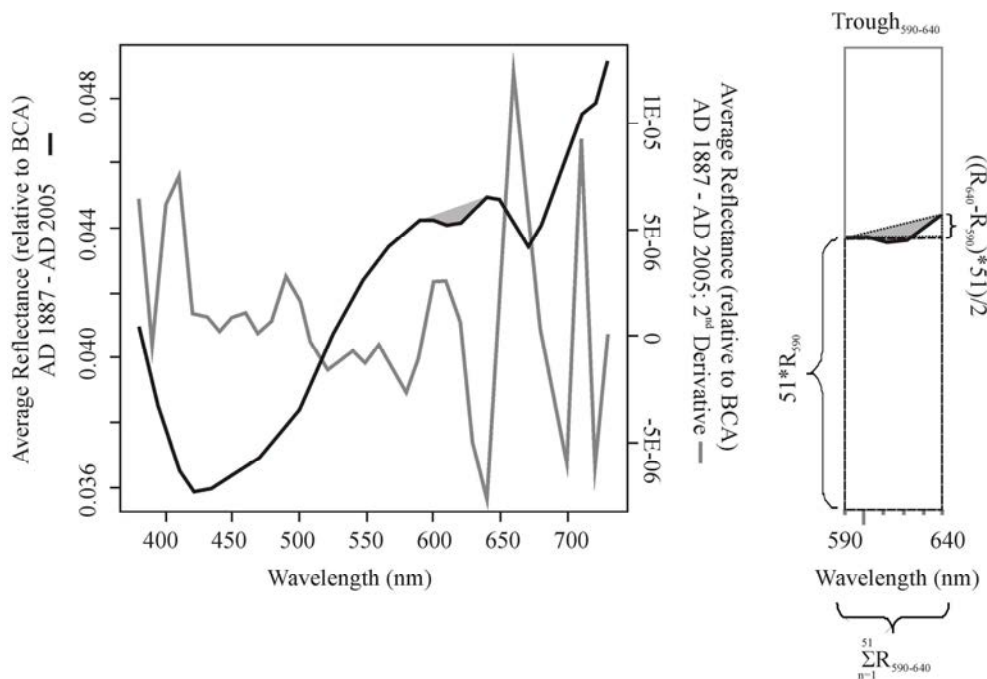


Figure 6.4 Average reflectance spectrum overlain by the second derivative (left) and calculation of the Trough₅₉₀₋₆₂₀ (right).

Algorithm	
Troughs ₅₉₀₋₆₄₀	$\frac{[(R_{590} * 51) + ((R_{640} - R_{590}) * 51) / 2] - \sum R_{590-640}}{\sum R_{590-640}}$
Troughs ₅₉₀₋₆₄₀ dR _{mean}	$\frac{[(R_{590} * 51) + ((R_{640} - R_{590}) * 51) / 2] - \sum R_{590-640}}{R_{mean}}$

Table 6.2 Custom reflectance algorithms used for the sediments of Lake Seeberg

In addition, we transformed the reflectance spectra of Lake Seeberg sediments into the L*a*b* color space. First, raw reflectance spectra were transformed into an XYZ coordinate system where Y indicates luminance (i.e. greyscale), and X and Z represent colors. In an additional step, the XYZ coordinate system was transformed into L*a*b*. Details regarding the calculations can be found in Nederbragt et al. (2004) and Lindbloom (2011).

The color of sediments can indicate changes in composition (e.g. mineralogy, pore water content) related to the provenance or depositional environment (Andrews and Freeman, 1996). In the L*a*b* color space, L* values range from 0 (black) to 100 (white), indicating the lightness of sediments. a* reflects changes from green (negative values) to red (positive values). b* indicates changes from blue (negative) to yellow (positive) (Nederbragt et al., 2004).

Although L*a*b* has typically been applied to studies of marine (rather than lake; e.g. Andrews and Freeman, 1996) sediments, we assume that L*a*b* is equally sensitive to changes in the composition of lake sediments.

To verify our reflectance results, we applied spectrophotometry to twelve ca. 1 cm³ sub-samples from the Lake Seeberg gravity core (0-15 cm depth with sub-samples at 2, 4 and 14 cm excluded). The sediments were freeze-dried and approximately 200 mg of each sample was placed in a 22 ml tube. Acetone was used to extract organic pigments (Routh et al., 2009) in a 200 Dionex Accelerated Solvent Extractor (ASE). The sediment residue was flushed with 60% of the initial solvent volume (ca. 14 ml) and the extracts were poured into 50 ml volumetric flasks to achieve equal concentrations.

A Shimadzu Spectrophotometer UV-1800 measured absorption spectra (330 nm to 800 nm; 1 nm resolution) for the extracts. The results were opened with UVProbe software. This revealed an absorption pattern consistent with the average reflectance spectrum of the Lake Seeberg freeze core (i.e. an absorption maximum at 610 nm and an absorption maximum at 665 nm).

According to Louda et al. (2002), reflectance minima (or absorption maxima) around 610 nm and 665 nm indicate chlorophyll degradation products. Thus, changes in these reflectance minima could reflect variable organic contents.

Sub-sampling

The remaining sediments from Lake Seeberg (i.e. those not used for the chronology or reflectance spectroscopy; ca. 0-25 cm) were sub-sampled at up-to-annual resolution for mass accumulation rates (MAR), biogenic silica (bSi), median grain size (D_{50}) and loss-on-ignition (LOI).

The frozen sediments were placed in a metal core holder lined with blocks of dry ice to prevent thawing during sub-sampling. Thumb-tacks were inserted into the sediments at ca. 10 year intervals according to the age-depth model. A hand-held band saw was used to remove near-annual layers of frozen sediment. Half of each sub-sample was put aside for measurements of MAR, bSi and D_{50} . The other half of each sub-sample was reserved for LOI. In some instances, these sub-samples represented small amounts of sediment (i.e. freeze-dried, ca. 50 mg). Therefore, adjacent pairs of samples were combined prior to measuring bSi, D_{50} and LOI. These results were regularized to obtain annual values.

Mass Accumulation Rate

Mass accumulation rates were determined from sedimentation rates and porosity using a modified (i.e. organic carbon was not included in the calculation) version of the methods of Berner (1971) and Niessen et al. (1992). Sedimentation rates were approximated through linear interpolation between age-depth model points. Because the age-depth model consisted of only 17 data points, sedimentation rates (and MAR) should be interpreted cautiously. Porosity was determined from water content (i.e. the loss in sediment weight following freeze-drying), dried sediment density (ca. 2.65 g/cm^3 for quartz; Blass et al., 2007a) and pore water density.

Biogenic silica

Biogenic silica concentrations (%bSi) were measured on ca. 100 mg of sediment per sub-sample following the method of Ohlendorf and Sturm (2008). Organic matter was removed with H_2O_2 (30%). The sediments were cleaned with distilled water, freeze-dried and placed in tubes. Each tube received 10 ml of 1 M NaOH and was placed in an ultrasonic bath. Upon removal, the tubes were capped, shook with a mini-shaker ($>2500/\text{minute}$), and placed for one hour in an oven heated to 90°C . These last three steps were repeated three times. The tubes were centrifuged and, in separate tubes, $700 \mu\text{l}$ of the supernatant was combined with $70 \mu\text{l}$ of 65% HNO_3 and Milli-Q-Water. %bSi was measured on an inductively coupled plasma optical emission spectrometer (ICP-OES) at the Paul Scherrer Institute (Switzerland). Results were

corrected for lithogenic silica (Al:Si ratio 2:1) and %bSi was converted to bSi flux by multiplying by MAR (Blass et al., 2007a; Ohlendorf and Sturm, 2008). Because of the influence of sedimentation rates and MAR on the structure of bSi flux, these values should be interpreted prudently. %bSi was also presented as %bSiO₂ (for calculation of %AUTO) using the relative atomic mass of Si (28) and O₂ (2*16).

Grain size

Laser particle size was measured on sediments following digestion of organic matter with H₂O₂ (30%) and bSi with NaOH (1 M). Each measurement was repeated three times on a Malvern Mastersizer Hydro 200S at the ETH Zurich (Switzerland). Values are presented as the median grain size (D₅₀).

Loss-on-ignition

Sequential loss-on-ignition was measured according to the protocols of Dean (1974) and Heiri et al. (2001). First, sediments were oven-dried at 105°C, homogenized with a mortar and pestle and placed in pre-weighed crucibles. The weight of the dried sediments (=DW₁₀₅) was recorded. The crucibles were transferred to a furnace for one hour at 550°C. The crucibles were removed from the furnace, placed in a desiccator containing blue silica crystals to prevent uptake of moisture during cooling and then reweighed (=DW₅₅₀). The crucibles were returned to the furnace for one hour of heating at 950°C. Again, the crucibles were removed from the furnace and placed in the desiccator containing blue silica crystals to cool prior to reweighing (=DW₉₅₀).

The percent loss of weight between DW₁₀₅ and DW₅₅₀, %LOI₅₅₀, is composed of CH₂O. This was multiplied by the relative atomic mass of CH₂O (30) divided by the relative atomic mass of C (12) to find organic carbon (%C_{org}). The percent loss of weight between DW₅₅₀ and DW₉₅₀, %LOI₉₅₀, consists of carbon dioxide (CO₂) and was multiplied by the relative atomic mass of CaCO₃ (100.088) divided by the relative atomic mass of CO₂ (44.009) for an estimate of calcium carbonate (%CaCO₃) (adapted from Heiri et al., 2001).

Percent Autochthonous Sediments and Percent Allochthonous Sediments

For an estimate of the autochthonous proportion (%AUTO) of sediments, we found the sum of %bSiO₂, %C_{org} and %CaCO₃. The percent of allochthonous sediment (i.e. %ALLO; e.g. quartz, clays, plagioclase and K-feldspar, and limestone) was estimated from 100% - %AUTO, plus %CaCO₃. Please note that %CaCO₃ was included in both variables because it

is presently not known whether this fraction is composed of primarily marl or detrital carbonates. Consequently, both %AUTO and %ALLO should be interpreted conservatively.

Statistical Methods

Results were analysed with R Statistical Software (R Development Core Team, 2009). Correlation coefficients (r_{Pearson}) and p values were corrected for trends and autocorrelation (p_{corr}) using the method of Trenberth (1984). The sedimentary proxy and meteorological data with the most promising correlation was smoothed with three, five and seven year running averages to determine the amount of smoothing which maximizes the correlation coefficient without losing statistical significance.

The sedimentary proxy and meteorological data were smoothed accordingly, and checked for autocorrelation after one year lag. Then, the two time series were divided into a calibration (AD 1961 – AD 2004) and a verification period (AD 1902 – AD 1960) (i.e. cross-validation split-periods; Cook et al., 1994) separated at the start of the increasing trend in both temperature and proxy (AD 1960). These periods were established to test the quality of the ordinary least squares (OLS) regression model and the influence of the increasing trend. The reduction of error (RE), coefficient of efficiency (CE) and the root mean squared error of prediction (RMSEP) were quantified (Cook et al., 1994).

In a next step, we used the entire calibration period to develop an OLS regression model which includes the complete range of calibration period climate variability. The reconstruction error was determined with a ten-fold cross-validation (RMSEP; Venables and Ripley, 2002; Peters and Hothorn, 2009; R Development Core Team, 2009; Therneau and Lumley, 2009; Leisch and Dimitriadou, 2010; Therneau et al., 2010).

e. Results

Chronology

^{210}Pb dates from the unconstrained CRS model had large uncertainties, were inconsistent with the SCP peak, and were barely consistent with the ^{137}Cs peak. Alternatively, the unconstrained SIT model had an almost identical shape to the constrained SIT model. Therefore, constraining the SIT model by the peak of ^{137}Cs at ca. AD 1963 only reduced dating uncertainties. Because the constrained SIT model was consistent with two of three independent chronological markers (i.e. the SCP Peak and the start of ^{137}Cs), it was elected to be the calibration period chronology. The chronology extended back to ca. AD 1878 with an average uncertainty of +/-3 years (maximum +/-6 years) (Figures 6.5a, b).

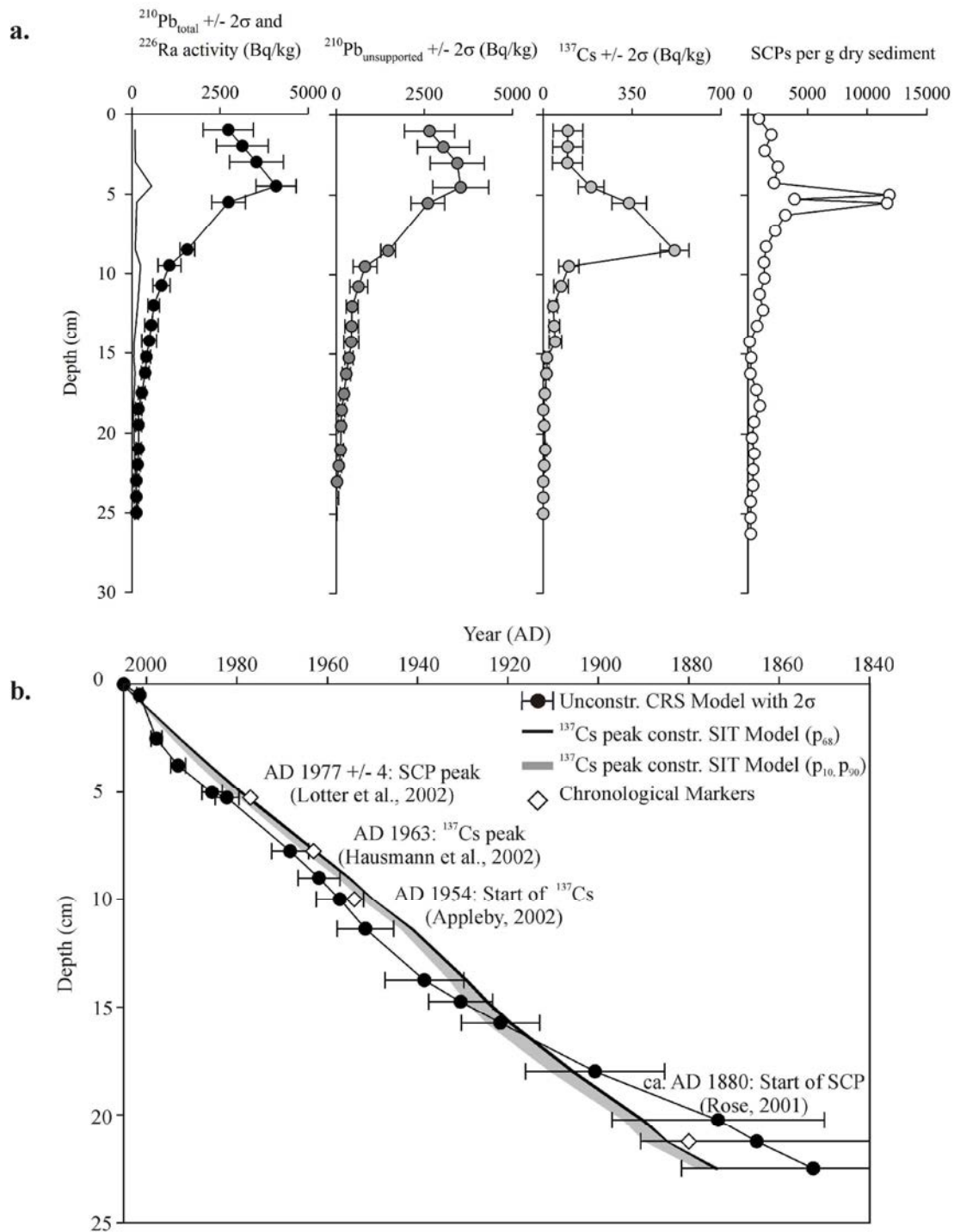


Figure 6.5 (a.) $^{210}\text{Pb}_{\text{total}}$, ^{226}Ra , $^{210}\text{Pb}_{\text{unsupported}}$, ^{137}Cs and Spheroidal Carbonaceous Particles (SCPs) per gram of dry sediment, (b.) two potential age-depth models for the calibration period with references for the chronological markers denoted with white diamonds.

This chronology was consistently several centimeters offset from the age-depth model in Hausmann et al. (2002; and personal communication). Considering that nine years have lapsed since the coring of Hausmann et al. (2002), this would suggest a sedimentation rate of 0.2 cm/year (=ca. 2 cm/9 years).

Scanning Reflectance Spectroscopy and Spectrophotometry

The average reflectance spectrum of the Lake Seeberg freeze core included a trough spanning R_{590} to R_{640} and a trough from R_{640} to R_{720} . However, these features only existed prior to AD 1955 (Figure 6.6b). Between AD 1955 and AD 2005, the reflectance spectra had an overall decreasing reflectance and increasing variability for wavelengths exceeding 630 nm (Figure 6.6a).

Consequently, the two trough areas (and the relative absorption band depth, RABD) resulted in different values for sediment younger and older than AD 1955 (Figures 6.6c, d, e and f). Specifically, trough areas and RABD were more variable after AD 1955.

A similar change in sediments was evident in $L^*a^*b^*$ results (Figures 6.6g, h and i). L^* indicated dark sediments from ca. AD 1878 to AD 2005 with higher variability after AD 1955. a^* indicated a larger proportion of green (relative to red) from AD 1955 to AD 2005 and higher variability than prior to AD 1955. Furthermore, b^* showed a transition from a higher proportion of blue (relative to yellow) from AD 1955 to AD 2005, to a higher proportion of yellow (relative to blue) before AD 1955.

Spectrophotometry absorption of sediments from the gravity core was used to validate the reflectance spectra of the freeze core. In contrast to the spectrolino data, this revealed the constant presence of the two reflectance troughs (as absorption maxima) at 610 nm and 665 nm from AD 1955 to AD 2005 (Figure 6.7).

Sedimentation Rate and Mass Accumulation Rate

Sedimentation rates and MAR were calculated at uneven temporal resolution and regularized to acquire annual values. Therefore, as stated in the methods, changes in these two variables may be related to sampling resolution and should be interpreted prudently.

Sedimentation rates averaged ca. 0.2 cm/yr with the lowest values around AD 1965 (Figure 6.8a). From moderate-to-low values around AD 1878, sedimentation rates increased (also in terms of variability) until the record maximum at ca. AD 1925. After ca. AD 1925, sedimentation rates decreased until ca. AD 1965 and then increased towards AD 2005.

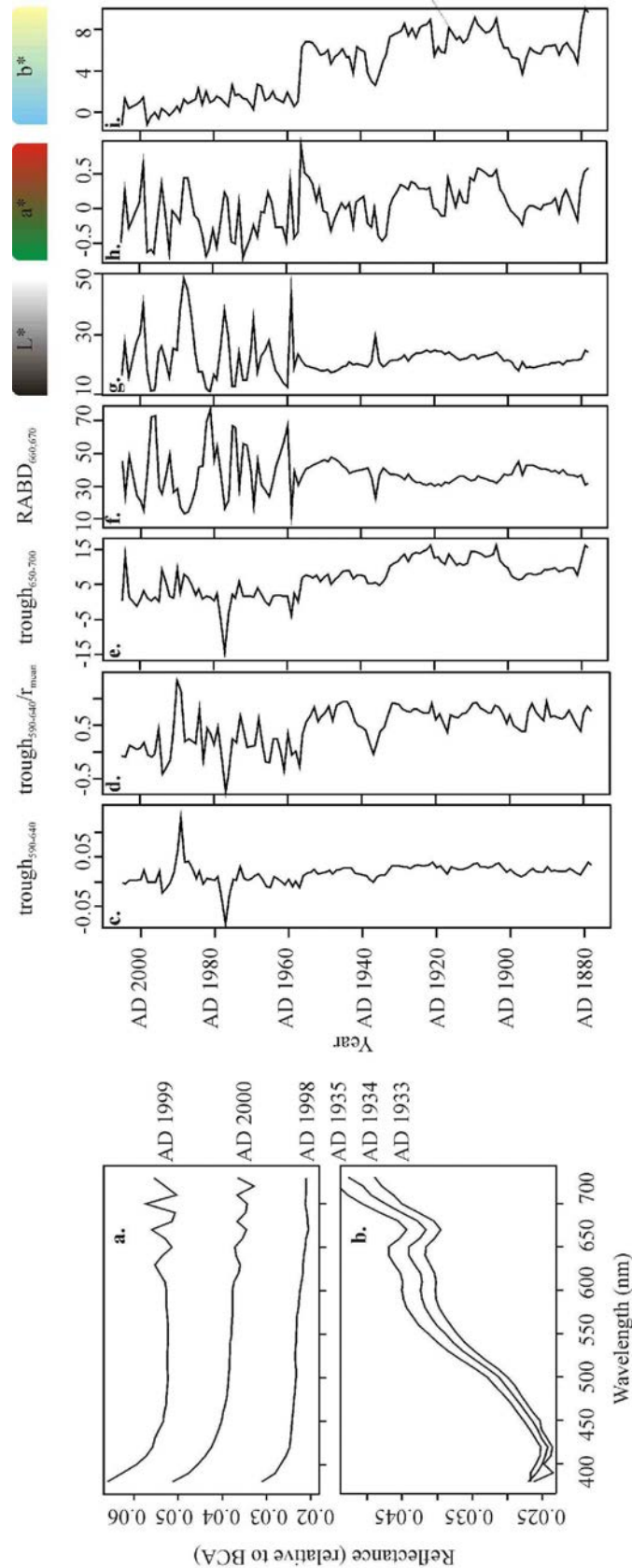


Figure 6.6 (a.) examples of reflectance spectra from ca. AD 1955 - AD 2005, (b.) examples of reflectance spectra from ca. AD 1878 to AD 1955, (c.) Trough₅₉₀₋₆₄₀ (d.) Trough₅₉₀₋₆₄₀dR_{mean}, (e.) Trough₆₅₀₋₇₀₀, (f.) RABD_{660:670}, (g.) L*, (h.) a*, and (i.) b*.

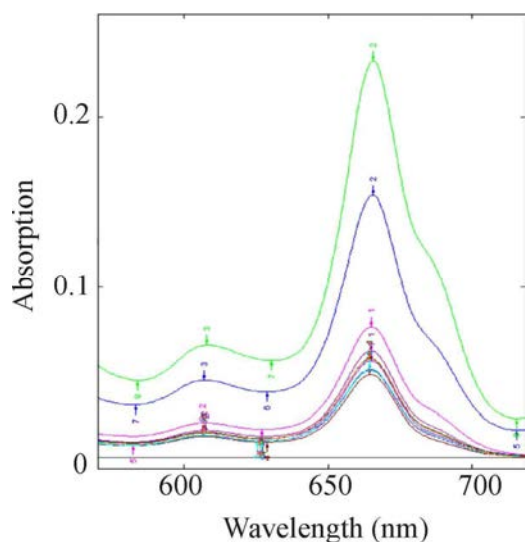


Figure 6.7 Spectrophotometer absorption results

MAR averaged $8.4E-03$ $\text{mg}/\text{cm}^2/\text{yr}$ (Figure 6.8b). At the start of the record (ca. AD 1878), values were moderate-to-high. MAR (and variability) increased to the record maximum around AD 1925. After AD 1925, MAR decreased steadily until ca. AD 1965. MAR temporarily increased around AD 1980 and then resumed its decline. Minimum MAR values were reached in AD 2003.

Differences between sedimentation rates and MAR are likely related to increasing water content in younger sediments which is accounted for in MAR. Water contents reached 99% at the top of the sediment core and gradually decreased to 92% by ca. AD 1878.

Biogenic silica

Concentrations of bSi averaged 5.6% (average $\%b\text{SiO}_2=11.9\%$) (Figure 6.8c). Between ca. AD 1878 and AD 1960, %bSi was reduced. Values of %bSi (and variability) began to increase after AD 1960, temporarily reached a plateau around AD 1980 and then continued to increase until AD 2005. The maximum %bSi (and variability) was achieved around AD 2002.

Bsi fluxes appear to be strongly influenced by the interpolated sedimentation rates. The fluxes had a mean of $3.6E-02$ $\text{mg}/\text{cm}^2/\text{yr}$ with maximum values (and variability) around AD 1925 (Figure 6.8d). Minimum values (albeit high variability) were found just after AD 1960. From the start of the record (ca. AD 1878) to AD 1900, bSi fluxes increased slightly. There was a temporary decrease in bSi fluxes from AD 1900 to AD 1920 followed by a peak at AD 1925. Between AD 1925 and AD 1960, bSi fluxes decreased steadily. After reaching the record minimum around AD 1960, bSi fluxes increased rapidly, reaching $5E-02$ $\text{mg}/\text{cm}^2/\text{yr}$ by AD 1975. Values were moderate-to-high for the remainder of the record.

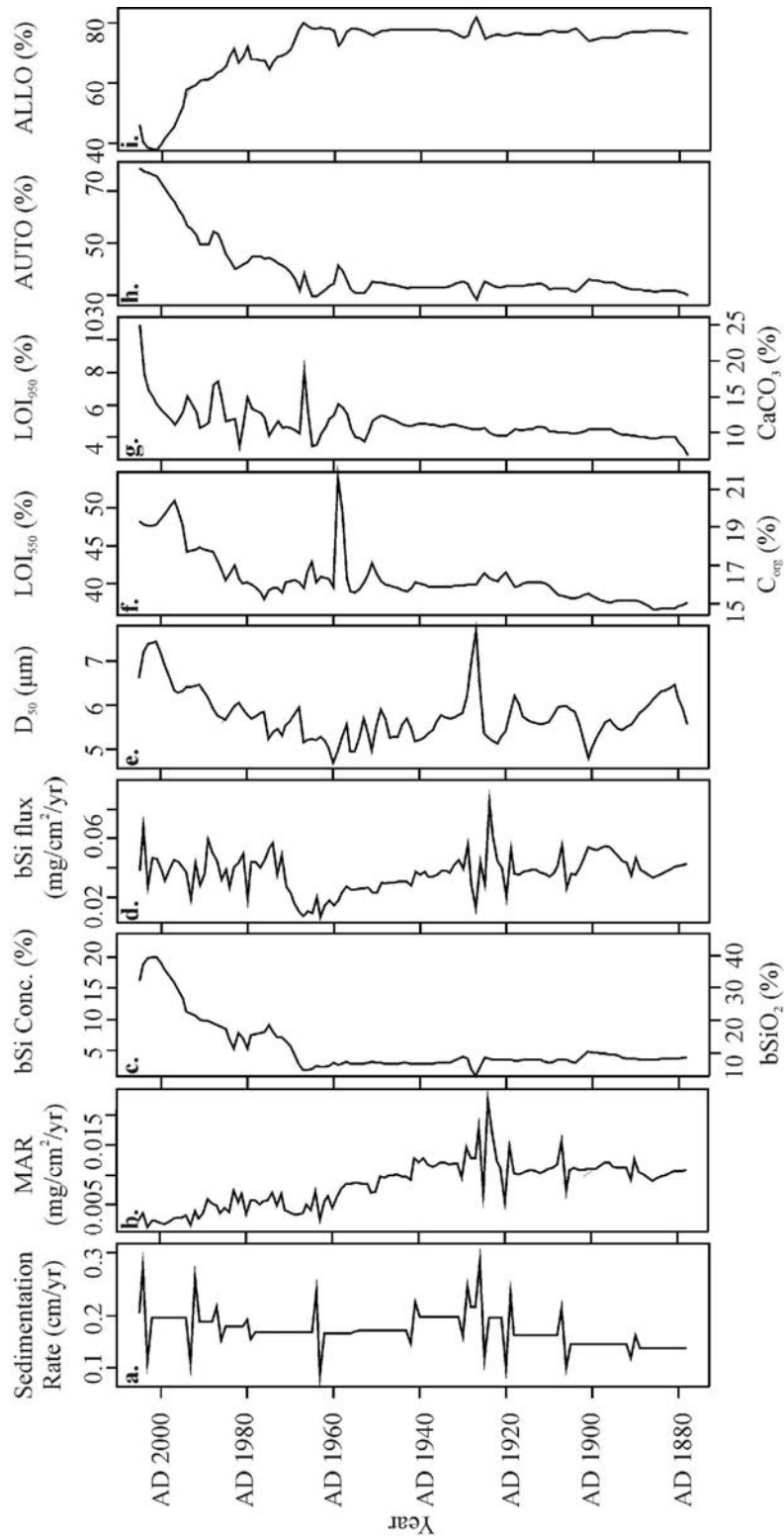


Figure 6.8 Results of (a.) sedimentation rates, (b.) mass accumulation rates (MAR), (c.) biogenic silica concentrations (as %bSi or %bSiO₂), (d.) biogenic silica fluxes, (e.) median grain sizes (D_{50}), (f.) loss-on-ignition at 550°C (as %LOI₅₅₀ or %C_{org}), (g.) loss-on-ignition at 950°C (as %LOI₉₅₀ or %CaCO₃), (h.) percent autochthonous sedimentation (%AUTO; estimated from %bSiO₂, %C_{org} and %CaCO₃), (i.) percent allochthonous sedimentation (%ALLO; estimated from 100% - %AUTO, plus %CaCO₃).

Grain size

Median grain sizes averaged 5.8 μm with minimum values at ca. AD 1900 and ca. AD 1960 (Figure 6.8e). Maximum median grain sizes (and variability) occurred around AD 1927. From ca. AD 1880, values decreased. After reaching a minimum around AD 1900, grain sizes increased slowly until AD 1920 and then rapidly reached the maximum value around AD 1927. From AD 1927 to AD 1960, median grain sizes decreased. After AD 1960, median grain sizes increased steadily. Around AD 2001, median grain sizes reached 7.4 μm .

Loss-on-ignition

%LOI₅₅₀ averaged 40.7% (average %C_{org}=16.3) (Figure 6.8f). Highest values were found around AD 1960 and AD 1997. From ca. AD 1878 to AD 1940, %LOI₅₅₀ was moderate-to-low with a gentle increasing (long-term) trend. Values peaked briefly around AD 1950 and then increased rapidly to the record maximum (and highest variability) by AD 1960. After AD 1960, %LOI₅₅₀ decreased to pre-AD 1940 levels. After ca. AD 1980, %LOI₅₅₀ began to increase again reaching 50.8% by ca. AD 1997.

Alternatively, %LOI₉₅₀ averaged 4.8% (average %CaCO₃=10.9%) (Figure 6.8g). The lowest %LOI₉₅₀ was found at the start of the record (ca. AD 1878) whereas maximum values (and variability) were found near AD 2005. After the minimum at ca. AD 1878, %LOI₉₅₀ had low variability and increased slowly towards ca. AD 1948. Higher variability was found after ca. AD 1948. Low %LOI₉₅₀ values were identified around AD 1965 and AD 1982. After ca. AD 1997, %LOI₉₅₀ increased rapidly, reaching the record maximum around AD 2005.

Percent Autochthonous Sediments and Percent Allochthonous Sediments

%AUTO (our estimate of autochthonous sediments assuming that most %CaCO₃ is produced in lake) averaged 39% with maximum values around AD 2005 and minimum values at ca. AD 1927 (Figure 6.8h). From ca. AD 1878 to ca. AD 1960, values were minimal with no apparent increasing or decreasing (long-term) trend. Around AD 1960, values temporarily peaked at 41%. From ca. AD 1965 to AD 2005, %AUTO increased rapidly. Highest variability was found around AD 1997.

%ALLO (our estimate of allochthonous sediments assuming that most %CaCO₃ is produced out of the lake) averaged 71.8% with maximum values around AD 1927 and minimum values around AD 2001 (Figure 6.8i). From ca. AD 1878 to ca. AD 1960, values were high without an increasing or decreasing (long-term) trend. Elevated values around AD

1927 were brief. From AD 1960, %ALLO began to decline. By AD 2001, values were as low as 38%.

Calibration Model

Correlation matrices presenting the relationship between sedimentary variables and meteorological (i.e. temperature and precipitation) data from Château-d'Oex show strong, significant ($p_{\text{corr}} < 0.01$) correlations between unsmoothed sedimentary indicators of in-lake productivity and warm season temperatures (e.g. May-June-July-August-September; MJJAS; Appendix B). However, no high and significant correlations could be found with precipitation. Reflectance-based variables were not included in the correlation matrices due to the anomalous results after AD 1955.

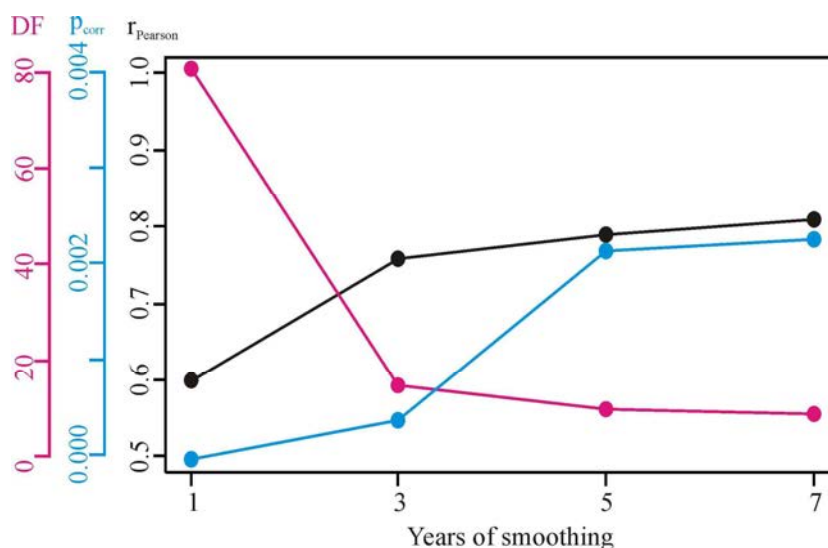


Figure 6.9 The impact of three, five and seven years of smoothing on r_{Pearson} , p_{corr} and Degrees of Freedom (DF) for %AUTO and MJJAS temperatures from Château-d'Oex.

The sedimentary variable with the highest correlation to temperature was %AUTO (%AUTO and MJJAS temperature $r_{\text{Pearson}}=0.60$, $p_{\text{corr}} < 0.01$). High, significant correlations to warm-season temperatures were also found for %bSi (or %bSiO₂), %LOI₅₅₀ (or %C_{org}), D₅₀ and %LOI₉₅₀ (or %CaCO₃). Although %AUTO was chosen to develop a calibration-in-time, other sedimentary variables indicative of autochthonous productivity would likely give similar results.

Figure 6.9 demonstrates that smoothing of %AUTO and MJJAS temperatures by three, five and seven years caused negligible changes to p_{corr} (< 0.01) but considerably

increased r_{Pearson} . The largest increase in r_{Pearson} was found after three years of smoothing. Therefore, both %AUTO and MJJAS temperatures were smoothed by only three years to conserve degrees of freedom in the calibration and verification periods.

In Figure 6.10, three year smoothed %AUTO and MJJAS temperatures are presented. Both time series have a similar increasing (long-term) trend after AD 1960. However, MJJAS temperatures have greater high-frequency variability than %AUTO. This may be related to sample pooling. This is confirmed by an autocorrelation of 0.86 (MJJAS temperatures) and of 0.94 (%AUTO) after a lag of one year.

Split-period calibration (AD 1961 to AD 2004) and verification (AD 1902 to AD 1960) of the OLS model resulted in an RMSEP of 0.51°C , a high RE (0.62) and a positive CE (0.03). The RMSEP was probably inflated and the CE was probably weakened by the different structure of proxy and temperature during the calibration (i.e. steep increasing trend, higher average) and verification periods.

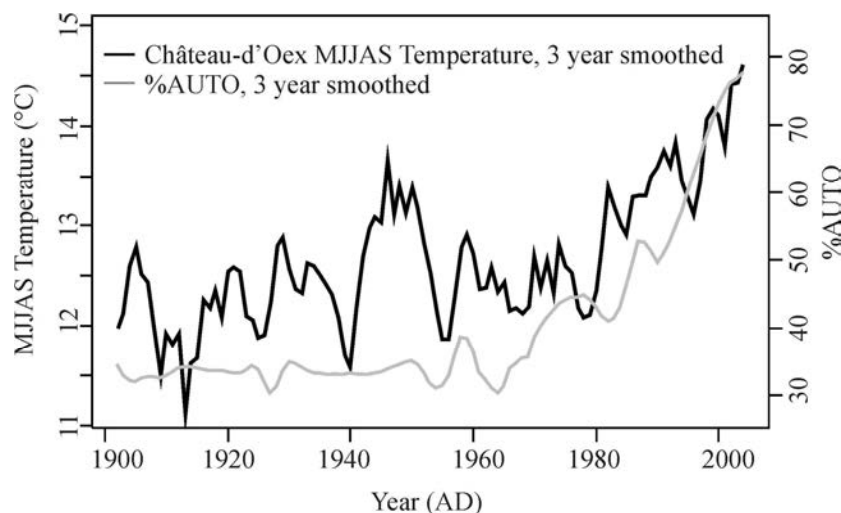


Figure 6.10 Three year smoothed %AUTO and three year smoothed MJJAS temperatures from Château-d'Oex.

To address this issue, the entire calibration period was used to develop an OLS regression model which represents the gamut of MJJAS temperature variability. This had a three year smoothed $r_{\text{Pearson}}=0.76$, $p_{\text{corr}}<0.01$, and a ten-fold cross-validated RMSEP of 0.45°C . This RMSEP is better than the value found through split-period calibration. Considering the amplitude of temperatures found during the calibration period (ca. 3.5°C), this RMSEP is promising.

f. Discussion

(1.) How have recent sediments in Lake Seeberg changed?

The most striking change in recent sediments is the reflectance of the freeze core after AD 1955. However, spectrophotometry on sediments from the gravity core did not indicate any change in absorption after AD 1955. Furthermore, Lake Seeberg became anoxic after ca. AD 1960 (Larocque-Tobler et al., accepted). As shown by Bianchi et al. (2000), anoxia at the sediment-water interface should favor pigment preservation.

We suggest that these conflicting results are related to the water content of the sediment which may be an artefact of the coring method because both the freeze core and gravity core were recovered during the same field excursion (winter, 2005) and from the same basin in Lake Seeberg.

The freeze core had a higher water content (AD 1878 to AD 2005, average=95%) than the gravity core (estimated average=40%). According to Stephenson et al. (1996), freeze cores can have considerably higher water contents than other core types because of an increase of sediment pore water during ice crystal formation. Balsam et al. (1998) found that high water contents can cause a darkening of sediments. This is consistent with the extremely low L^* values for the Lake Seeberg sediment core. During reflectance spectroscopy, excess water may interfere with light reaching the sedimentary target. Balsam et al. (1998) found that dividing reflectance values by the average reflectance (R_{mean}) can account for variable water contents in deep-sea sediment cores. However, this was only tested on sediments with water contents of 35% (Balsam et al., 1998). Therefore, it may not apply to sediments with considerably higher saturation.

In addition to enhancing the pore water of sediments, freeze coring can impact pigments directly. The average reflectance spectrum of the Lake Seeberg freeze core included a trough spanning R_{590} to R_{640} and a trough from R_{640} to R_{720} . According to the spectrophotometry results, there were absorption maxima at 610 nm and at 665 nm. Louda et al. (2002) showed that absorption maxima (i.e. reflectance minima) around 610 nm and 665 nm are associated with chlorophyll degradation products. During freezing and thawing of the sediment core, damage to the structure of cells may have accelerated diagenesis of these pigments (B. Rein, personal communication).

Alternatively, all of the (non-reflectance) variables except for MAR and %ALLO had moderate-to-low values until ca. AD 1965. After AD 1965, an increasing (long-term) trend was observed among productivity-indicating sedimentary variables including %bSi, bSi

fluxes, D_{50} , %LOI₅₅₀, %LOI₉₅₀, and %AUTO. Several of these variables reached their maximum values around AD 2005.

Grain size had a similar increasing trend. This may be related to an increase in carbonate precipitation by warmer lake waters and enhanced bacterial and algal metabolism (Wetzel, 2001). This might explain the similar increase in %LOI₉₅₀.

Meanwhile, %ALLO and MAR decreased from AD 1965 to AD 2005. The decrease in %ALLO is consistent with the C/N results of Hausmann et al. (2002).

(2.) Can changes in sediments coinciding with the instrumental period (AD 1901 - AD 2005) be attributed to climate (temperature or precipitation) and be used to develop a calibration-in-time in order to reconstruct past climate?

As described by Hausmann et al. (2002) and Thompson et al. (2005), Alpine lakes such as Lake Seeberg are sensitive to changes in climate. In particular, warmer temperatures dictate the duration of ice-cover which influences water-column (and nutrient) circulation and radiation balances (Battarbee, 2000; Lotter and Bigler, 2000).

However, intensified land-use and influxes of nutrients can distort the climate signature in lake sediments (e.g. Heiri and Lotter, 2005). For instance, in Lake Silvaplana, Switzerland, eutrophication from land-use masked any influence of warming temperatures on productivity (Blass et al., 2007b).

Alternatively, changes to in-lake productivity in Lake Seeberg between ca. AD 1878 and AD 2005 may be related to climate (e.g. warming summer temperatures, shorter ice-cover period). A similar finding has been described in high-altitude (and/or high-latitude) lakes such as Hallet Lake, Alaska (i.e. parallel increases in %bSi and June-July-August temperatures; McKay et al., 2008) and six lakes on Baffin Island, Canada (i.e. matching increasing trends in reflectance-inferred chlorophyll-a and temperature; Michelutti et al., 2005).

In Lake Seeberg, immutable evidence of eutrophication during the 20th century could not be found. In van der Knaap et al. (2000), enhanced grazing was inferred from pollen. However, diatom-inferred total phosphorus (TP) and eutrophication-indicating diatoms (e.g. *Stephanodiscus parvus*) were relatively low during the 20th century (Hausmann et al., 2002). Furthermore, Larocque-Tobler et al. (accepted) suggested an increase in anoxia (chironomid-inferred) after AD 1960 was due to an increase in organic matter which may be temperature driven. Consequently, we suggest that %AUTO in Lake Seeberg is a reflection of MJJAS temperatures rather than eutrophication and the use of %AUTO to reconstruct MJJAS temperatures back in time would be appropriate for changes exceeding 0.45°C. Unfortunately,

long-term applications of the OLS model are limited by hypertrophy of the lake beyond AD 1680 (Hausmann et al., 2002). However, the findings of this study, including the impact of water content in sediments on spectral reflectance and the development of an algorithm to quantify the reflectance $\text{Trough}_{590-620}/R_{\text{mean}}$ may have applications for other studies.

g. Summary and Conclusions

Warming in Central Europe and the Alps during the 20th century has raised concerns about anthropogenic contributions to climate variability. Since instrumental meteorological data preceding the 20th century are sparse, quantitative, up-to-annually resolved and long-duration climate reconstructions derived from archives (e.g. lake sediments) are needed.

Here, sediments from Lake Seeberg (Bernese Oberland, Switzerland) were evaluated for their potential as a climate archive. A focus was placed on recent sediments (ca. AD 1878 - AD 2005) and the Château-d'Oex instrumental period (AD 1901 - AD 2005).

Up-to-annual measurements of sedimentation rates, mass accumulation rates (MAR), biogenic silica (bSi), median grain size (D_{50}) and loss-on-ignition (LOI) were supplemented with non-destructive measurements of scanning reflectance spectroscopy and spectrophotometry. bSi and LOI were used to estimate total autochthonous productivity (%AUTO) and total detrital sediments (%ALLO). In combination, these results provided a record of changes in sedimentation and sediment composition.

Anomalous results of scanning reflectance spectroscopy were attributed to high water contents of the sediment possibly related to the coring method. Consequently, reflectance values were not explored as a climate proxy.

Alternatively, we found a close relationship between sedimentary variables indicative of autochthonous productivity and warm-season temperatures at Château-d'Oex (i.e. %AUTO and MJJAS). Statistics from a split-period (i.e. calibration and verification) Ordinary Least Squares (OLS) regression between three year smoothed %AUTO and MJJAS appear to be influenced by difference proxy and temperature characteristics (e.g. trends; means) during the two periods. However, an OLS model of %AUTO and MJJAS temperatures for the entire calibration period resulted in a low error.

These statistics suggest that %AUTO can be used to reconstruct MJJAS temperatures. However, uncertainties regarding the trophic status of the lake should be further explored. Furthermore, applications of this OLS model in the past are limited by hypertrophy of the lake beyond AD 1680 (Hausmann et al., 2002).

References

- Abramoff, M.D., Magelhaes, P.J., Ram, S.J. 2004. Image processing with ImageJ. *Biophotonics International* 11 (7): 36-42.
- Andrews, J.T., Freeman, W. 1996. The Measurement of Sediment Color Using the Colortron Spectrophotometer. *Arctic and Alpine Research* 28 (4): 524-528.
- Appleby, P.G. 1997. Sediment records of fallout radionuclides and their application to studies of sediment-water interactions. *Water, Air and Soil Pollution* 99: 573-586.
- Appleby, P.G. 2002. Chronostratigraphic techniques in recent sediments, In: Last, W.M., Smol, J.P. (eds.), *Tracking Environmental Change Using Lake Sediments, Volume 1: Basin Analysis, Coring and Chronological Techniques*. The Netherlands: Kluwer Academic Publishers, 171-203.
- Balsam, W.L., Deaton, B.C., Damuth, J.E. 1998. The effects of water content on diffuse reflectance spectrophotometry studies of deep-sea sediment cores. *Marine Geology* 149: 177-189.
- Battarbee, R.W. 2000. Palaeolimnological approaches to climate change, with special regard to the biological record. *Quaternary Science Reviews* 19: 107-124.
- Berner, R.A. 1971. *Principles of chemical sedimentology*. McGraw-Hill Book Company.
- Bianchi, T.S., Johansson, B., Elmgren, R. 2000. Breakdown of phytoplankton pigments in Baltic sediments: effects of anoxia and loss of deposit-feeding macrofauna. *Journal of Experimental Marine Biology and Ecology* 251: 161-183.
- Blass, A., Grosjean, M., Troxler, A., Sturm, M. 2007a. How stable are twentieth-century calibration models? A high-resolution summer temperature reconstruction for the eastern Swiss Alps back to AD 1580 derived from proglacial varved sediments. *The Holocene* 17: 51-63.
- Blass, A., Bigler, C., Grosjean, M., Sturm, M. 2007b. Decadal-scale autumn temperature reconstruction back to AD 1580 inferred from the varved sediments of Lake Silvaplana (southeastern Swiss Alps). *Quaternary Research* 68: 184-195.
- Carroll, J., Lerche, I. 2003. *Sedimentary processes: quantification using radionuclides*. Elsevier, Oxford.
- Christensen, J.H., Christensen, O.B. 2003. Climate modelling: Severe summertime flooding in Europe. *Nature* 421: 805-806.
- Cook, E.R., Briffa, K.R., Jones, P.D. 1994. Spatial regression methods in dendroclimatology - a review and comparison of 2 techniques. *International Journal of Climatology* 14: 379-402.
- Dean, W. E. Jr. 1974. Determination of carbonate and organic matter in calcareous sediments and sedimentary rocks by loss on ignition: Comparison with other methods. *Journal of Sedimentary Petrology* 44: 242-248.

- Esper, J., Wilson, R.J.S., Frank, D.C., Moberg, A., Wanner, H., Luterbacher, J. 2005. Climate: past ranges and future changes. *Quaternary Science Reviews* 24: 2164-2166.
- Frei, C., Schär, C. 2001. Detection probability of trends in rare events: Theory and application to heavy precipitation in the Alpine region. *Journal of Climate* 14: 1568-1584.
- Grob, P. 2008. Spheroidal carbonaceous particles SCPs als Indikatoren der Umweltbelastung und als Datierungsmethode junger Seesedimente. MSc Thesis. University of Bern, Bern.
- Guthruf, J., Guthruf-Seilber, K., Zeh, M. 1999. Kleinseen im Kanton Bern. Bern: Paul Haup AG.
- Hausmann, S., Lotter, A.F., van Leeuwen, J.F.N., Ohlendorf, C., Lemcke, G., Grönlund, E., Sturm, M. 2002. Interactions of climate and land-use documented in the varved sediments of Seebergsee in the Swiss Alps. *The Holocene* 12 (3): 279-289.
- Heiri, O., Lotter, A.F., Lemcke, G. 2001. Loss-on-ignition as a method for estimating organic and carbonate content of sediments: reproducibility and comparability of results. *Journal of Paleolimnology* 25: 101-110.
- Heiri, O., Lotter, A.F. 2005. Holocene and Lateglacial summer temperature reconstruction in the Swiss Alps based on fossil assemblages of aquatic organisms. A review. *Boreas* 34: 506-516.
- Kuglitsch, F.G., Toreti, A., Xoplaki, E., Della-Marta, P.M., Luterbacher, J., Wanner, H. 2009. Homogenization of Daily Maximum Temperature Series in the Mediterranean. *Journal of Geophysical Research* 114.
- Lamoureux, S.F. 1994. Embedding unfrozen lake sediments for thin section preparation. *Journal of Paleolimnology* 10: 141-146.
- Larocque-Tobler, I., Quinlan, R., Stewart, M., Grosjean, M. (accepted) Chironomid-inferred temperature changes of the last century in Lake Seeberg (Seebergsee), Switzerland: assessment of two calibration methods. *Quaternary Science Reviews*.
- Leisch, F., Dimitriadou, E. 2010. mlbench: Machine Learning Benchmark Problems. R package version 2.1-0.
- Lindbloom, B. 2011. Color calculators and spreadsheets. <http://www.brucelindbloom.com>
- Liu, J., Carroll, J.L., Lerche, I. 1991. A technique for disentangling temporal source and sediment variations from radioactive isotope measurements with depth. *Nuclear Geophysics* 5: 31-45.
- Lotter, A.F., Appleby, P.G., Bindler, R., Dearing, J.A., Grytnes, J.A., Hofmann, W., Kamenik, C., Lami, A., Livingstone, D.M., Ohlendorf, C., Rose, N., Sturm, M. 2002. The sediment record of the past 200 years in a Swiss high-alpine lake: Hagelseewli (2339 m a.s.l.). *Journal of Paleolimnology* 22: 111-127.
- Lotter, A.F., Bigler, C. 2000. Do diatoms in the Swiss Alps reflect the length of ice-cover? *Aquatic Sciences* 62: 125-141.

Lotter, A.F., Lemcke, G. 1999. Methods for preparing and counting biochemical varves. *Boreas* 28: 243-252.

Louda, J.W., Liu, L., Baker, E.W. 2002. Senescence- and death-related alteration of chlorophylls and carotenoids in marine phytoplankton. *Organic Geochemistry* 33: 1635-1653.

Mappad Free Software 1996. <http://www.ngdc.noaa.gov/paleo/paleo.html>

McKay, N.P., Kaufman, D.S., Michelutti, N. 2008. Biogenic silica concentration as a high-resolution, quantitative temperature proxy at Hallet Lake, south-central Alaska. *Geophysical Research Letters* 35.

MeteoSchweiz 2010. (http://www.meteoschweiz.admin.ch/web/de/klima/klima_heute/Homogene_reihen.Par.0019.DownloadFile.ext.tmp/chateaudoex.txt)

Michelutti, N., Wolfe, A.P., Vinebrooke, R.D., Rivard, B., Briner, J.P. 2005. Recent productivity increases in arctic lakes. *Geophysical Research Letters* 32.

Nederbragt, A.J., Francus, P., Bollmann, J., Soreghan, M.J. 2004. Image Calibration, Filtering, and Processing, In: Francus, P. (ed.), *Tracking Environmental Change Using Lake Sediments, Volume 7: Image Analysis, Sediments and Palaeoenvironments*. The Netherlands: Springer, 35-58.

Niessen, F., Wick, L., Bonani, G., Chondrogianni, C., Siegenthaler, C. 1992. Aquatic system response to climatic and human changes: productivity, bottom water oxygen status, and sapropel formation in Lake Lugano over the last 10,000 years. *Aquatic Sciences* 54: 257-276.

Ohlendorf, C., Sturm, M. 2008. A modified method for biogenic silica determination. *Journal of Paleolimnology* 39: 137-142.

Parey, S., Dacunha-Castelle, D., Huong Hoang, TT. 2010. Mean and variance evolutions of the hot and cold temperatures in Europe. *Climate Dynamics* 34: 345-359.

Peel, M.C., Finlayson, B.L., McMahon, T.A. 2007. Updated world map of the Köppen-Geiger climate classification. *Hydrological Earth Systems Science* 11: 1633-1644.

Peters, A., Hothorn, T. 2009. ipred: Improved Predictors. R package version 0.8-8. <http://CRAN.R-project.org/package=ipred>

R Development Core Team 2009. R: A language and environment for statistical computing. R Foundation for Statistical Computing. Vienna, Austria. ISBN 3-900051-07-0, URL <http://www.R-project.org>.

Rein, B., Sirocko, F. 2002. In-situ reflectance spectroscopy - analyzing techniques for high-resolution pigment logging in sediment cores. *International Journal of Earth Science* 91: 950-954.

Rose, N.L. 2001. Fly-ash particles, In: Last, W.M., Smol, J.P (eds.), *Tracking Environmental Change Using Lake Sediments, Volume 2: Physical and Chemical Techniques*. The Netherlands: Kluwer Academic Publishers, 319-349.

Routh, J., Choudhary, P., Meyers, P.A., Kumar, B. 2008. A sediment record of recent nutrient loading and trophic state change in Lake Norrviken, Sweden. *Journal of Palaeolimnology* 42 (3): 325-341.

Schär, C., Vidale, P.L., Lüthi, D., Frei, C., Häberli, C., Liniger, M.A., Appenzeller, C. 2004. The role of increasing temperature variability in European summer heatwaves. *Nature* 427: 332-336.

Scherrer, S.C., Appenzeller, C., Liniger, M.A. 2006. Temperature trends in Switzerland and Europe: Implications for climate normals. *International Journal of Climatology* 26: 565-580.

‘Seebergsee.’ 43° 34’ 39.11” N, 7° 26’ 36.19” E. Google Earth. January 1, 1997. January 1, 2010.

Seneviratne, S.I., Lüthi, D., Litschi, M., Schär, C. 2006. Land-atmosphere coupling and climate change in Europe. *Nature* 443: 205-209.

Smol, J.P. 1988. Paleoclimate proxy data from freshwater arctic diatoms. *Verhandlungen der Internationale Vereinigung für Theoretische und Angewandte Limnologie* 24: 1240-1246.

Stephens, F.C., Louchard, E.M., Reid, R.P., Maffione, R.A. 2003. Effects of microalgal communities on reflectance spectra of carbonate sediments in subtidal optically shallow marine environments. *Limnology Oceanography* 42 (1, 2): 535-546.

Stephenson, M., Klaverkamp, J., Motycka, M., Baron, C., Schwartz, W. 1996. Coring artifacts and contaminant inventories in lake sediment. *Journal of Paleolimnology* 15: 99-106.

Stewart, M., Larocque-Tobler, I., Grosjean, M. (accepted) Quantitative inter-annual and decadal summer temperature variability ca. 570 BC - AD 120 (Iron Age - Roman Period) reconstructed from the varved sediments of Lake Silvaplana, Switzerland. *Journal of Quaternary Science*.

Therneau, T.M., Atkinson, B., Ripley, B. 2010. rpart: Recursive Partitioning. R package version 3.1-46. <http://CRAN.R-project.org/package=rpart>

Therneau, T.M., Lumley, T. 2009. survival: Survival analysis, including penalised likelihood. R package version 2.35-8. <http://CRAN.R-project.org/package=survival>

Thompson, R., Kamenik, C., Schmidt, R. 2005. Ultra-sensitive Alpine lakes and climate change. *Journal of Limnology* 64: 139-152.

Trachsel, M., Grosjean, M., Larocque-Tobler, I., Schwikowski, M., Blass, A., Sturm, M. 2010a. Quantitative summer temperature reconstruction derived from combined biogenic Si and chironomid record from varved sediments of Lake Silvaplana (south-eastern Swiss Alps) back to AD 1177. *Quaternary Science Reviews* 29 (19-20): 2719-2730.

Trachsel, M., Grosjean, M., Schnyder, D., Kamenik, C., Rein, B. 2010b. Scanning reflectance spectroscopy (380-730 nm): a novel method for quantitative high-resolution climate reconstructions from minerogenic lake sediments. *Journal of Paleolimnology* 44 (4): 979-994.

- Trenberth, K.E. 1984. Some effects of finite sample size and persistence on meteorological statistics. Part I: Autocorrelation. *Monthly Weather Review* 112: 2359-2368.
- van der Knaap, W.O., van Leeuwen, J.F.N., Fankhauser, A., Ammann, B. 2000. Palynostratigraphy of the last centuries in Switzerland based on 23 lake and mire deposits: chronostratigraphic pollen markers, regional patterns, and local histories. *Review of Palaeobotany and Palynology* 108: 85-142.
- von Gunten, L., Grosjean, M., Rein, B., Urrutia, R., Appleby, P. 2009. A quantitative high-resolution summer temperature reconstruction based on sedimentary pigments from Laguna Aculeo, central Chile, back to AD 850. *The Holocene* 19 (6): 873-881.
- Venables, W.N., Ripley, B.D. 2002. Modern Applied Statistics with S. Fourth Edition. New York: Springer, ISBN 0-387-95457-0
- Wetzel, R.G. 2001. Limnology: Lake and River Ecosystems Third Ed. San Diego: Academic Press, 1006 pp.
- Wolfe, A.P., Vinebrooke, R.D., Michelutti, N., Rivard, B., Das, B. 2006. Experimental calibration of lake-sediment spectra reflectance to chlorophyll a concentrations: methodology and paleolimnological validation. *Journal of Paleolimnology* 36: 91-100.

8. Conclusions and outlook

a. Conclusions

Regional climate models suggest that Central Europe and the Alps are highly sensitive to climate change. As warming continues, the region is expected to become a ‘hotspot’ of inter-annual summer temperature variability (Schär et al., 2004; Scherrer et al., 2006; Seneviratne et al., 2006; Parey et al., 2010) with an elevated risk of drought (IPCC, 2007) and a higher occurrence of extreme precipitation events (Arnell and Liu, 2001; Christensen and Christensen, 2003; Kundzewicz et al., 2005).

Since instrumental records in Central Europe and the Alps are limited to the past ca. 150 years, there are considerable uncertainties about natural climate variability (e.g. forcings, feedbacks and thresholds) in this region which make it difficult to interpret warming of the 20th century and to evaluate regional climate model projections for the 21st century.

In this thesis, multiple proxies in the sediments of Lake Silvaplana (e.g. biogenic silica (bSi) fluxes, chironomids, mass accumulation rates (MAR) and turbidite thicknesses) were used to reconstruct the late Holocene climate of Central Europe and the Alps (i.e. air temperature, palaeofloods, glacier activity and cool/wet or warm/dry climate phases). Sediments from this lake were used because they consist of annual laminations (varves) which provide an accurate chronology and facilitate high-resolution sampling. Furthermore, previous studies of Lake Silvaplana have shown a close relationship between sediment composition and climate (e.g. Blass et al., 2007; Trachsel et al., 2010a, b; Larocque-Tobler et al., 2010; de Jong and Kamenik, accepted). Emphasis was placed on ca. 570 BC - AD 120 because published (lower resolution) climate records illustrate that it was warmer than the last millennium, including a warmer (Early Iron Age; in Central Europe ‘Hallstatt’), a cooler (Late Iron Age; in Central Europe ‘La Tène’), and a moderate-to-warm Roman Period (Tinner et al., 2003).

Specifically, in Chapter 4, bSi fluxes and chironomids were used to reconstruct annually resolved June-July-August (JJA) temperatures (ca. 570 BC - AD 120). In Chapter 5, turbidite thicknesses provided a record of palaeoflood frequencies and magnitudes during cool/wet and warm/dry climate phases as inferred from MAR (ca. 1450 BC - AD 420).

These records were compared to instrumental (JJA temperatures at Sils Maria from ca. AD 1950 - AD 2005; MeteoSchweiz, 2010), reconstructed (JJA temperatures between ca. AD 1177 - AD 1950, Trachsel et al., 2010a; palaeofloods from ca. AD 1580 - AD 1950, Blass, 2006) and historical (flood records; Caviezel, 2007) climate data to address the first three research questions of this thesis.

1. What was the extent of natural climate variability in Central Europe and the Alps during the late Holocene?

Inter-annual and decadal JJA temperature variability from ca. 570 BC - AD 120 surpassed values from the last millennium. However, multi-decadal and lower frequency variability were comparable. Warm and variable JJA temperatures were noted at the Late Iron Age - Roman Period transition (approximately 50 BC to AD 100 in this region) and a cold anomaly was recognized around 470 BC (Early - Late Iron Age). The warmest JJA temperatures occurred from ca. 570 BC - 351 BC (11.2°C) and the coolest were found from AD 1351 - AD 1700 (8.8°C).

2. How did the climate from AD 1950 - AD 2000 in Central Europe and the Alps compare to 'naturally' warm climates such as the Roman Climate Optimum?

Relative to 'naturally' warm climates from ca. 570 BC to AD 120, the JJA temperature mean and rate of increase from AD 1950 - AD 2000 was not unprecedented. Specifically, we found 130 windows of 50 year JJA temperatures with an increasing trend and mean JJA temperature exceeding the Sils Maria AD 1950 - AD 2000 reference period (Sils Maria AD 1950 - AD 2000 JJA temperature trend=0.02°C/yr, p=0.02; average=9.8°C; MeteoSchweiz, 2010).

We used the thickness and frequency of turbidites during these windows to approximate the magnitude and frequency of palaeofloods (or extreme precipitation). We found that only 31 (24%) of the windows had a turbidite thickness and 35 (27%) had a turbidite frequency exceeding the average 50 year values from ca. 1450 BC - AD 420 (0.38 mm and 0.05 per year, respectively).

3. How realistic are the projections of global and regional climate models in the context of past climate in Central Europe and the Alps?

A Mean-Variability Change plot of reconstructed JJA temperatures from ca. 570 BC - AD 120 and AD 1177 - AD 1950 (Trachsel et al., 2010a), and instrumental JJA temperatures from AD 1950 - AD 2000 (Sils Maria; MeteoSchweiz, 2010), was consistent with projections of regional climate models for the 21st century (Schär et al., 2004; Scherrer et al., 2006; Seneviratne et al., 2006; Parey et al., 2010). Specifically, heteroscedasticity was recognized above a mean temperature threshold (ca. 9.8-10.7°C). Above a second threshold (ca. 12-13°C; not included in our data), we propose that the relationship between mean and inter-annual temperature variability should weaken.

Contrary to regional climate models (e.g. HIRHAM4 of E.U. PRUDENCE; Christensen and Christensen, 2003) which project that future climate warming in Central Europe will bring more intense precipitation events (e.g. summer-autumn floods) (Arnell and Liu, 2001; Kundzewicz et al., 2005), we could not find evidence that summer-autumn floods would increase in magnitude or frequency in the eastern Swiss Alps in a warmer climate of the 21st century.

Finally, we used sediments from Lake Seeberg (Bernese Oberland) to explore the fourth research question in Chapter 7.

4. Can the calibration-in-time method which was effective in Lake Silvaplana be applied to other lakes?

We chose to use sediments from Lake Seeberg to test the calibration-in-time method because the setting of Lake Seeberg (e.g. geological, glacial cover, land-use) is different from Lake Silvaplana. Therefore, the composition of sediments in both lakes is distinct. Lake Seeberg has varved sediments below ca. 15 cm which is useful for sampling at high temporal resolution. Furthermore, the composition of sediments from Lake Seeberg is known to contain a climate signature (e.g. Hausmann et al., 2002; Larocque-Tobler et al., accepted).

It was possible to develop a calibration-in-time using the proxy %AUTO (an estimate of autochthonous productivity) in the sediments of Lake Seeberg and May-June-July-August-September (MJJAS) temperatures from Château-d'Oex. However, this calibration-in-time was weakened by several factors. The upper ca. 15 cm of sediments were not varved therefore, establishing a highly accurate chronology (and sampling at high resolution) for this section of sediment was difficult. Furthermore, the low sedimentation rates required sample pooling. The correlation between %AUTO and May-June-July-August-September (MJJAS) temperature was likely due to the similar increasing trend after AD 1960 in both the proxy and the temperature data. We could not find irrefutable evidence that this trend was related to eutrophication. However, this should be further investigated. Finally, applications of the calibration-in-time to reconstruct past temperatures are limited because hypertrophy in Lake Seeberg prior to AD 1680.

b. Outlook

The findings of this thesis offer insight into natural climate variability of the past. However, they also highlight challenges in palaeoclimate reconstructions and the need for future studies. These challenges range from: selecting an appropriate site and coring method, establishing an accurate chronology for the sediment core, selecting the types of measurements to make on the sediment core, developing a statistical calibration method which captures the range of variability in the calibration period, and using the resulting reconstruction to address important questions about past and future climate.

Site selection depends on the objectives of the palaeoclimate study. For this thesis, a focus was placed on JJA temperatures in Central Europe and the Alps. Because JJA temperatures in the Engadine are highly spatially correlated to most of Central Europe (Trachsel et al., 2010a), sediments from Lake Silvaplana were an ideal choice.

Currently, most palaeoclimate reconstructions are concentrated in Europe and North America. However, lakes in other regions of the world should be explored for their potential to reconstruct past climate.

In Chapter 6, a highly significant relationship was found between %AUTO (an estimate of autochthonous productivity) in Lake Seeberg and warm-season temperatures. However, scanning reflectance spectroscopy revealed no reflectance minima (indicative of chlorins) around 660-670 nm. We propose applying scanning reflectance spectroscopy to the Lake Seeberg gravity core to verify whether anomalous reflectance results from the freeze core are related to the water content (possibly due to the coring method). If so, we suggest testing the potential of reflectance (including $\text{Trough}_{590-620}\text{dR}_{\text{mean}}$) as a climate proxy.

Developing an accurate chronology for the sediments of Lake Silvaplana and Lake Seeberg was challenging. In Mauchle (2010), XRF elemental mapping was used to identify changes in mineralogy and the start of varves. In Trachsel (2010), it was suggested that chronological uncertainties be presented on the x-axis of climate reconstructions.

An additional challenge was finding a nearby meteo-station with homogenized temperature and precipitation data for developing a calibration-in-time. As evident on the MeteoSchweiz website, only twelve meteo-stations across Switzerland have homogenized monthly temperature and/or precipitation data. Errors introduced by (e.g.) station relocations or changes in equipment can introduce errors in the climate data. This can impact the correlation between sedimentary proxies and climate data and the resulting calibration model. Consequently, a project is underway to homogenize monthly to sub-daily temperature series of more than 50 stations in Switzerland (personal communication, F.G. Kuglitsch).

For Lake Seeberg, we chose an ordinary least squares (split-period and whole period) model to develop a calibration-in-time with homogenized instrumental temperature data. However, many other calibration methods (and measures) could be explored to optimize temperature amplitudes (Esper et al., 2005; Trachsel et al., 2010a).

Finally, in this study we considered regional climate model projections for an increase in inter-annual temperature variability and extreme precipitation (flooding) with continued climate warming. However, regional climate models also project more frequent droughts, heatwaves, and reduced winter temperature variability with continued warming. Climate reconstructions derived from lake sediments can provide insight into the relationship between mean temperatures, winter temperature variability, and extremes such as droughts, heatwaves, in the past (IPCC, 2007).

References

- Arnell, N., Liu, C. 2001. Hydrology and water resources, In: McCarthy, J.J., Canziani, O.F., Leary, N.A., Dokken, D.J., White, K.S. (eds.), *Climate Change 2001: Impacts, Adaptation and Vulnerability. Contribution of Working Group II to the Third Assessment Report of the Intergovernmental Panel on Climate Change*. Cambridge: Cambridge University Press, Chapter 4.
- Blass, A. 2006. Sediments of two high-altitude Swiss lakes as high-resolution late Holocene paleoclimate archives. Inauguraldissertation der Philosophisch-naturwissenschaftlichen Fakultät der Universität Bern.
- Blass, A., Bigler, C., Grosjean, M., Sturm, M. 2007. Decadal-scale autumn temperature reconstruction back to AD 1580 inferred from the varved sediments of Lake Silvaplana (southeastern Swiss Alps). *Quaternary Research* 68: 184-195.
- Caviezel, G. 2007. Hochwasser und ihre Bewältigung anhand des Beispiels Oberengadin 1750-1900. Master's thesis for the History Institute of the Universität Bern.
- Christensen, J.H., Christensen, O.B. 2003. Climate modelling: Severe summertime flooding in Europe. *Nature* 421: 805-806.
- Christensen, J.H., Hewitson, B., Busuioc, A., Chen, A., Gao, X., Held, I., Jones, R., Kolli, R.K., Kwon, W.T., Laprise, R., Magaña Rueda, V., Mearns, L., Menéndez, C.G., Räisänen, J., Rinke, A., Sarr, A., Whetton, P. 2007. Regional climate projections, In: Solomon, S., Qin, D., Manning, M., Chen, Z., Marquis, M.C., Averyt, K.B., Tignor, M., Miller, H.L. (eds.), *Climate Change 2007. The Physical Science Basis. Contribution of WG I to the Fourth Assessment Report of the Intergovernmental Panel on Climate Change*. Cambridge: Cambridge University Press.
- de Jong, R., Kamenik, C. (accepted) Validation of a chrysophyte stomatocyst-based cold-season climate reconstruction from high-Alpine Lake Silvaplana. *Journal of Quaternary Science*.
- Esper, J., Frank, D.C., Wilson, R.J.S., Briffa, K.B. 2005. Effect of scaling and regression on reconstructed temperature amplitude for the past millennium. *Geophysical Research Letters* 32.
- Hausmann, S., Lotter, A.F., van Leeuwen, J.F.N., Ohlendorf, C., Lemcke, G., Grönlund, E., Sturm, M. 2002. Interactions of climate and land-use documented in the varved sediments of Seebergsee in the Swiss Alps. *The Holocene* 12 (3): 279-289.
- Kundzewicz, Z.W., Ulbrich, U., Brücher, T., Graczyk, D., Krüger, A., Leckebusch, G.C., Menzel, L., Pińskwar, I., Radziejewski, M., Szwed, M. 2005. Summer Floods in Central Europe - Climate Change Track? *Natural Hazards* 36: 165-189.
- Larocque-Tobler, I., Grosjean, M., Heiri, O., Trachsel, M., Kamenik, C. 2010. Thousand years of climate change reconstructed from chironomid subfossils preserved in varved Lake Silvaplana, Engadine, Switzerland. *Quaternary Science Reviews* 29: 1940-1949.

Larocque-Tobler, I., Quinlan, R., Stewart, M., Grosjean, M. (accepted) Chironomid-inferred temperature changes of the last century in Lake Seeberg (Seebergsee), Switzerland: assessment of two calibration methods. *Quaternary Science Reviews*.

Mauchle, F. 2010. The modern sediments of Lake Oeschinen (Swiss Alps) as an archive for climatic and meteorological events. Master's thesis for the Faculty of Science of the University of Bern.

MeteoSchweiz 2010. (http://www.meteoschweiz.admin.ch/web/de/klima/klima_heute/jahresverlaeufo_nbcn/Segl_Maria.html)

Parey, S., Dacunha-Castelle, D., Huong Hoang, T.T. 2010. Mean and variance evolutions of the hot and cold temperatures in Europe. *Climate Dynamics* 34: 345-359.

Schär, C., Vidale, P.L., Lüthi, D., Frei, C., Häberli, C., Liniger, M.A., Appenzeller, C. 2004. The role of increasing temperature variability in European summer heatwaves. *Nature* 427: 332-336.

Scherrer, S.C., Appenzeller, C., Liniger, M.A. 2006. Temperature trends in Switzerland and Europe: Implications for climate normals. *International Journal of Climatology* 26: 565-580.

Seneviratne, S.I., Lüthi, D., Litschi, M., Schär, C. 2006. Land-atmosphere coupling and climate change in Europe. *Nature* 443: 205-209.

Tinner, W., Lotter, A.F., Ammann, B., Conedera, M., Hubschmid, P., van Leeuwen, J.F.N., Wehrli, M. 2003. Climatic change and contemporaneous land-use phases north and south of the Alps 2300 BC to 800 AD. *Quaternary Science Reviews* 22: 1447-1460.

Trachsel, M. 2010. Climate variability over the last millennium as recorded in the sediments of high-altitude Lake Silvaplana, Switzerland: data, methods and limitations. Inauguraldissertation der Philosophisch-naturwissenschaftlichen Fakultät der Universität Bern.

Trachsel, M., Grosjean, M., Larocque-Tobler, I., Schwikowski, M., Blass, A., Sturm, M. 2010a. Quantitative summer temperature reconstruction derived from combined biogenic Si and chironomid record from varved sediments of Lake Silvaplana (south-eastern Swiss Alps) back to AD 1177. *Quaternary Science Reviews* 29 (19-20): 2719-2730.

Trachsel, M., Grosjean, M., Schnyder, D., Kamenik, C., Rein, B. 2010b. Scanning reflectance spectroscopy (380-730 nm): a novel method for quantitative high-resolution climate reconstructions from minerogenic lake sediments. *Journal of Paleolimnology* 44: 979-994.

van der Knaap, W.O., van Leeuwen, J.F.N., Fankhauser, A., Ammann, B. 2000. Palynostratigraphy of the last centuries in Switzerland based on 23 lake and mire deposits: chronostratigraphic pollen markers, regional patterns, and local histories. *Review of Palaeobotany and Palynology* 108: 85-142.

Acknowledgements

First and foremost, I would like to recognize Martin Grosjean for providing guidance and support during the past three years. Throughout this project, financial support was provided by the SNF Enlarge II fund.

Lakes Silvaplana and Seeberg were cored in 2005, prior to the start of this thesis. Field-work by Richard Niederreiter, Mathias Trachsel and Lucien von Gunten provided beautiful, well-preserved sediment cores from each site.

Many hands make light work, especially in the field. Rixt de Jong, Pascal Dessarzin, Nicholas Greber, Sam Hagnauer, Stefan Hunziker, Christian Kamenik, Fabian Mauchle, Mathias Trachsel, Richard Wartenburger and Lucien von Gunten assisted on field excursions to Lake Seeberg. Mathias Trachsel was especially invaluable for maintaining a good relationship with the local farmers.

Successful coring campaigns and frequent field excursions provided plenty of material for the laboratory. Fortunately, assistance was provided by Daniela Fischer (measuring biogenic silica at the Paul Scherrer Institute, providing standardized instructions for the laboratory methods and keeping things in the laboratory running smoothly), Pascal Dessarzin (preparing resin-embedded blocks, leaching biogenic silica and measuring scanning reflectance spectroscopy), Fabian Mauchle (cutting the sediment cores varve-by-varve and making grain size measurements at the Geological Institute, ETH-Zurich), Stefan Hunziker (running sequential loss-on-ignition), Lukas Siffert (conducting spectrophotometry), Markus Jungo (counting SCPs), Philip Grob (providing instructions on SCP counting) and Petra Kaltenrieder (identifying terrestrial microfossils for radiocarbon dating).

External laboratory assistance was provided by Willy Tschüdin at GEOPREP (cutting and polishing resin-embedded blocks and making thin sections), Tomasz Goslar (Radiocarbon Dating at Poznań Laboratory) and Marian Fujak (Lead and Cesium Dating at EAWAG).

Interpreting results required careful selection and implementation of statistical methods and many discussions. Collaborations with Petra Breitenmoser, Rixt de Jong, Christian Kamenik, Franz Gunther Kuglitsch, Jürg Luterbacher, Samuel Nussbaumer, Christoph Raible, Krystyna Saunders, Andrea Toreti and Mathias Trachsel were particularly fruitful.

Meteorological data was provided by Raphael Neukom and Nadja Riedwyl and access to data from previous studies of Lake Silvaplana were available from Alex Blass, Andreas Leemann, Christian Ohlendorf, and Mathias Trachsel. Data from Lake Seeberg was generously provided by Sonia Hausmann.

Administrative assistance was provided by Margaret Mohl and Monika Wälti at the Oeschger Centre for Climate Change Research and by Isabella Geissbühler and Marlis Röthlisberger of the Geographical Institute. Technical (IT) assistance was provided by Basilio Ferrante and Thomas Trüssel.

Last but not least, I would like to thank my family and friends for their support over the years and for keeping what's important in perspective. I thoroughly enjoyed reconnecting with my Swiss roots and having a home away from home in Muri. I especially appreciated partaking in Christmas festivities in Gstaad, skiing with Irene and party-planning with Cögg! It was lovely visiting my family in Boston each summer and having them visit me here in Bern. Thanks mom and dad for being such a great support system and for all of your love! Finally, I would like to thank Franz for being such a great support, distraction and partner. Trips to Milan, Strasbourg, Budapest, Vienna, Freiburg, Boston and Mallorca helped me to remember what is important in life!

Appendix A

SVP 06 2 V

Wet core



Frozen core



SVP 06 2 VI

Wet core



Frozen core



Wet core



Frozen core



Resin-Embedded Blocks & Varve Identification



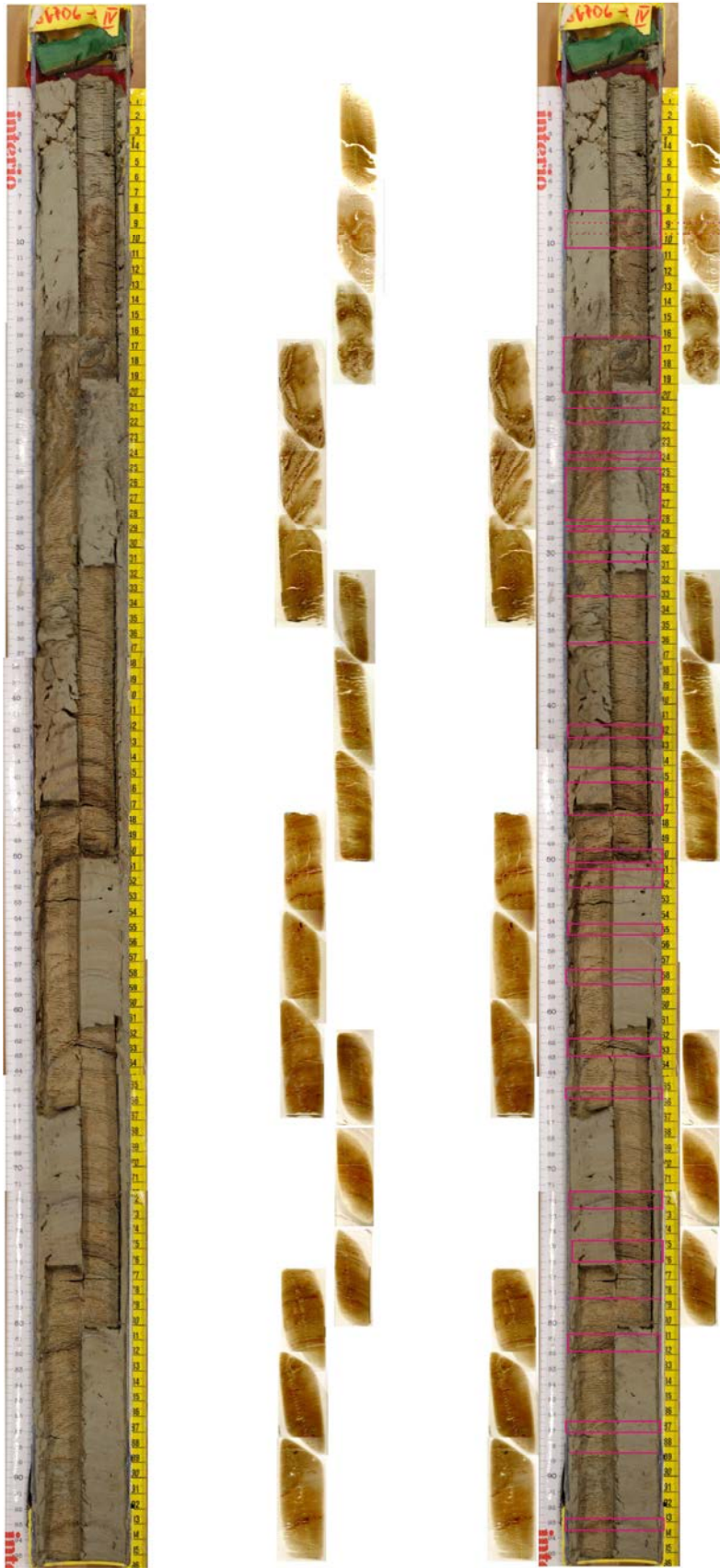
SVP 06 2 IX

Wet core



Frozen core





SVP 06 3 V

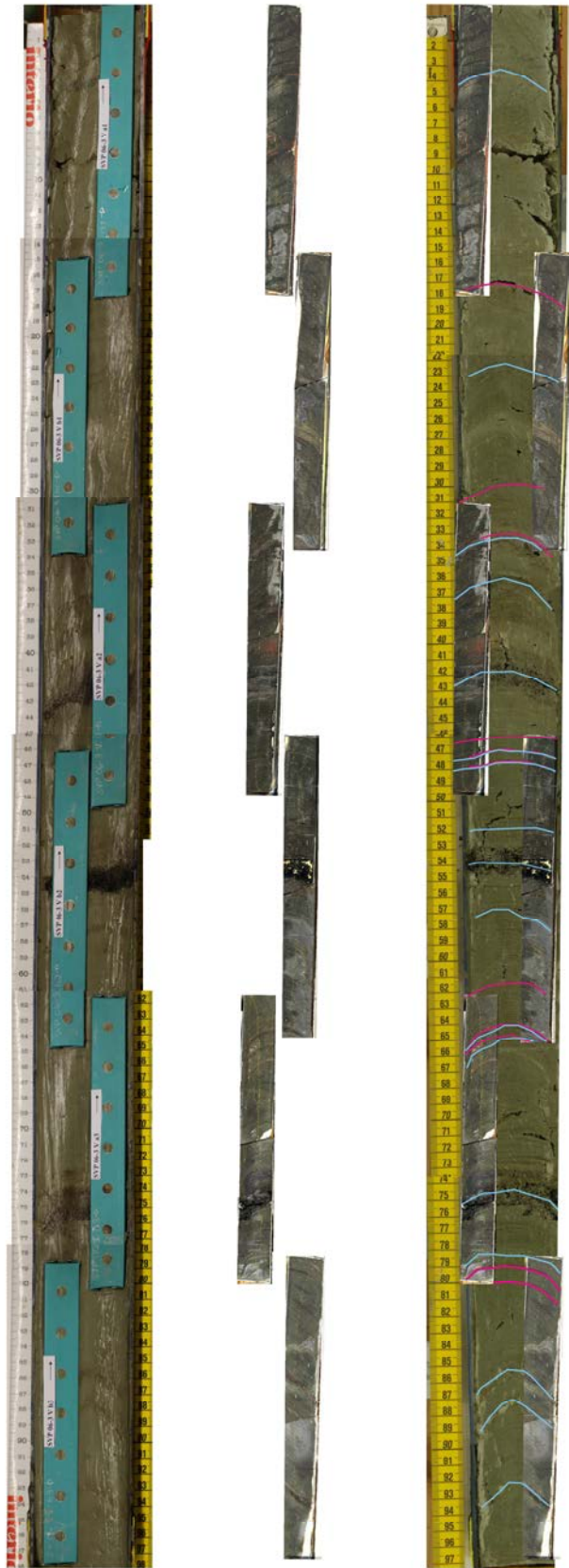
Wet core



Frozen Core



Resin-Embedded Blocks & Varve Identification



SVP 06 3 V

Sampling Intervals



Wet core



Frozen Core

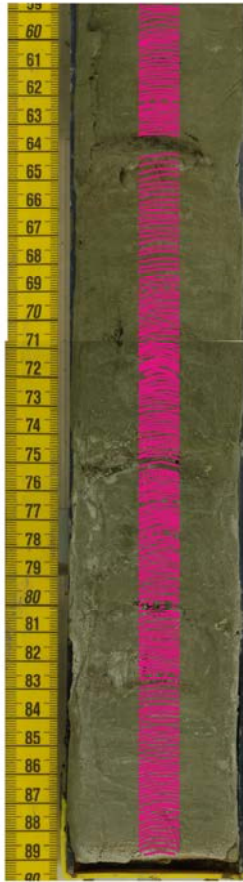


Resin-Embedded Blocks & Varve Identification



SVP 06 3 VI

Sampling Intervals



SVP 06 3 VII

Wet core

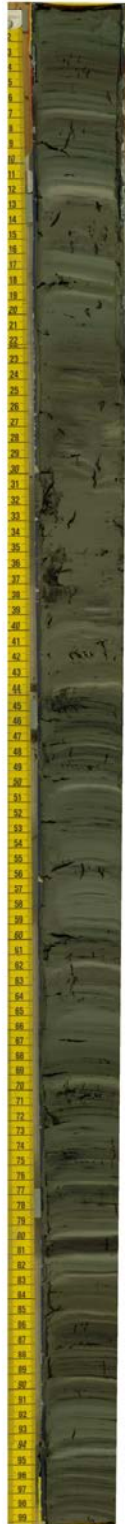


Frozen Core



SVP 06 3 VIII

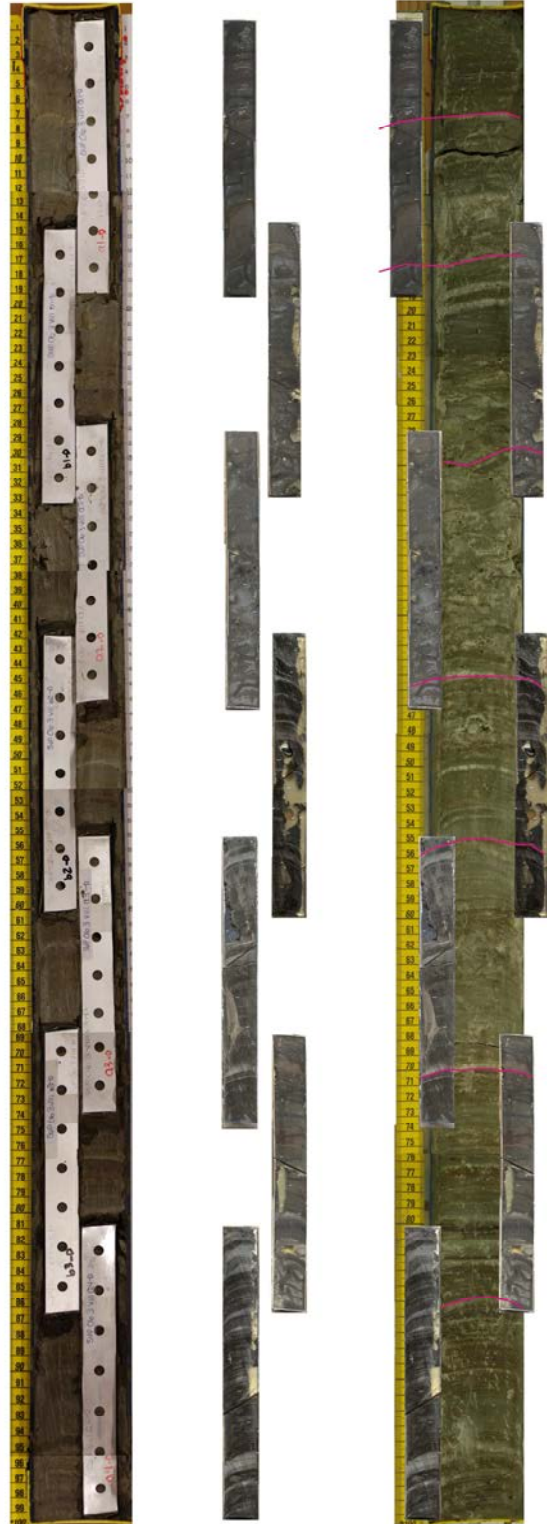
Wet core



Frozen Core



Resin-Embedded Blocks & Varve Identification



SVP 06 3 IX

Wet core



Frozen Core



Resin-Embedded Blocks & Varve Identification



SBS B1

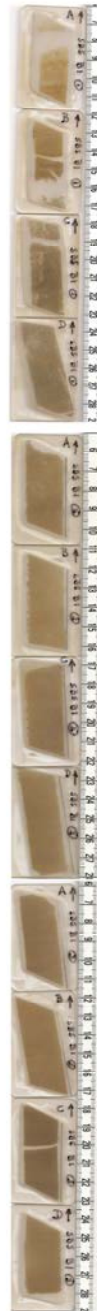
Frozen core



Resin-embedded blocks



Thin sections

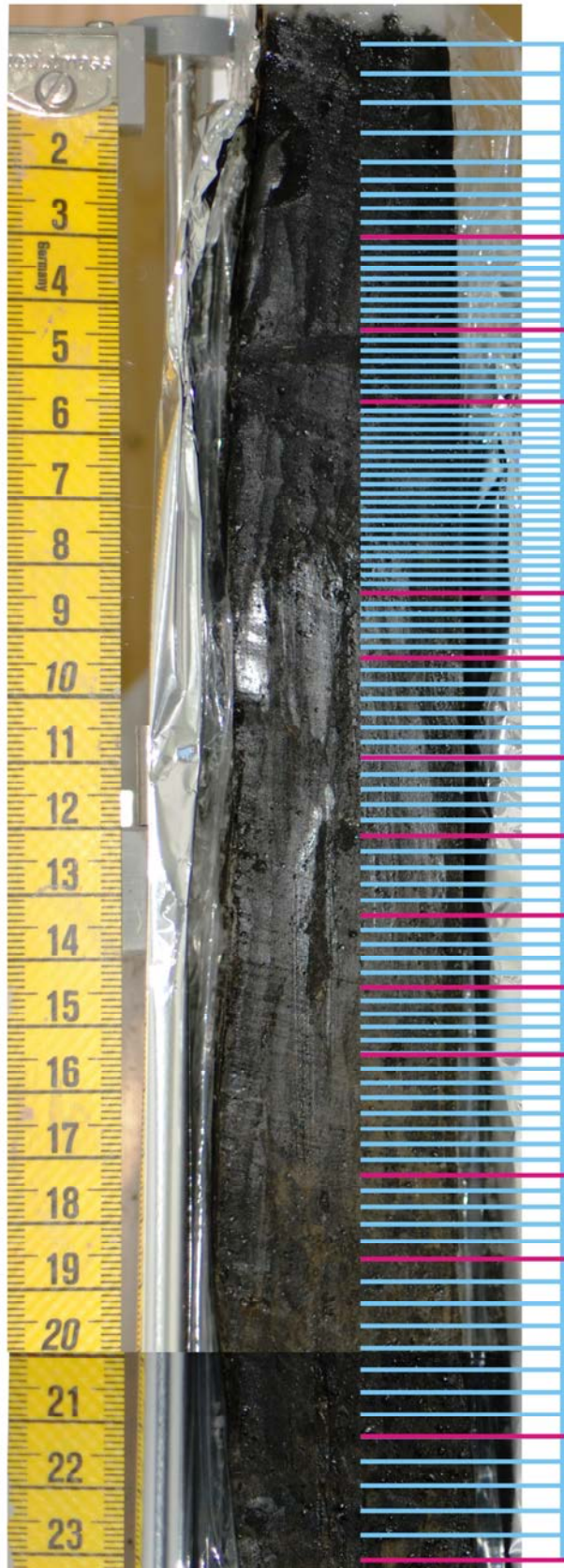


SBS B1

Frozen core



Sampled section



Sampling intervals

- (0) 2005
- (1) 2004
- (2) 2003
- (3) 2002
- (4) 2001
- (5) 2000
- (6) 1999
- (7) 1998
- (8) 1997
- (9) 1996
- (10) 1995
- (11) 1994
- (12) 1993
- (13) 1992
- (14) 1991
- (15) 1990
- (16) 1989
- (17) 1988
- (18) 1987
- (19) 1986
- (20) 1985
- (21) 1984
- (22) 1983
- (23) 1982
- (24) 1981
- (25) 1980
- (26) 1979
- (27) 1978
- (28) 1977
- (29) 1976
- (30) 1975
- (31) 1974
- (32) 1973
- (33) 1972
- (34) 1971
- (35) 1970
- (36) 1969
- (37) 1968
- (38) 1967
- (39) 1966
- (40) 1965
- (41) 1964
- (42) 1963
- (43) 1962
- (44) 1961
- (45) 1960
- (46) 1959
- (47) 1958
- (48) 1957
- (49) 1956
- (50) 1955
- (51) 1954
- (52) 1953
- (53) 1952
- (54) 1951
- (55) 1950
- (56) 1949
- (57) 1948
- (58) 1947
- (59) 1946
- (60) 1945
- (61) 1944
- (62) 1943
- (63) 1942
- (64) 1941
- (65) 1940
- (66) 1939
- (67) 1938
- (68) 1937
- (69) 1936
- (70) 1935
- (71) 1934
- (72) 1933
- (73) 1932
- (74) 1931
- (75) 1930
- (76) 1929
- (77) 1928
- (78) 1927
- (79) 1926
- (80) 1925
- (81) 1924
- (82) 1923
- (83) 1922
- (84) 1921
- (85) 1920
- (86) 1919
- (87) 1918
- (88) 1917
- (89) 1916
- (90) 1915
- (91) 1914
- (92) 1913
- (93) 1912
- (94) 1911
- (95) 1910
- (96) 1909
- (97) 1908
- (98) 1907
- (99) 1906
- (100) 1905
- (101) 1904
- (102) 1903
- (103) 1902
- (104) 1901
- (105) 1900

SBS B2

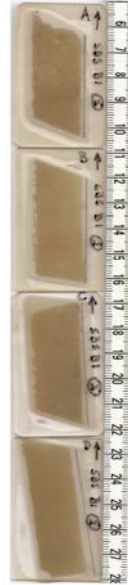
Frozen core



Resin-embedded blocks



Thin sections



SBS B3

Frozen core



Resin-embedded blocks



SBS B4

Frozen core



Resin-embedded blocks



Appendix B

Proxies AD 1878 - AD 2005	Sedimentation Rate (mm/yr)	MAR (mg/cm ² /yr)	bSi Conc. or bSiO ₂ (%)	bSi Flux (mg/cm ² /yr)	LOI ₅₅₀ or C _{org} (%)	LOI ₉₅₀ or CaCO ₃ (%)	Total auto. (%)	Total allo. (%)	D ₅₀ (µm)
Sedimentation rate (mm/yr)	1.00	-0.05 0.54	0.23 <0.01	0.24 <0.01	0.36 <0.01	0.28 <0.01	0.28 <0.01	-0.26 <0.01	0.26 <0.01
MAR (mg/cm ² /yr)	-0.05 0.54	1.00	-0.63 <0.01	0.31 <0.01	-0.54 <0.01	-0.47 <0.01	-0.65 <0.01	0.66 <0.01	-0.36 <0.01
bSi Conc. or bSiO ₂ (%)	0.23 <0.01	-0.63 <0.01	1.00	0.28 0.05	0.71 <0.01	0.54 <0.01	0.98 <0.01	-0.99 <0.01	0.64 0.02
bSi Flux (mg/cm ² /yr)	0.24 <0.01	0.31 <0.01	0.28 0.05	1.00	-0.06 0.64	-0.04 0.74	0.21 0.15	-0.23 0.15	0.15 0.28
LOI ₅₅₀ or C _{org} (%)	0.36 <0.01	-0.54 <0.01	0.71 <0.01	-0.06 0.64	1.00	0.56 <0.01	0.79 <0.01	-0.77 <0.01	0.39 0.03
LOI ₉₅₀ or CaCO ₃ (%)	0.28 <0.01	-0.47 <0.01	0.54 <0.01	-0.04 0.74	0.56 <0.01	1.00	0.69 <0.01	-0.56 <0.01	0.27 0.04
Total auto. (%)	0.28 <0.01	-0.65 <0.01	0.98 <0.01	0.21 0.15	0.79 <0.01	0.69 <0.01	1.00	-0.98 <0.01	0.60 0.02
Total allo. (%)	-0.28 <0.01	0.65 <0.01	-0.98 <0.01	-0.21 0.15	-0.79 <0.01	-0.69 <0.01	-1.00 <0.01	1.00	-0.60 0.02
D ₅₀ (µm)	0.26 <0.01	-0.36 <0.01	0.64 0.02	0.15 0.28	0.39 0.03	0.27 0.04	0.60 0.02	-0.63 0.02	1.00

Château-d'Oex
T emp. (°C)

AD 1901 - AD 2005

	Sedimentation Rate (mm/yr)	MAR (mg/cm ² /yr)	bSI Conc. or bSI(O ₂ (%))	bSI Flux (mg/cm ² /yr)	LOI ₅₅₀ or C _{org} (%)	LOI ₅₅₀ or CaCO ₃ (%)	Total auto. (%)	Total allo. (%)	D ₅₀ (µm)
January	T _{year} P _{corr} -0.01 0.90	-0.24 0.01	0.27 < 0.01	0.04 0.64	0.23 0.01	0.09 0.35	0.26 < 0.01	-0.27 < 0.01	0.18 0.05
February	T _{year} P _{corr} 0.17 0.08	-0.23 0.02	0.23 0.01	-0.03 0.76	0.27 < 0.01	0.17 0.08	0.25 < 0.01	-0.24 < 0.01	0.17 0.07
March	T _{year} P _{corr} 0.11 0.26	-0.23 0.02	0.34 < 0.01	0.07 0.48	0.31 < 0.01	0.20 0.04	0.34 < 0.01	-0.34 < 0.01	0.30 < 0.01
April	T _{year} P _{corr} -0.03 0.75	-0.17 0.08	0.19 0.05	-0.06 0.55	0.20 0.04	0.17 0.08	0.20 0.03	-0.19 0.04	0.12 0.22
May	T _{year} P _{corr} -0.06 0.54	-0.23 0.01	0.32 < 0.01	0.00 0.96	0.34 < 0.01	0.14 0.14	0.33 < 0.01	-0.33 < 0.01	0.23 0.02
June	T _{year} P _{corr} -0.04 0.66	-0.26 < 0.01	0.38 < 0.01	-0.01 0.89	0.33 < 0.01	0.29 < 0.01	0.40 < 0.01	-0.38 < 0.01	0.28 < 0.01
July	T _{year} P _{corr} 0.06 0.52	-0.27 < 0.01	0.31 < 0.01	0.02 0.81	0.31 < 0.01	0.22 0.03	0.33 < 0.01	-0.32 < 0.01	0.26 0.01
August	T _{year} P _{corr} 0.16 0.11	-0.40 < 0.01	0.56 < 0.01	0.07 0.48	0.43 < 0.01	0.30 < 0.01	0.55 < 0.01	-0.56 < 0.01	0.47 < 0.01
September	T _{year} P _{corr} 0.23 0.02	-0.17 0.07	0.20 0.01	0.01 0.91	0.24 < 0.01	0.26 < 0.01	0.24 < 0.01	-0.21 < 0.01	0.15 0.07
October	T _{year} P _{corr} 0.10 0.29	-0.37 < 0.01	0.37 < 0.01	-0.03 0.81	0.33 < 0.01	0.38 < 0.01	0.40 < 0.01	-0.37 < 0.01	0.29 < 0.01
November	T _{year} P _{corr} 0.18 0.07	-0.14 0.15	0.11 0.24	-0.06 0.55	0.11 0.25	0.12 0.21	0.12 0.19	-0.10 0.23	0.19 0.03
December	T _{year} P _{corr} 0.04 0.72	-0.10 0.29	0.24 0.01	0.18 0.06	0.25 < 0.01	0.03 0.76	0.22 0.02	-0.25 0.01	0.16 0.11
JJA average	T _{year} P _{corr} 0.08 0.39	-0.43 < 0.01	0.57 < 0.01	0.04 0.71	0.49 < 0.01	0.37 < 0.01	0.58 < 0.01	-0.58 < 0.01	0.47 < 0.01
JJAS average	T _{year} P _{corr} 0.15 0.10	-0.41 < 0.01	0.54 < 0.01	0.04 0.73	0.49 < 0.01	0.40 < 0.01	0.56 < 0.01	-0.55 < 0.01	0.43 < 0.01
MIJAS average	T _{year} P _{corr} 0.11 0.24	-0.43 < 0.01	0.58 < 0.01	0.03 0.76	0.54 < 0.01	0.40 < 0.01	0.60 < 0.01	-0.59 < 0.01	0.45 < 0.01

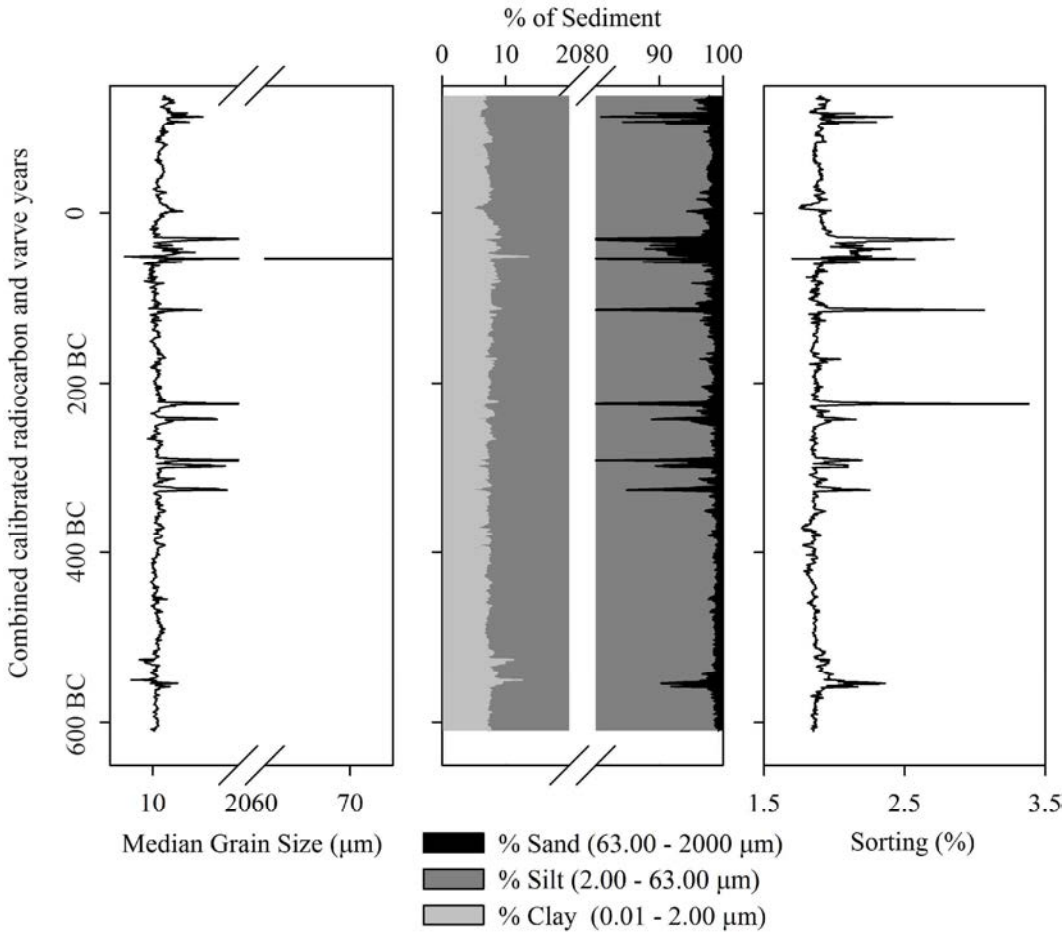
Château-d'Oex

Precip. (mm)

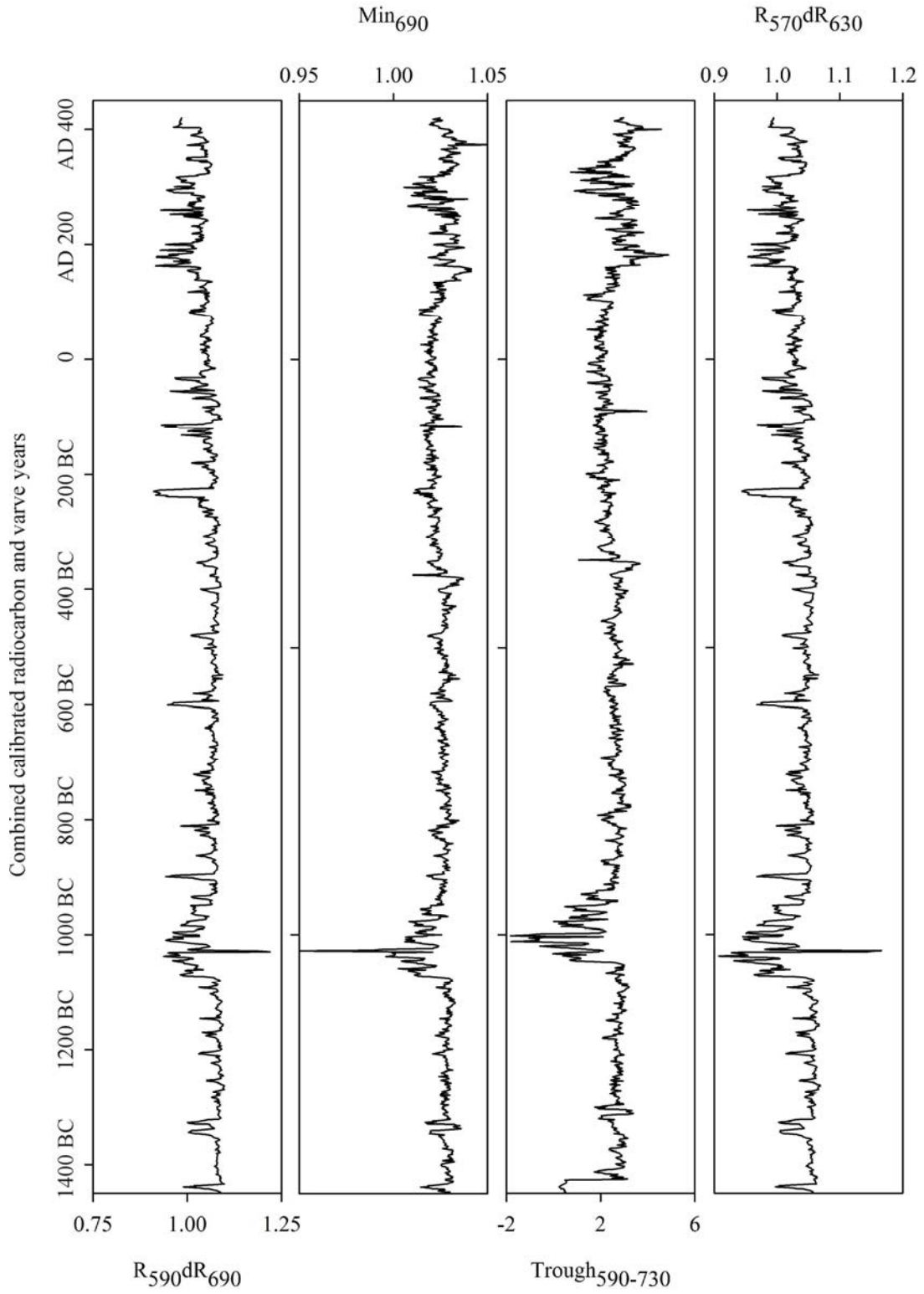
AD 1901 - AD 2005

	Sedimentation Rate (mm/yr)	MAR (mg/cm ² /yr)	bSi Conc. or bSiO ₂ (%)	bSi Flux (mg/cm ² /yr)	LOI ₅₅₀ or C _{org} (%)	LOI ₅₅₀ or CaCO ₃ (%)	Total auto. (%)	Total allo. (%)	D ₅₀ (µm)
January	0.03 <i>P_{corr}</i>	-0.10 0.29	0.02 0.83	-0.14 0.15	0.07 0.47	0.12 0.19	0.05 0.62	-0.03 0.77	-0.03 0.73
February	0.02 <i>P_{corr}</i>	-0.13 0.15	0.04 0.63	-0.16 0.07	0.06 0.52	0.12 0.18	0.06 0.46	-0.04 0.60	-0.02 0.83
March	0.01 <i>P_{corr}</i>	-0.04 0.97	-0.01 0.83	-0.04 0.48	-0.02 0.58	0.08 0.44	0.01 0.94	0.01 0.94	0.03 0.79
April	0.06 <i>P_{corr}</i>	0.06 0.53	0.01 0.86	0.07 0.45	0.02 0.86	-0.05 0.61	0.00 0.96	-0.01 0.86	0.05 0.54
May	0.08 <i>P_{corr}</i>	-0.04 0.68	0.08 0.46	0.03 0.78	0.03 0.74	0.11 0.27	0.09 0.39	-0.07 0.47	-0.02 0.84
June	0.05 <i>P_{corr}</i>	0.00 0.98	-0.02 0.86	0.02 0.85	-0.03 0.75	-0.11 0.24	-0.04 0.67	0.02 0.84	-0.03 0.71
July	-0.03 <i>P_{corr}</i>	-0.03 0.72	0.01 0.87	-0.05 0.59	0.02 0.81	-0.03 0.73	0.01 0.93	-0.02 0.86	0.00 0.97
August	0.01 <i>P_{corr}</i>	-0.01 0.96	-0.05 0.55	-0.13 0.15	0.00 0.98	0.05 0.59	-0.03 0.71	0.05 0.59	-0.01 0.93
September	-0.02 <i>P_{corr}</i>	-0.02 0.85	-0.04 0.64	-0.13 0.16	0.03 0.74	-0.08 0.38	-0.05 0.61	0.04 0.70	0.06 0.54
October	0.17 <i>P_{corr}</i>	0.07 0.46	0.09 0.38	0.25 0.01	0.02 0.83	0.03 0.78	0.08 0.44	-0.08 0.41	0.05 0.62
November	0.02 <i>P_{corr}</i>	-0.09 0.37	-0.01 0.92	-0.09 0.32	-0.05 0.61	-0.14 0.13	-0.04 0.67	0.01 0.88	-0.02 0.82
December	-0.06 <i>P_{corr}</i>	-0.02 0.79	-0.03 0.73	-0.02 0.86	0.05 0.59	-0.02 0.86	-0.02 0.79	0.02 0.80	-0.03 0.79
JJA sum	0.02 <i>P_{corr}</i>	-0.02 0.82	-0.03 0.61	-0.10 0.21	0.00 0.98	-0.04 0.60	-0.04 0.59	0.03 0.64	-0.02 0.73
JJAS sum	0.01 <i>P_{corr}</i>	-0.03 0.77	-0.05 0.50	-0.15 0.08	0.01 0.87	-0.08 0.37	-0.05 0.47	0.04 0.55	0.01 0.94
MJJAS sum	0.03 <i>P_{corr}</i>	-0.04 0.68	-0.02 0.78	-0.14 0.13	0.02 0.78	-0.04 0.67	-0.02 0.78	0.02 0.82	0.00 0.99
SON sum	0.10 <i>P_{corr}</i>	-0.02 0.82	0.02 0.79	0.01 0.86	0.00 0.98	-0.11 0.23	0.00 0.97	-0.02 0.82	0.04 0.64

Appendix C

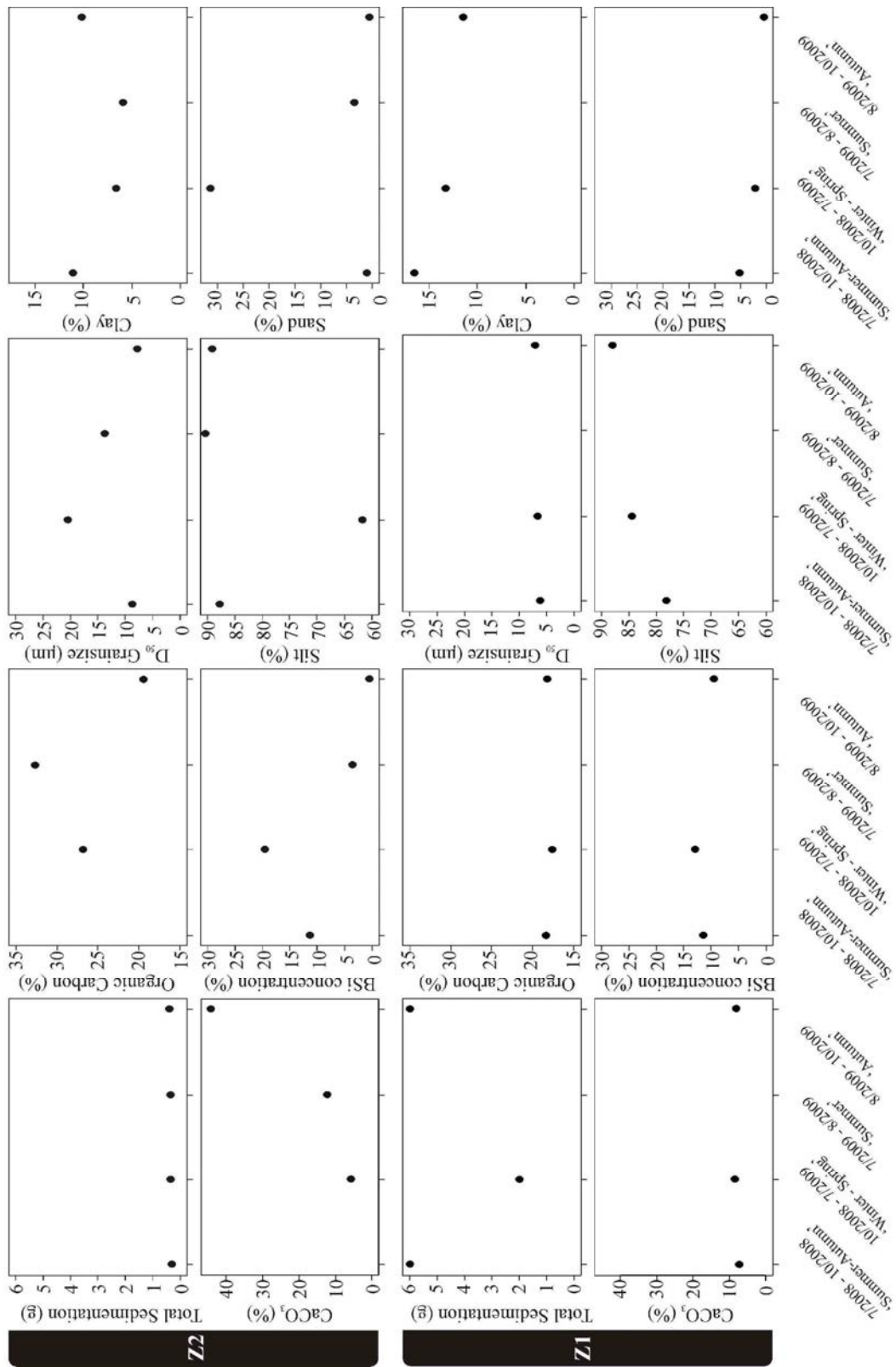


Annual grain size results from Lake Silvaplana ca. 600 BC – AD 120



Annual Spectrolino results from Lake Silvaplana ca. 1450 BC – AD 420

Appendix D



Sediment trap data from Lake Seeberg (Z1 depth: 12.5 m - 10.5 m; Z2 depth: 6.5 m - 4.5 m)

Erklärung

gemäss Art. 28 Abs. 2 RSL 05

Name/Vorname: Monique M. Stewart.....

Matrikelnummer: 08-132-037.....

Studiengang: 1 Februar 2008.....

Bachelor

Master

Dissertation

Titel der Arbeit: High-resolution, multi-proxy climate reconstructions of the late Holocene
derived from the varved sediments of two lakes in the Swiss Alps

LeiterIn der Arbeit: Prof. Dr. Martin Grosjean.....
.....

Ich erkläre hiermit, dass ich diese Arbeit selbständig verfasst und keine anderen als die angegebenen Quellen benutzt habe. Alle Stellen, die wörtlich oder sinngemäss aus Quellen entnommen wurden, habe ich als solche gekennzeichnet. Mir ist bekannt, dass andernfalls der Senat gemäss Artikel 36 Absatz 1 Buchstabe o des Gesetzes vom 5. September 1996 über die Universität zum Entzug des auf Grund dieser Arbeit verliehenen Titels berechtigt ist.

Bern/8 Marz 2011

Ort/Datum

Monique M. Stewart.....

Unterschrift

MONIQUE M. STEWART
 Kanonenweg 18 Bern 3012
 Phone: + 76 471 4854, Email: stewart@giub.unibe.ch
 Nationality: U.S. / Swiss, Profession: Scientist

EDUCATION

- 2008 – 2011 **Ph.D. student in Climate Sciences**
Supervisor: Prof. Dr. Martin Grosjean
 Oeschger Centre of Climate Research
 Institute of Geography
 University of Bern
 Bern, Switzerland
- 2006 – 2008 **M.Sc. in Physical Geography**
Supervisor: Prof. Dr. Joseph Desloges
 Department of Geography
 University of Toronto
 Toronto, ON, Canada
- 2000 – 2005 **B.A.H. in Physical Geography & French**
 Faculty of Arts & Sciences
 Queen's University
 Kingston, ON, Canada
- 2001 Semester Abroad
 Faculty of Arts & Sciences
 Harvard University
 Cambridge, MA, U.S.A.
- 1996 – 2000 **High School Diploma**
 Lexington High School
 Lexington, MA, U.S.A.

PROFESSIONAL EXPERIENCE

- September 2006 – May 2007 **Instructor**
Field Methods in Physical Geography
Geomorphology
 Department of Geography
 University of Toronto
 Toronto, ON, Canada
- May – June 2002 **Intern (Energy Consumption Research)**
 Exec. Office of Environmental Affairs
 Boston, MA, U.S.A.

PUBLICATIONS

PEER-REVIEWED JOURNAL ARTICLES:

Larocque-Tobler I, Quinlan R, **Stewart M**, Grosjean M, 2010. Chironomid-inferred temperature changes of the last century in meromictic lake Seeberg, Switzerland: assessment of two calibration methods. *Quaternary Science Reviews*, *Accepted*.

Stewart M, Larocque-Tobler I, Grosjean M, 2010. Quantitative inter-annual and decadal summer temperature variability 570 BC - AD 120 (Iron Age - Roman Period) as reconstructed from the varved sediments of Lake Silvaplana, Switzerland. *Journal of Quaternary Sciences*, *Accepted*.

Stewart M, Grosjean M, Kuglitsch FG, Nussbaumer SU, von Gunten L. Reconstructions of Late Holocene palaeofloods and glacier activity in the Upper Engadine, Switzerland (ca. 1450 BC – AD 420). *Palaeography, Palaeoclimatology, Palaeoecology*, *Submitted*.

BOOK CHAPTERS:

Larocque-Tobler I, Laurion I, Moschen R, **Stewart M**, 2010. Climate and Lacustrine Ecosystems. *In*: J. Dodson (Ed.), *Changing Climates, Earth Systems and Society*, International Year of Planet Earth, Springer Science + Business Media, p. 123 – 160.

MONOGRAPHS:

Stewart M, 2011. High-resolution, multi-proxy climate reconstructions of the late Holocene derived from the varved sediments of two lakes in the Swiss Alps. Ph.D. Thesis, University of Bern, Bern, Switzerland, 167 pp.

Stewart M, 2008. The sediment accumulation record at glacial-fed Kinaskan Lake: Implications for changes in Holocene hydrology and climate in the Upper Iskut River Watershed, British Columbia. M.Sc. Thesis, University of Toronto, Toronto, Ontario, Canada, 145 pp.

CONFERENCE CONTRIBUTIONS

Stewart M, Larocque-Tobler I, Grosjean M. Quantitative inter-annual and decadal June-July-August temperature variability 570 BC - AD 120 (Iron Age - Roman Period) as reconstructed from the varved sediments of Lake Silvaplana, Switzerland. International Quaternary Association (INQUA), Bern, Switzerland, July 2011, ORAL.

Desloges JR, **Stewart M**, Chow N, Gilbert R. Extreme events interpreted from the clastic accumulation record of large glacier-fed lakes of north western Canada. International Quaternary Association (INQUA), Bern, Switzerland, July 2011, POSTER.

Stewart M, Larocque-Tobler I, Grosjean M. A multi-proxy warm season temperature reconstruction (3400 cal yr BP - 1500 cal yr BP) from the varved sediments of Lake Silvaplana. European Geophysical Union (EGU) General Assembly, Vienna, Austria, May 2011, POSTER.

Stewart M, Larocque-Tobler I, Grosjean M. A multi-proxy warm season temperature reconstruction (3400 cal yr BP - 1500 cal yr BP) from the varved sediments of Lake Silvaplana. Swiss Global Change Day, Bern, Switzerland, April 2011, POSTER.

Stewart M, Grosjean M. Climate reconstructions from varved Alpine lake sediments for the last 3500 years. Swiss Global Change Day, Bern, Switzerland, March 2009, POSTER.

Stewart M, Desloges JR. Spatial and temporal trends of sedimentation in Kinaskan Lake, British Columbia, Canada. Annual Meeting of Swiss Sedimentologists, Fribourg, Switzerland, February 2009, ORAL.

Stewart M, Grosjean M. Climate reconstructions from varved Alpine lake sediments for the last 3500 years. NCCR Climate Summer School, Monte Verità, Switzerland, September 2008, POSTER.

MEMBERSHIPS

European Geophysical Union

Swiss Sedimentologists

INTERESTS

Palaeo- (late Holocene) climatology

Reconstruction of extreme weather and climate events

Limnogeology and geomorphology

Travel, Sports, Arts, Culture